Structural elucidation of asphalt using NMR spectroscopy and GPC fractionation with laser desorption mass spectrometry
by Jacqueline Eileen Fonnesbeck

A dissertation submitted in partial fulfillment of the requirements for the degree of Doctor of Philosophy in Chemistry
Montana State University

Abstract:
Asphalt is a very complex mixture containing polyaromatic hydrocarbons bearing long chain aliphatics and few functional groups including phenols, carboxylic acids, amines, and sulfides. Vanadium, nickel, and iron are also found in trace amounts. When asphalt is used in pavement it is exposed to environmental weathering which changes it chemically and hence, physically, causing it to harden. This hardening makes the asphalt more susceptible to cracking and has been thought to be caused mainly by the increase of polar interactions between asphalt molecules. This increase would be due to the production of additional polar functional groups by air oxidation which is a free-radical process called autoxidation. For this reason, it is important to be able to easily identify functional groups in asphalt and to determine how they are affected by weathering. Examination of functional groups before and after asphalt pavement weathering has been accomplished by NMR spectroscopy. Phenols have been derivitized using a novel method involving specific phenol methylation using sodium hydride and 13C enriched methyl iodide, NaH13 CH3I, in a one-step process. The methylated phenols have then been quantified using the Inverse Gated NMR experiment. Benzylic carbons are thought to be prime positions for the free-radical air oxidation forming benzylic ketones. The changes in these positions, upon both laboratory and actual road aging, have been relatively quantified using the 2D Inverse COLOC NMR experiment. It has been found that benzylic protons decrease in actual road aged asphalts. However, in laboratory aged asphalts, this is not neccessarily the case. In fact, benzylic protons sometimes increase upon laboratory aging. FT-IR spectroscopy has also confirmed the formation of carbonyl groups upon weathering which supports the benzylic carbon free-radical air oxidation theory. It has also been found that certain additives such as Mn02 tend to oxidize the benzylic carbons in neat, unweathered asphalt. Fingerprinting and mass identification of smaller molecules in asphalt has been accomplished through Gel Permeation Chromatograpy (GPC) Fractionation along with Laser Desorption Time-of- Flight Mass Spectrometry (LD TOF MS). Individual asphalts can be distinguished from the GPC fractions of the smaller molecules by recognizing that each asphalt gives a specific peak pattern in its LD mass spectrum. In addition, complete base line resolution of the LD mass spectra of the these lower molecular size GPC fractions has allowed identification of possible core molecules in asphalt that are alkyl substituted to varying degrees.

STRUCTURAL ELUCIDATION OF ASPHALT USING NMR SPECTROSCOPY AND GPC FRACTIONATION WITH LASER DESORPTION MASS SPECTROMETRY

by

Jacqueline Eileen Fonnesbeck

A dissertation submitted in partial fulfillment
of the requirements for the degree

of

Doctor of Philosophy

in

Chemistry

MONTANA STATE UNIVERSITY
Bozeman, Montana

May 1997

APPROVAL

of a thesis submitted by

Jacqueline Eileen Fonnesbeck

This dissertation has been read by each member of the thesis committee and has been found to be satisfactory regarding content, English usage, format, citations, bibliographic style, and consistency, and is ready for submission to the College of Graduate Studies.

Dr. Jan Sunner _____ (Signature) 5/6/97 Date

Approved for the Department of Chemistry

Dr. David M. Dooley _____ (Signature) 5/12/97 Date

Approved for the College of Graduate Studies

Dr. Robert Brown _____ (Signature) 5/14/97 Date

STATEMENT OF PERMISSION TO USE

In presenting this thesis in partial fulfillment of the requirements of a doctoral degree at Montana State University-Bozeman, I agree that the Library shall make it available to borrowers under rules of the Library. I further agree that copying of this dissertation is allowable only for scholarly purposes, consistent with "fair use" as prescribed in the U.S. Copyright Law. Requests for extensive copying or reproduction of this dissertation should be referred to University Microfilms International, 300 North Zeeb Road, Ann Arbor, Michigan 48106, to whom I have granted "the exclusive right to reproduce and distribute my dissertation in and from microform along with the non-exclusive right to reproduce and distribute my abstract in any format in whole or in part."

Signature Jacqueline Tonnesbeck

Date May 1, 1997

ACKNOWLEDGEMENTS

I gratefully acknowledge support for this work from funding received as fellowships from the State of Montana/Department of Energy EPsCOR program and the Associated Western Universities. In addition, laboratory space and equipment were provided by the Department of Energy at the Idaho National Engineering Laboratory under the direction of Dr. Eric S. Peterson. I also am grateful to Dr. Jan Sunner for the advice and assistance that he gave on much of this research project.

TABLE OF CONTENTS

TABLE OF CONTENTS (continued)

TABLE OF CONTENTS (continued)

LIST OF TABLES

LIST OF TABLES (continued)

LIST OF FIGURES

LIST OF FIGURES (continued)

LIST OF FIGURES (continued)

LIST OF FIGURES (continued)

LIST OF FIGURES (continued)

ABSTRACT

Asphalt is a very complex mixture containing polyaromatic hydrocarbons bearing long chain aliphatics and few functional groups including phenols, carboxylic acids, amines, and sulfides. Vanadium, nickel, and iron are also found in trace amounts. When asphalt is used in pavement it is exposed to environmental weathering which changes it chemically and hence, physically, causing it to harden. This hardening makes the asphalt more susceptible to cracking and has been thought to be caused mainly by the increase of polar interactions between asphalt molecules. This increase would be due to the production of additional polar functional groups by air oxidation which is a free-radical process called autoxidation. For this reason, it is important to be able to easily identify functional groups in asphalt and to determine how they are affected by weathering. Examination of functional groups before and after asphalt pavement weathering has been accomplished by NMR spectroscopy. Phenols have been derivitized using a novel method involving specific phenol methylation using sodium hydride and ^{13}C enriched methyl iodide, $NaH/^{13}CH_3I$, in a one-step process. The methylated phenols have then been quantified using the Inverse Gated NMR experiment. Benzylic carbons are thought to be prime positions for the free-radical air oxidation forming benzylic ketones. The changes in these positions, upon both laboratory and actual road aging, have been relatively quantified using the 2D Inverse COLOC NMR experiment. It has been found that benzylic protons decrease in actual road aged asphalts. However, in laboratory aged asphalts, this is not neccessarily the case. In fact, benzylic protons sometimes increase upon laboratory aging. FT-IR spectroscopy has also confirmed the formation of carbonyl groups upon weathering which supports the benzylic carbon free-radical air oxidation theory. It has also been found that certain additives such as MnO_2 tend to oxidize the benzylic carbons in neat, unweathered asphalt. Fingerprinting and mass identification of smaller molecules in asphalt has been accomplished through Gel Permeation Chromatograpy (GPC) Fractionation along with Laser Desorption Time-of- Flight Mass Spectrometry (LD TOF MS). Individual asphalts can be distinguished from the GPC fractions of the smaller molecules by recognizing that each asphalt gives a specific peak pattern in its LD mass spectrum. In addition, complete base line resolution of the LD mass spectra of the these lower molecular size GPC fractions has allowed identification of possible core molecules in asphalt that are alkyl substituted to varying degrees.

INTRODUCTION

Bitumens are complex mixtures of hydrocarbons. When a bitumen is combined with inorganic material such as vanadium, nickel, and iron, it is called asphalt. Both bitumens and asphalts occur in nature. However, as an industrial product, asphalt is obtained in petroleum refining as the heavy, non-volatile residue that remains after distilling crude oil. Naturally occurring asphalt is also derived from petroleum but through the natural process of slow evaporation of the volatile fractions that leave the asphalt fraction behind. Rock asphalt, for example, is a naturally occurring asphalt that has impregnated porous rock such as sandstone or limestone. Gilsonite is another form of natural asphalt that is hard and brittle and is mined from rock crevices and veins. The main source of asphalt however, is from petroleum refining. Figure 1 shows a schematic diagram of major types of products, including asphalt, that are produced by refining petroleum.

Petroleum products are extremely important to the world economy. For example, we may consider the wide variety of engineering and industrial uses of asphalt. It is not only used to pave streets, highways, and airfields, but is used to make roofing, waterproofing, and insulating materials. It is also used to line irrigation canals and reservoirs, and for the facing on dams and levees. Asphalt is also found in some paints and varnishes. However, asphalt is predominantly used for paving purposes where it is referred to as asphalt

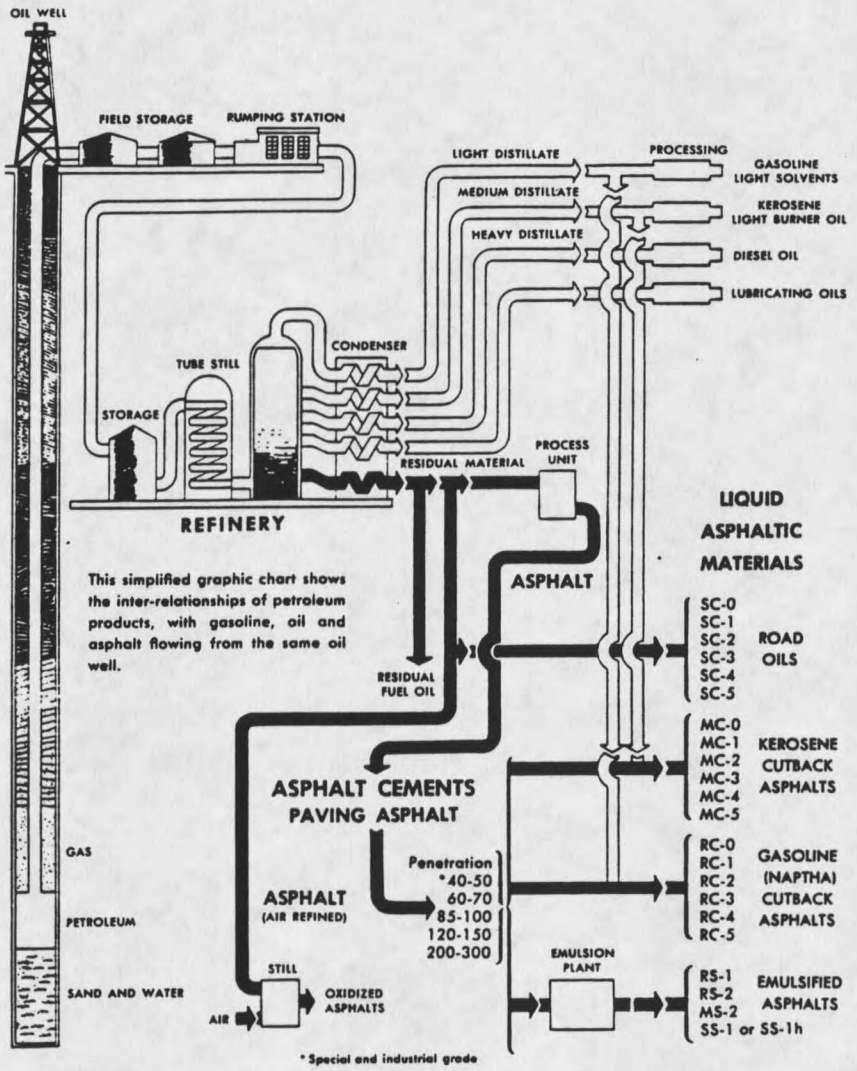

Figure 1. Petroleum asphalt flow diagram.(1)

cement. Asphalt cement, when mixed with rocks of various sizes and shapes is called pavement. The rock components are called aggregates and are commonly made up of broken stone and slag, crushed or uncrushed gravel, sand, crushed limestone, stone dust, silica, or hydrated lime. Aggregates normally constitute 90 percent or more by weight of the pavement mixture.(1)

It is apparent that asphalt is an important commodity, but as a resource it is limited. Due to the depletion of our own reserves, the U.S. dependency on foreign oil imports has grown rapidly since the 1960's. This is a good reason for U.S. researchers to develop asphalt pavements that have greater durability to weathering conditions and hence, longer service lifetimes. A logical approach would be to learn more about fundamental asphalt chemistry. Understanding the chemistry might enable us to eventually develop pavements that do not rut, crack, or crumble and that require little maintenance.

When used as a paving or roofing material, asphalt undergoes an aging process. The asphalt hardens, resulting in embrittlement, which causes it to crack and crumble. This age hardening has been attributed to two processes. First, as asphalt is exposed to UV radiation and oxygen in the atmosphere, it undergoes chemical oxidation.(2) The second process is dependent upon the first. Polar molecules within asphalt naturally cluster together through polar interactions.(3) These clusters are commonly called micelles and the process of molecular clustering in asphalt is referred to as "self-assembly".(4,5) This will be discussed in more detail later. When asphalt oxidizes, more polar groups

are formed. This affects the self-assembly in asphalt. The micelles in asphalt generally increase in size which raises the overall viscosity. The mobility of asphalt molecules is lowered preventing them from easily flowing past each other when stress is applied to the material.(2) The consequence is that asphalt pavement hardens and becomes more susceptible to cracking.

To understand asphalt properties and how they are affected when exposed to "aging" conditions, it is necessary to study the chemistry of asphalt. One may first ask the following two questions:

1. What is the chemical composition of asphalt?
2. What chemical changes occur as a result of aging?

These general questions are fundamental to understanding asphalt behavior and are the focus of this dissertation which includes the following research:

1. Quantifying the phenol content in asphalt. Phenols are important contributors to the self-assembly in asphalt.(2)
2. Observing benzylic hydrogens in asphalt by 2D NMR. Their disappearance upon aging would indicate possible benzylic carbon oxidation to benzylic ketones. This increase of carbonyl concentration would increase self-assembly and contribute to asphalt hardening.
3. Characterizing and fingerprinting asphalts by Laser Desorption Mass Spectrometry (LD-MS).

A Brief History

Skeletons of prehistoric vertebrates have been preserved intact in naturally occurring surface deposits of asphalts. The most famous example is

the La Brea tar pit in Los Angeles, California. Ice Age fossils have been found there due to the fact that animals became trapped when they came to drink from the shallow pool that covered the asphalt bog. La Brea asphalt was used by indians in the area to waterproof their baskets and canoes, and by early Spanish settlers to waterproof their adobe houses.(6) Recent archeological excavations have shown that between 3200 to 540 B.C. asphalt was used extensively in Mesopotamia and the Indus Valley as a cement for masonry and highway construction and as a waterproofing layer for temple baths and water tanks.(1) Around 300 B.C., asphalt was used in the mummification process in Egypt where the swathing bandages were smeared with an asphalt preservative.(7) Indeed, the Arabic word for mummy (*mumiya*) means bitumen. Rock asphalt found occasional use in the 19th century. For example, in 1802 it was used in France for floor, bridge, and sidewalk surfacing. In 1838, it was imported into Philadelphia for sidewalk construction. The interest in asphalt as a paving material started to grow appreciably after 1870 as evidenced by pavements laid between Newark, New Jersey and Washington D.C. from 1870 to 1876.(1)

During the first year of industrial petroleum refining in 1902, approximately 20,000 tons of asphalt were produced in the United States. The U.S. petroleum asphalt tonnage produced annually increased steadily to 3,000,000 tons in 1924 and to 19,000,000 tons in 1956.(1)

Asphalt Chemical Composition

Through the years much information on the chemical composition and molecular structure of asphalt components has been obtained from analytical techniques, such as: IR, NMR, GC-MS, GPC, etc. These studies have shown that asphalt is an extremely complex mixture of different hydrocarbons. However, the primary components are polynuclear aromatic ring systems with naphthenic structures bearing alkyl side chains as well as various polar functional groups containing oxygen, nitrogen, and sulfur. These structural elements are illustrated in Figure 2. Asphalt also contains parts-per-million amounts of organometallic iron, nickel, and vanadium compounds usually in the form of porphyrins.(2) Results from the elemental analysis of several representative asphalts can be seen in Table 1.(2) It is seen that the concentrations of heteroatoms vary somewhat and the concentrations of trace metals vary widely depending on the geological source of the petroleum.

The composition of asphalt is also influenced by the specific refinery process that was used to produce the asphalt. For instance, olefins do not generally occur in crude oils. Olefins are present in asphalt only as a result of the petroleum cracking process in which large hydrocarbon molecules are broken down into smaller molecules.

Each individual asphalt contains a wide variety of molecules ranging from nonpolar, non-aromatic hydrocarbons to highly polyaromatic hydrocarbons

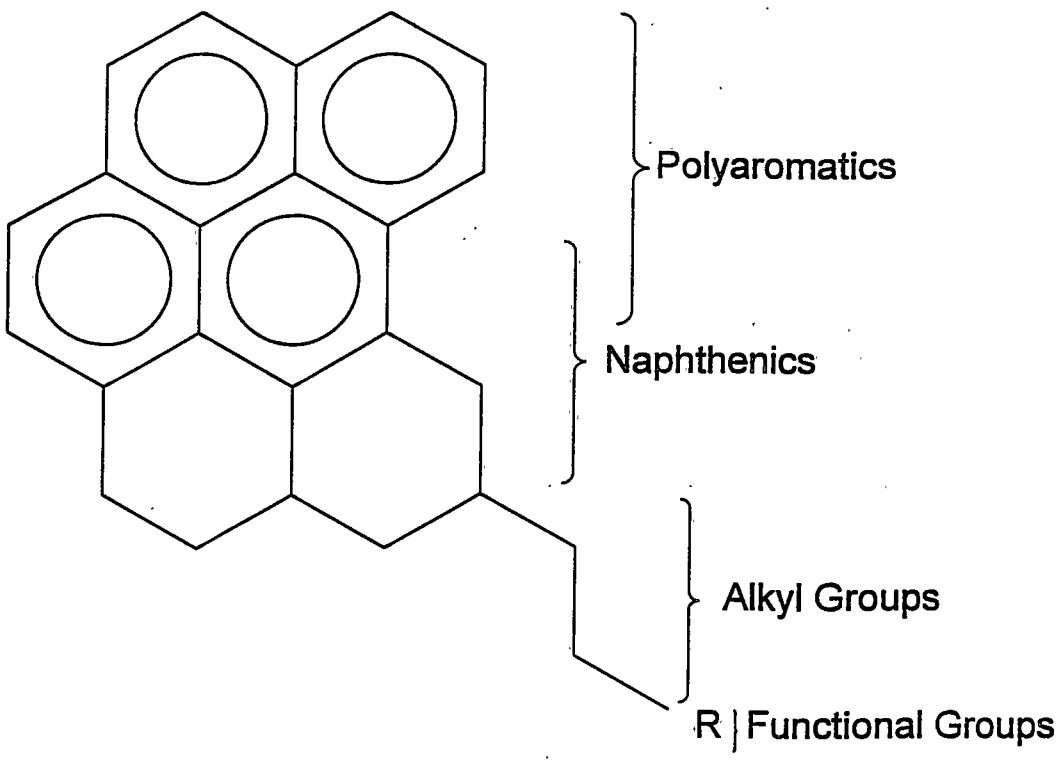

Where R = COOH, OH, SH, or NH

Figure 2. General structural features of asphalt.(3)

Table 1. Elemental analysis of representative petroleum asphalts (2).

Code Source	B-2959 Mexican blend	B-3036 Arkansas-Louisiana	B-3051 Boscan	B-3602 California
Carbon, %	83.77	85.78	82.90	86.77
Hydrogen, %	9.91	10.19	10.45	10.94
Nitrogen, %	0.28	0.26	0.78	1.10
Sulfur, %	5.25	3.41	5.43	0.99
Oxygen, %	0.77	0.36	0.29	0.20
Vanadium, ppm	180	7	1380	4
Nickel, ppm	22	0.4	190	6

(PAHs). Varying substitution with heteroatom functional groups as well as the presence of organometallic compounds dramatically increases the complexity of the mixture. One can still construct a hypothetical "average" asphalt molecule. This is the type of molecule that one might construct in order to explain the results of analytical methods used to characterize asphalt while assuming that these results were obtained for a pure substance and not for a complicated mixture. This may seem naive, but it has been an important step in the structural elucidation of asphalt components. By developing hypothetical structures one can obtain a general idea of asphalt structural features and mass information. Work has been done to determine the structures of compounds present in asphalt. Jennings *et al.* (3,8) constructed molecules that can be considered “typical” of those present in asphalt. An example of such a

structure is seen in Figure 3.

Functional Groups in Asphalt

Functional groups present in asphalt are known to be important for asphalt self-assembly(3,9) as well as sites for "oxidative aging".(2,10-13) A primary objective in asphalt research has therefore been to characterize these functional groups. Asphalt researchers have extensively employed IR spectrometry to detect, quantify, and characterize them.(2,14,15) IR spectra demonstrated that the functional groups include carboxylic acids, 2-quinolones, phenols, pyrrolics, pyridines, and sulfides. Upon oxidative aging new functional groups are formed which include ketones, sulfoxides, and anhydrides. Carboxylic acids are present in newly produced asphalt but their concentrations increase upon oxidative aging.(16) The structures of these functionalities are shown in Figure 4.

Asphalt Fractionation

A traditional approach to studying asphalt is to separate the complex asphalt mixture into fractions with different chemical properties. The group analysis methods, that were developed for this purpose, are based on the different solubilities of asphalt components in different solvents. The two most

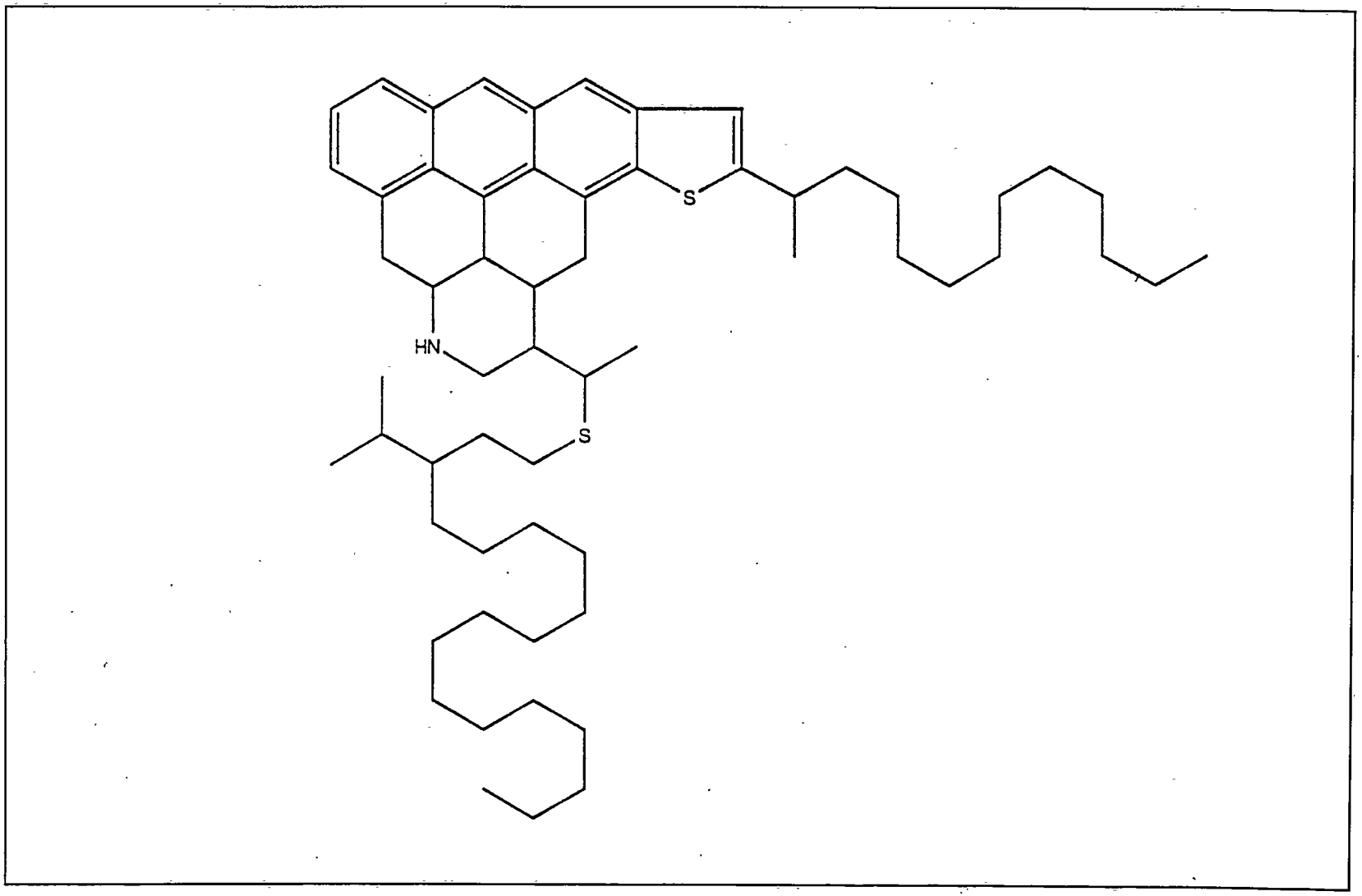

Figure 3. A hypothetical asphalt molecule.(8)

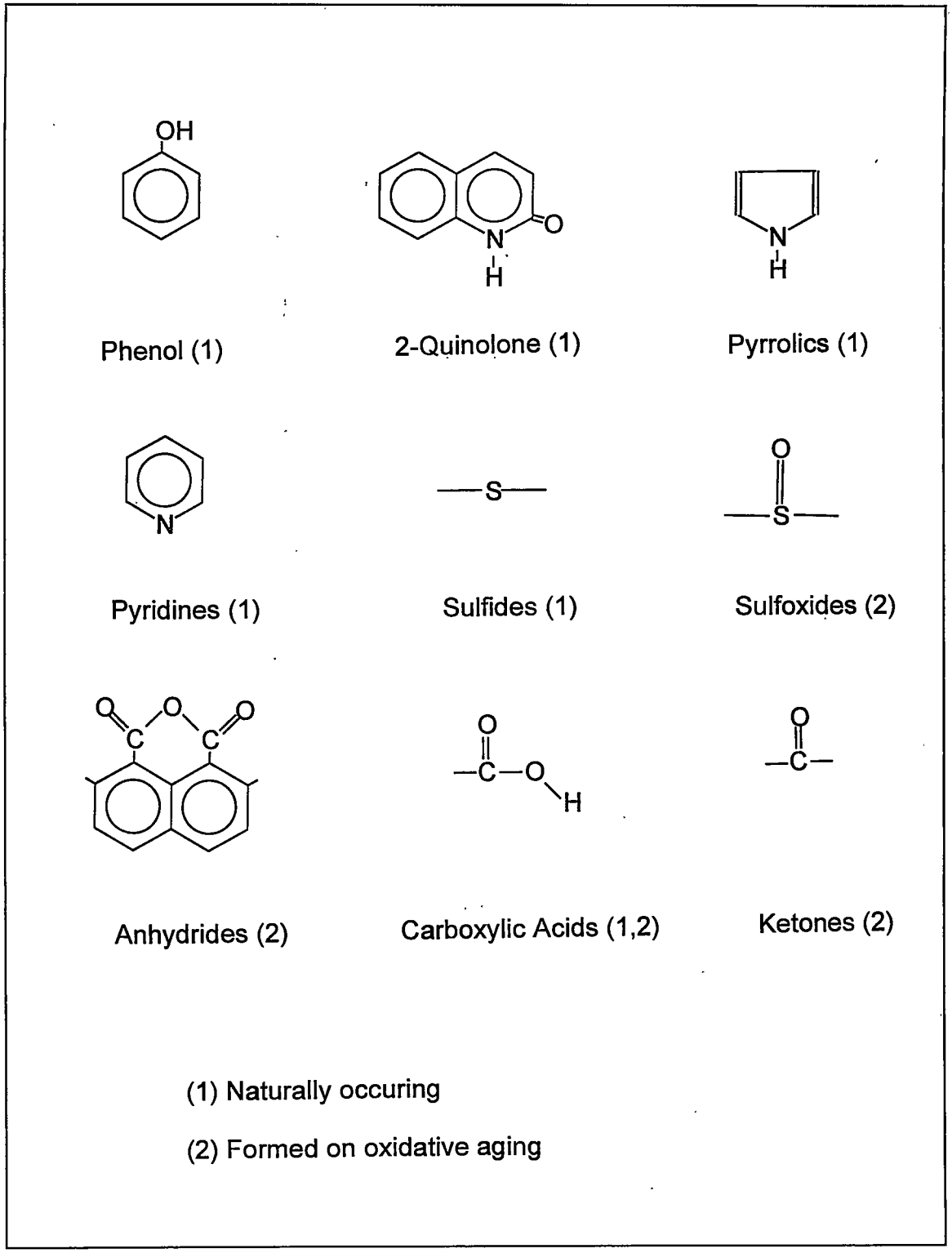

Figure 4. Examples of important chemical functionalities present in asphalt molecules.(16)

important compound groups in asphalt are asphaltenes and malthenes.(17) Asphaltenes are insoluble in low boiling point saturated hydrocarbons such as n-hexane but are soluble in carbon tetrachloride (or benzene). Asphaltenes consist mainly of the larger, polar PAHs. Malthenes, in contrast, are soluble in low boiling point saturated hydrocarbons (n-hexane). Malthenes consist mainly of the non-polar chain aliphatic hydrocarbons (paraffins).

Asphaltenes and malthenes are first separated by precipitating the asphaltenes in fifty times the asphalt volume with n-pentane. Malthenes can be further separated into fractions with different chemical properties. The separation procedure begins by dissolving the malthene fraction in pentane and new fractions are precipitated in sequence as shown below:(18)

Nitrogen bases	(N) :	Soluble in pentane and precipitatable with cold 85 percent sulfuric acid.
	(N_1):	Soluble in pentane and precipitatable with hydrogen chloride gas.
	(N_2):	That remaining portion which did not precipitate with HCl gas but precipitates with cold 85 percent sulfuric acid.
First Acidaffins	(A_1):	That portion which did not precipitate with cold 85 percent sulfuric acid but precipitates with cold concentrated (97-98%) sulfuric acid.
Second Acidaffins	(A_2):	Did not precipitate with cold concentrated sulfuric acid but precipitates with cold fuming

sulfuric acid.

Paraffins (P) : Did not precipitate with cold, fuming sulfuric acid.

Self-Assembly in Asphalt

The complexity of asphalt mixtures has presented a challenging problem for asphalt chemists for years. Over the years, much has indeed been learned about the chemical composition of asphalt and about the nature of asphalt self-assembly. However, the information is incomplete and fragmented, and the overall picture of asphalt must be put together like an extraordinarily convoluted puzzle. Several explanations have been proposed concerning the reason for asphalt self-assembly. It has been suggested that the flat polyaromatic molecules within asphalt stack via delocalization of the aromatic ring π electrons.(4,19-21) Hydrogen bonding is also believed to contribute to the self-assembly in asphalts.(3,9) This polar interaction would involve the heteroatoms oxygen and nitrogen. Although the total concentration of these heteroatoms is low, the energy of the hydrogen bonds is on the order of 5-10 kcal/mol, and this is large enough for hydrogen bonding to be important to self-assembly.(22) The third interaction involves the weak van der Waals forces that occur between all of the molecules. However, van der Waals forces are the only forces that occur between the long, unbranched, unsubstituted aliphatic chains

(paraffins) (23) found in asphalt.

Once formed, asphalt assemblies have been found to arrange themselves into even larger assemblies that are ellipsoidal (or nearly spherical) in shape and these are called micelles. Brulé et al. (24), from a Gel Permeation Chromatography (GPC) study, elaborated upon the micellar theory of asphalt. GPC separates molecules by size and shape of the molecules. The column is packed with porous beads of polystyrene. The smaller molecules are retained in the column longer than the largest molecules because they penetrate the beads. Whereas, the larger molecules, due to their size, cannot penetrate the beads and will travel through the column much more rapidly than smaller molecules.

GPC has also been used to study asphalt self-assembly in various solvents.(19-21) In an extensive GPC study by Jennings *et al.* (21,25), the tendency for self-assembly of molecules in asphalts was shown by studying the changes in their GPC curves when dissolved in different solvents. An increase in the GPC curve intensity at the beginning of the elution time, when the larger molecules come off of the column, would indicate an increased tendency for molecular associations. Asphalt samples were dissolved in THF, toluene, and in mixtures of THF and toluene. It was initially believed that toluene, a non-polar solvent, would encourage polar interactions but disrupt the pi electron interactions between asphalt sheet polyaromatics. However, tetrahydrofuran (THF) was expected to disrupt all but the most highly polar interactions. The

respective asphalt solutions were run through a GPC column. Figures 5 & 6 show two of the chromatograms (at 340 nm detection) of whole asphalts from the Jennings study. The superimposed GPC chromatograms are of the same asphalt, but dissolved in different concentrations of the solvent mixtures or pure solvent. The largest molecules or assemblies eluted from the column first. Curve C in Figures 5 and 6 has a higher absorbance between 12 and 16 minutes than the other curves. The larger assemblies or molecules should be eluting at this time. Curve C represents the asphalt dissolved in equal volumes of both THF and toluene. The increase showed that the largest size assemblies had formed in this solvent mixture. The conclusion was that the larger assemblies were held together by both polar and non-polar interactions. This study showed that different types of molecular interactions are involved in self-assembly. Some asphalts contain more polar groups than others, hence they will be more likely to form assemblies via dipole-dipole interactions in non-polar solvents. Other asphalts are less polar and more polyaromatic, hence they will be more likely to form assemblies via pi-pi stacking in polar solvents. Then again, other asphalts contain a more balanced composition between polar and non-polar constituents and assemblies in both polar and non-polar solvents are expected to form.

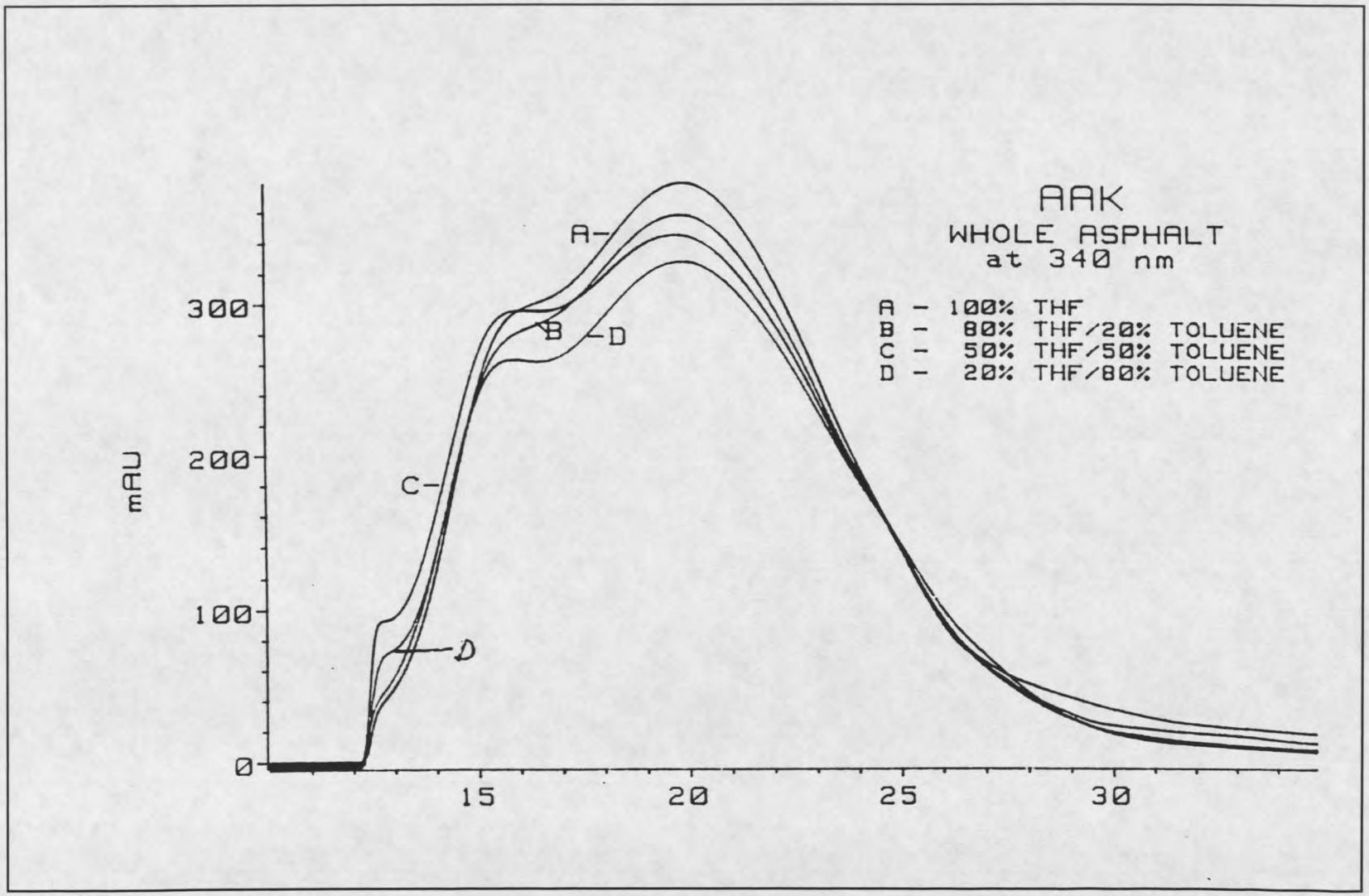

Figure 5. GPC chromatograms of a whole asphalt at different toluene/THF concentrations.(25)

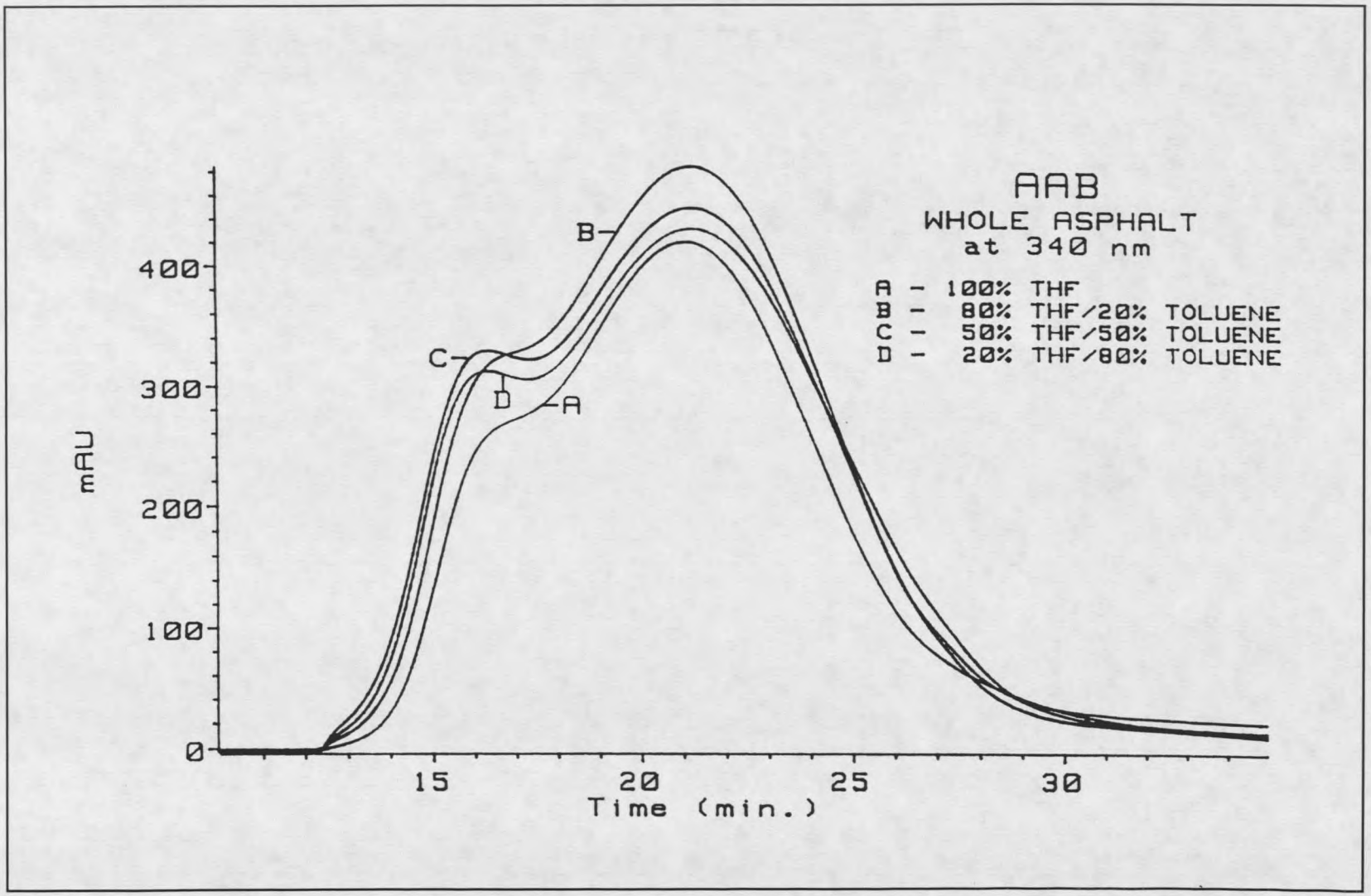

Figure 6. GPC chromatograms of a whole asphalt at different toluene/THF concentrations.(25)

Asphalt Age Hardening

Asphalt age hardening and embrittlement in pavements has long been recognized to be a function of asphalt composition.(2,5) However, as mentioned above, asphalt is a complex mixture, and its composition can vary significantly among asphalts from different sources. It is the broad range of substances that gives asphalt its unique properties.

It has long been thought that asphalt pavement age hardening occurs in two phases (11): First, there is a rapid, short-term aging that occurs when the asphalt is mixed with the aggregate material at elevated temperatures just prior to the actual paving. Second, there is a much slower aging process that occurs over time at ambient temperatures after the pavement has been laid. Poor pavement performance follows age hardening as the asphalt becomes brittle and cracks.

Three basic causes of asphalt pavement age hardening have been identified:

1. Loss of the paraffinic components i.e. aliphatics via evaporation or adsorption into the pores of the aggregate material(26).
2. Molecular structuring which causes steric hardening. (2,5) (reversible)
3. Changes in the chemical composition as a result of oxidation (irreversible).

Volatile loss, according to Peterson (2) appears not to be significant in the hardening of asphalt. "Molecular structuring" is a general term used relating

to the spatial rearrangements or microstructuring of molecules in asphalt that results from increased self assembly. This causes a reversible hardening referred to as "steric hardening".

Synthetic steric hardening in asphalt is accomplished by a process called "air blowing" (sometimes called "air conversion") where asphalt is simply exposed to a constant flow of pure oxygen for a specified amount of time.(27-30) Although many asphalt investigators have found that air blowing contributes to asphalt age hardening they have also found that this type of steric hardening is reversible.

Though changes in the microstructure of asphalt contributes to age hardening, age hardening is not exclusively due to molecular structuring. The main cause seems to be irreversible changes in asphalt due to chemical changes which, in turn, influence asphalt microstructuring. The main chemical reaction is believed to be autoxidation, which is a free-radical process initiated by atmospheric oxygen.(2) The oxidation can also occur catalytically at the interface between the asphalt binder and the mineral aggregate in pavement.(10) Vanadium, which occurs in trace amounts in asphalt, has also been shown to promote oxidation.(31)

Two standardized laboratory procedures have been developed to simulate oxidative asphalt aging processes.(11,32) The Thin Film Oven Test (TFOT) is designed to mimic the short-term hot-mix aging process, and the Pressure Oxygen Vessel (POV) test is designed to mimic long-term weathering

aging. See Figure 7 for a schematic diagram of a Pressure Oxygen Vessel. These laboratory aging processes will be mentioned throughout this dissertation since asphalt samples aged by these methods were used extensively in this research.

Application of Nuclear Magnetic Resonance Spectroscopy for Asphalt Analysis

One-dimensional ^{1}H and ^{13}C NMR spectroscopy has been used extensively in the last decade to characterize asphalt.(33-36) Figures 8 and 9 show typical 1D ^{1}H and ^{13}C NMR spectra of asphalt. In Figure 8, aliphatic proton peaks resonate between 0 and 2 ppm. Benzylic, amine, and sulfide protons resonate between 2 and 4 ppm. Aromatic proton peaks are between 7 and 8.5 ppm. In Figure 9, aliphatic carbons are between 11 and 40 ppm. Aromatic carbons are between 120 and 150 ppm. Both proton and carbon NMR spectra are unremarkable in the sense that all asphalt 1D NMR spectra are very similar. However, unique information can be obtained by NMR using more sophisticated pulse experiments. For example, Jennings, *et al.* (3,8,33) were able to determine the ratio of asphalt aromatic/aliphatic carbons using the Distortionless Enhancement by Polarization Transfer (DEPT) NMR experiment. The DEPT experiment was used to differentiate among methyl (CH_3), methylene (CH_2), and methine (CH) groups to clarify the aliphaltic region of ^{13}C

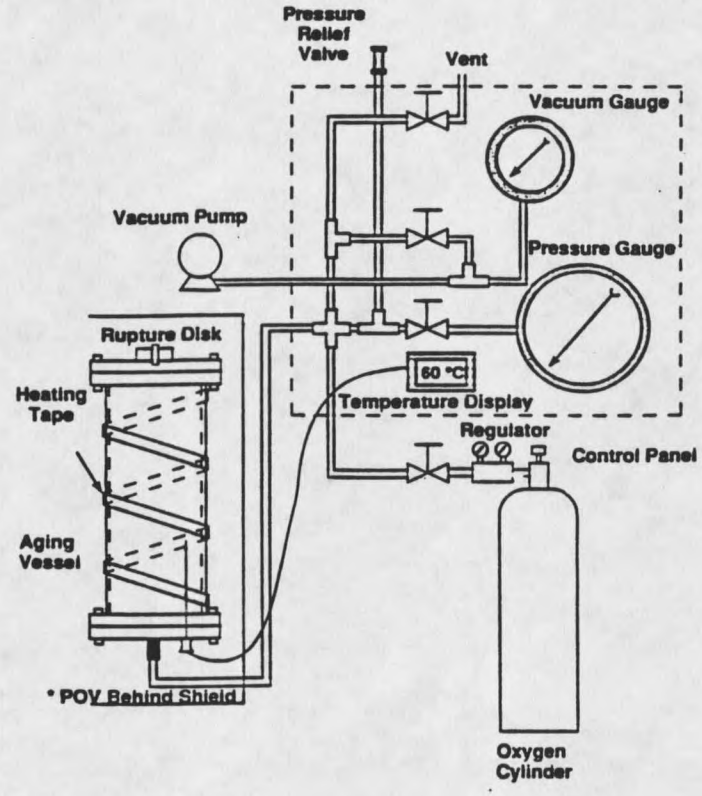

Figure 7. Pressure Oxygen Vessel (POV) apparatus.(32)

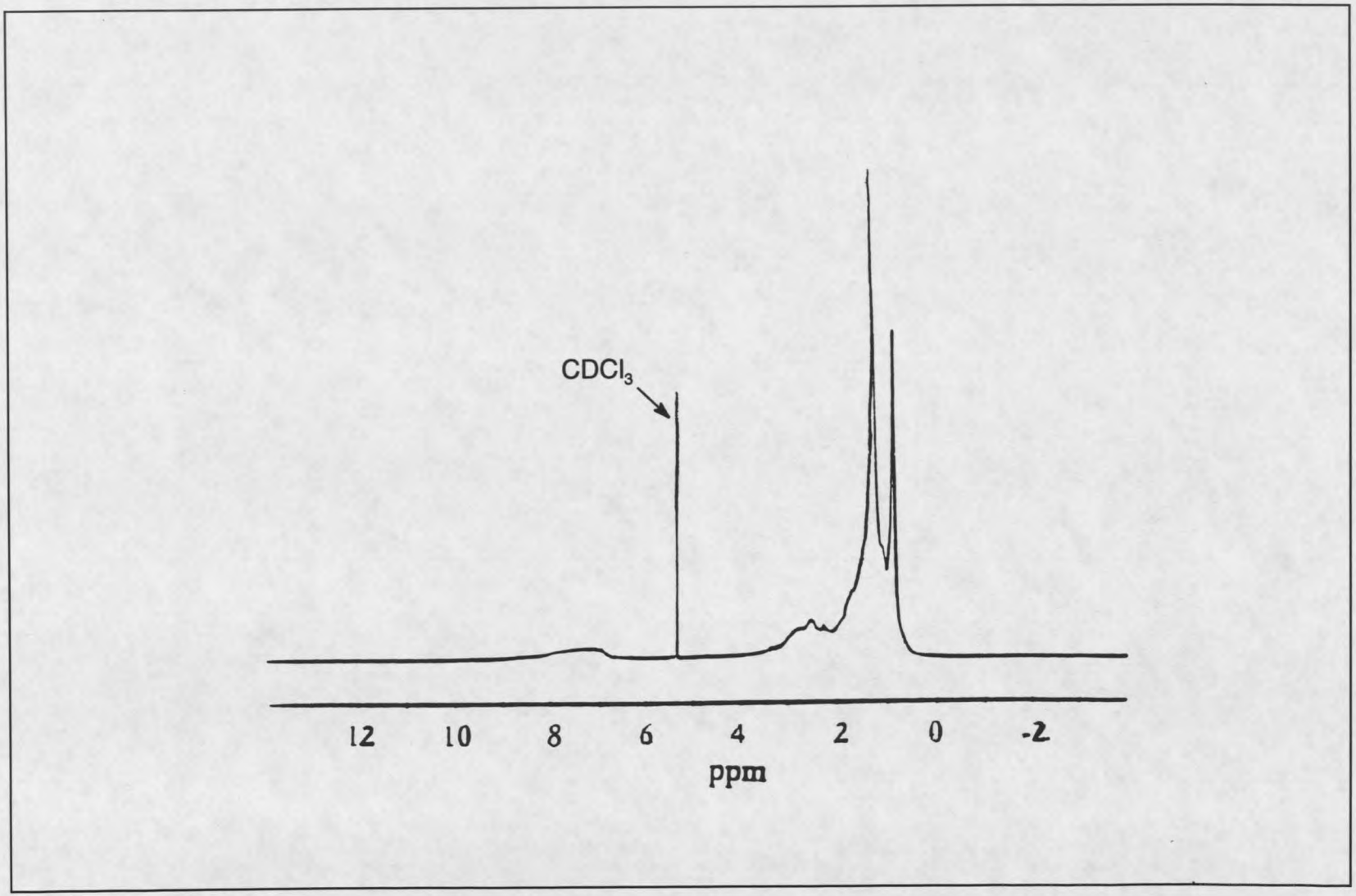

Figure 8. Example of a typical ^{1}H-NMR spectrum of asphalt in deuterated chloroform ($CDCl_3$).(3)

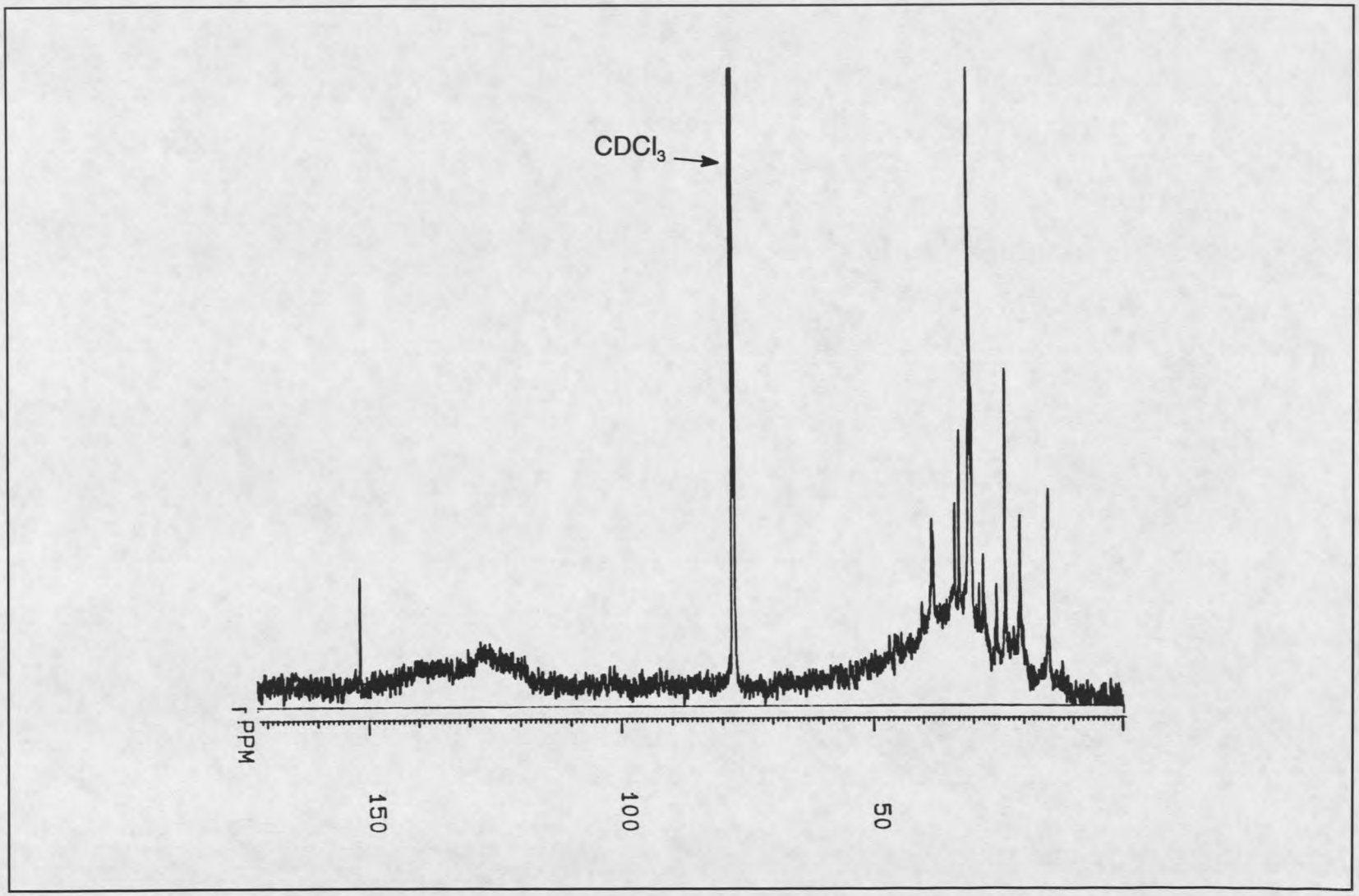

Figure 9. Example of a typical ^{13}C-NMR spectrum of asphalt in deuterated chloroform ($CDCl_3$).(3)

spectra. Shown in Figure 10 are the DEPT spectra of 10a, the whole asphalt; 10b, its strong acid fraction; and 10c, its neutral fraction. Methyl and methine carbons are displayed as positive signals, whereas the methylene carbons are negative, or inverted signals.

NMR spectrometry has also been used to quantify functional groups in asphalt which include phenols, amines, and carboxylic acids.(3,35,36)

Phenols in Asphalt

As mentioned earlier, phenols occur naturally in asphalt. Phenols are believed to play an important role in asphalt. Their potential for hydrogen bonding means that there is a high probability that they contribute to the microstructuring of the polar components in asphalt. This is particularly true because the O---HO hydrogen bond is stronger than the N---HN hydrogen bond, 5 kcal/mol as opposed to 3 kcal/mol.(22) This is due to the fact that oxygen is more electronegative than nitrogen and thus, has a greater tendency to withdraw electron density from the proton. Phenols could also be involved in aromatic electrophilic substitution reactions in asphalt. For these reasons, their detection and quantitation are important issues.

Phenols in asphalt are methylated prior to NMR detection because the acidic protons are difficult to detect in the proton NMR spectrum. However, upon methylation using ^{13}C enriched methyl iodide one can observe a

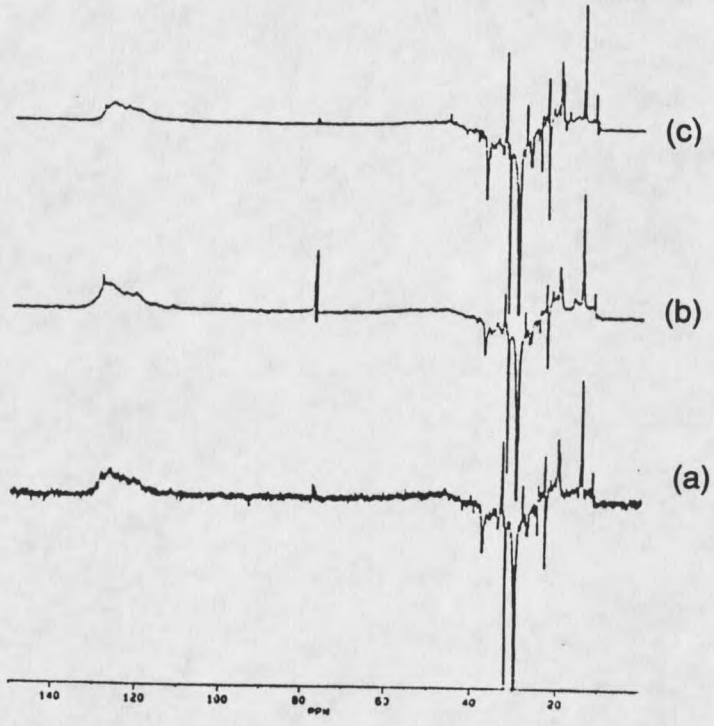

Figure 10. DEPT 135 for (a) a whole asphalt, (b) its strong acid fraction, and (c) its neutral fraction.(35)

corresponding ^{13}C NMR signal from the methoxy carbon. Fortunately, in asphalt, no other peaks occur in that region of the NMR spectrum which ranges from about 50 to 60 ppm.

When using ^{13}C NMR spectroscopy for the analysis of phenols in asphalt, one observes two types: hindered and non-hindered phenols. Hindered phenols have substituents on either one or both ortho positions relative to the hydroxy group. See Figure 11 for their general structures. Figure 12 shows the NMR peaks in the methoxy region of the ^{13}C NMR spectrum of both hindered and non-hindered phenols as well as of methylated carboxylic acids. In preparation for NMR analysis, phenols in asphalt have been first methylated by the Short Term Phase Transfer (STPT) methylation using tetra-n-butylammonium hydroxide and 99% ^{13}C enriched methyl iodide where asphalt phenols are deprotonated and subsequently methylated (Figure 13).(3,33) However, the chemistry is long and arduous. In addition, this method is non-phenol specific. Carboxylic acids (-COOH) as well as imino (=NH), and thiol (-SH) groups are methylated as well.

Carboxylic acids in asphalt have been identified and quantified using another selective process. After deprotonation, methylation of the carboxylate anion is accomplished by using ^{13}C enriched diazomethane to form esters.(3) To produce integratable ^{13}C NMR spectra, an inverse gated experiment was employed. In this pulse sequence, protons are decoupled from carbons only during ^{13}C signal acquisition as to not allow Nuclear Overhauser Enhancements

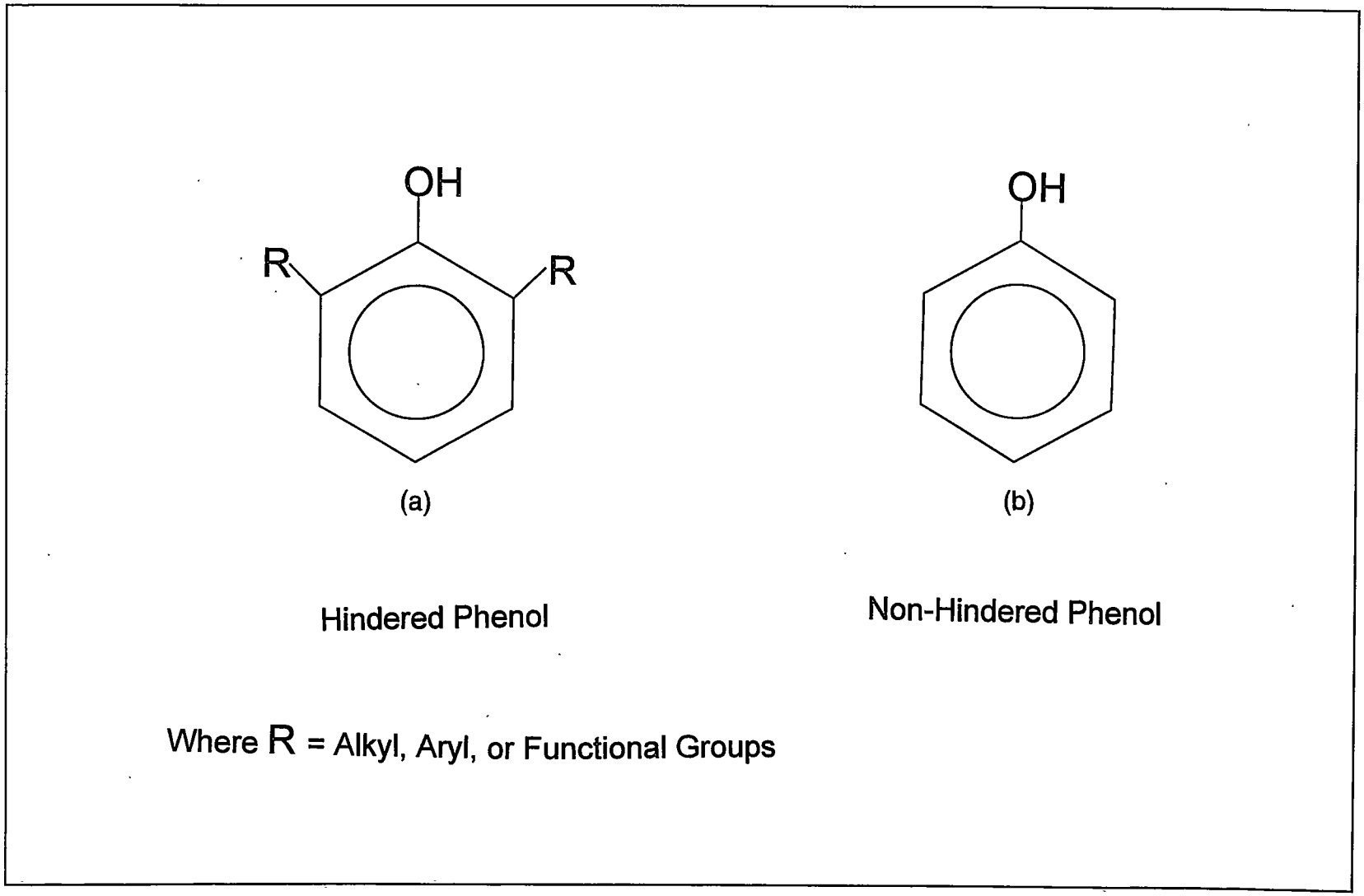

Figure 11. General structure of (a) a hindered and (b) a non-hindered phenol.

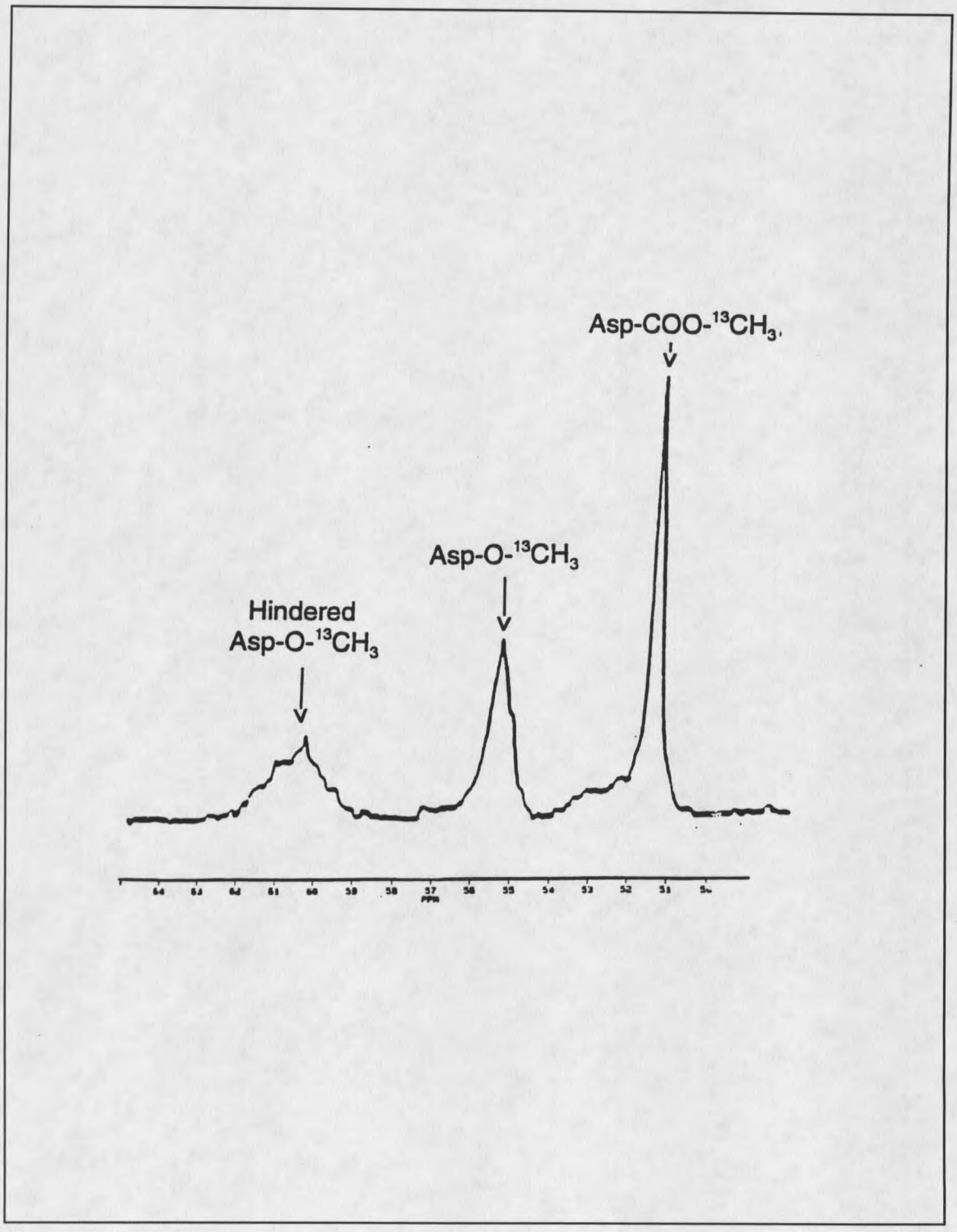

Figure 12. Methoxy region of the ^{13}C-NMR spectrum showing the chemical shifts for methylated hindered and non-hindered phenols as well as for methylated carboxylic acids.(3)

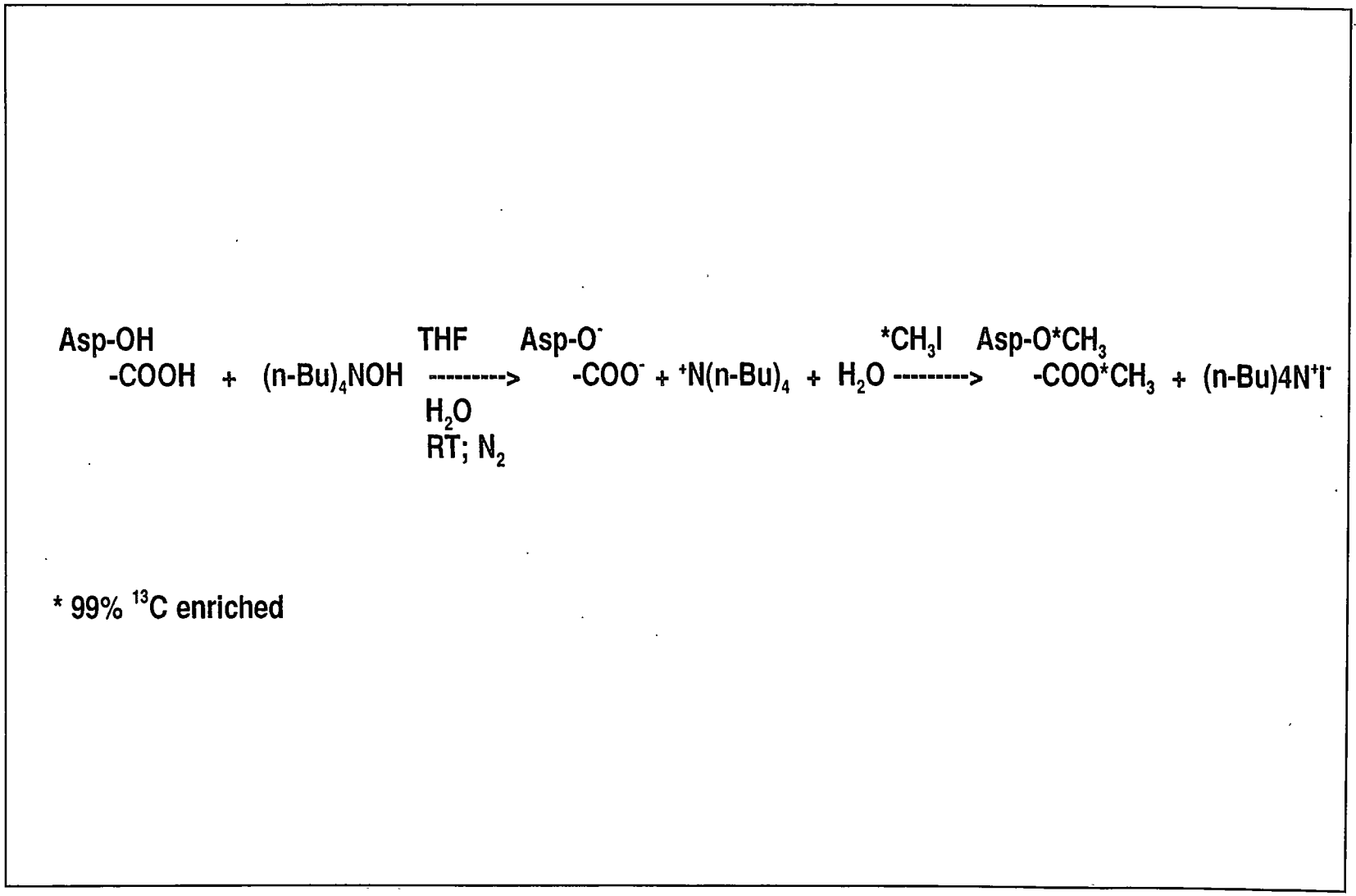

Figure 13. Short-Term Phase Transfer Methylation reaction.(3)

(NOEs) to occur, which affect signal intensities. Figure 12 shows the methoxy ^{13}C peak in the NMR spectrum of methylated carboxylic acids using the inverse gated experiment.

One of the problems dealt with in this work was to find a methodology that would simplify the methylation of phenols in asphalt. It was found in the literature that rapid, stereoselective methylation of alcohols and phenols could be accomplished with sodium hydride and methyl iodide.(37,38) The reaction scheme is shown in Figure 14. The results on asphalts will be discussed in some detail in the Results and Discussion section.

Benzylic Carbons in Asphalt

The moiety present in asphalt most susceptible to oxidative aging is thought to be the benzylic carbon.(2) This is the carbon directly adjacent to the aromatic ring and is thought to undergo a free-radical oxidation. Figure 15 depicts the suggested mechanism.(2) The agent responsible for initiating this mechanism is still unknown, but the possibilities include U.V. light; oxygen; metal catalysts i.e. vanadium; and mineral aggregate surfaces.

Not all benzylic carbons react at the same rate. Methyl benzylic carbons are the least reactive and methine benzylic carbons are the most reactive towards autoxidation.(Figure 16) There are two reasons for this. First, C-H bond strengths as shown in Figure 17 affect reaction rates. A tertiary C-H bond

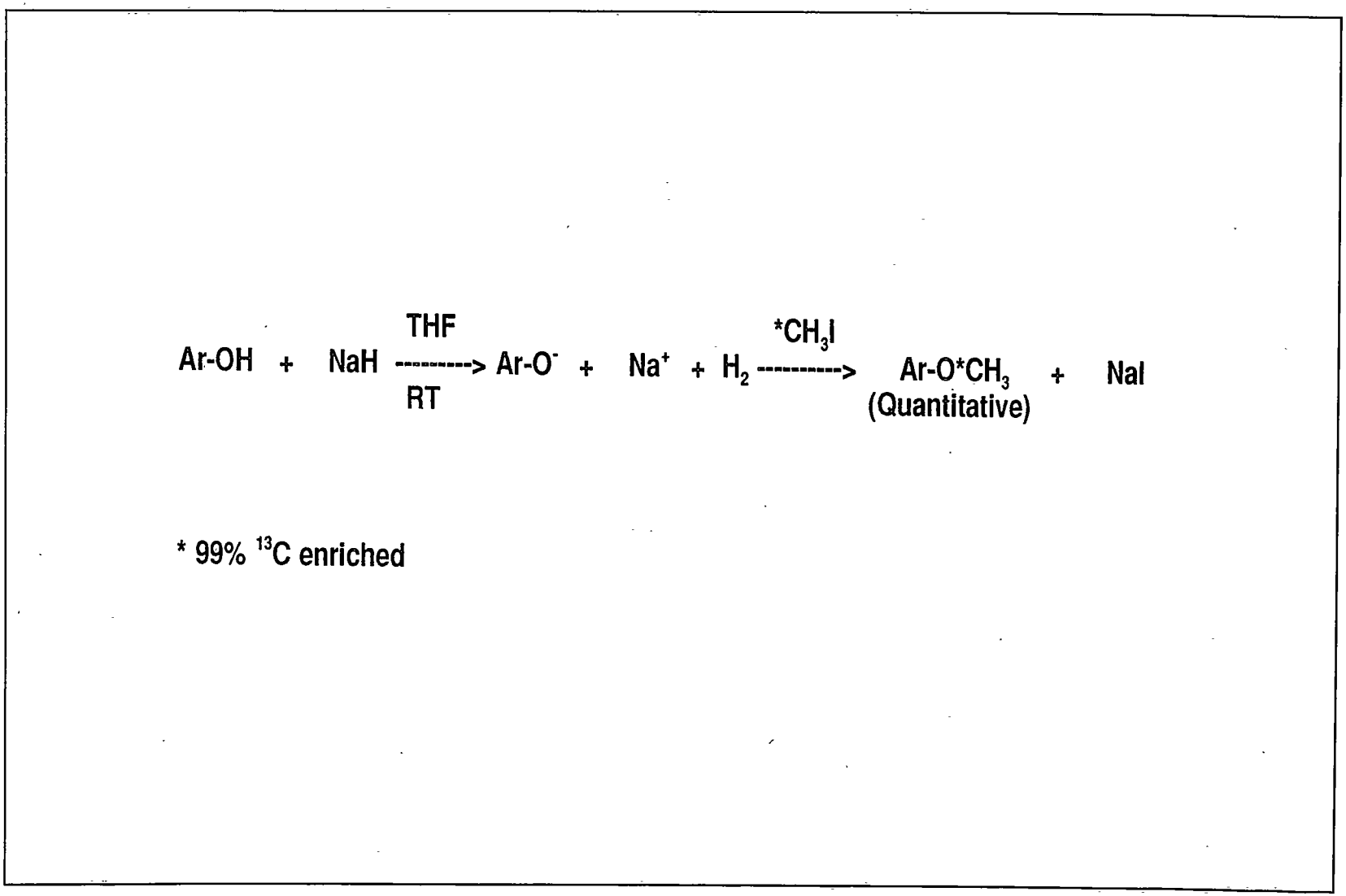

Figure 14. Sodium hydride/methyl iodide methylation reaction.(37)

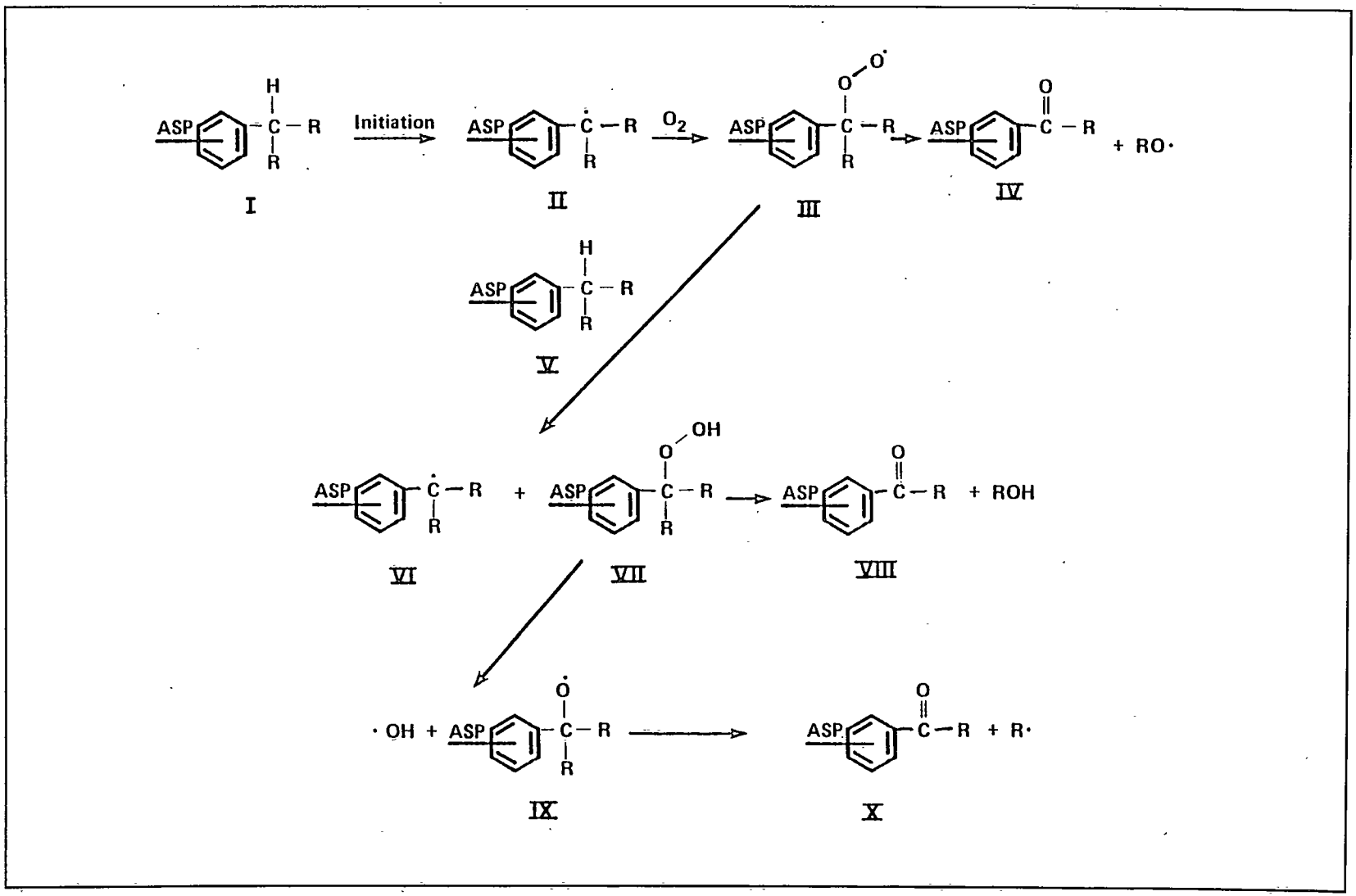

Figure 15. A suggested mechanism for the free-radical air oxidation of asphalt.(2)

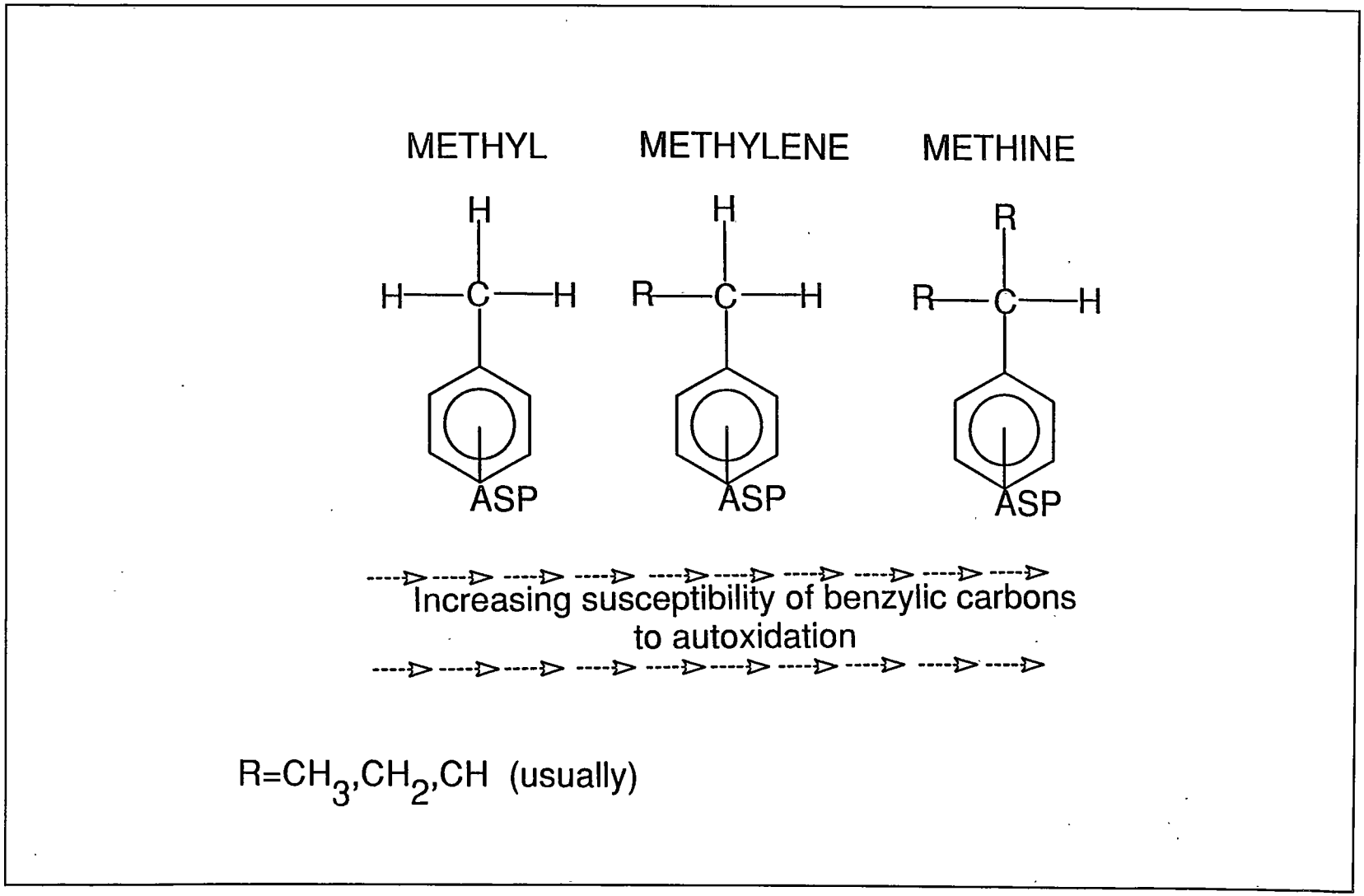

Figure 16. Order of increasing benzylic carbon susceptibility to autoxidation.

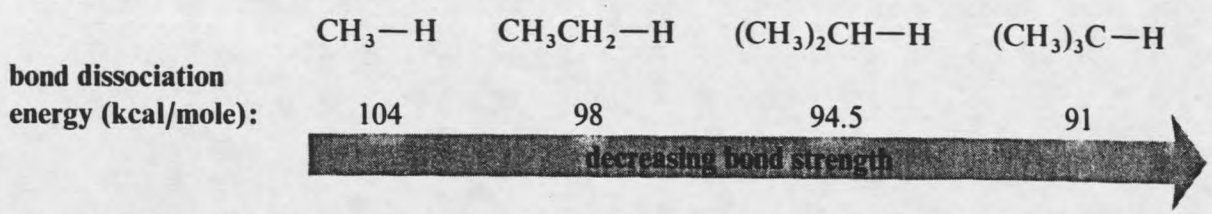

Figure 17. Order of decreasing C-H bond strength.(22)

is weaker than a secondary C-H bond which, in turn, in weaker than a primary C-H bond. The second possible reason supporting the order of reactivity is the relative stability of the intermediate radical through hyperconjugation where benzylic carbon p-orbital radicals are stabilized by delocalization with beta proton nuclei.(Figure 18)

An understanding of the process of the oxidation of benzylic carbons in asphalt is an important goal for asphalt chemists. In particular, it would be important to be able to observe chemical changes at the benzylic carbons upon actual road weathering. The problem is that it is very difficult to obtain an NMR signal from the benzylic carbons in asphalt because of the complicated nature of the mixture. Some preliminary attempts were made by Jennings *et al.* (33). These authors employed a 2-dimensional NMR INVERSE COLOC experiment, which allows one to observe long range couplings, i.e. through two or more bonds. They optimized the experimental parameters to enhance the ^{2}J coupling between an alkyl substituted aromatic carbon and the benzylic protons (or proton) two bonds away. This was a novel approach towards spectroscopically "viewing" the benzylic position. This experiment enabled them to indirectly observe the benzylic carbons by cross peaks in the 2D spectrum caused by the ^{2}J couplings. In this work, the COLOC experiment has been used to obtain more detailed information on the actual chemical changes that occur at the benzylic carbons upon asphalt aging.

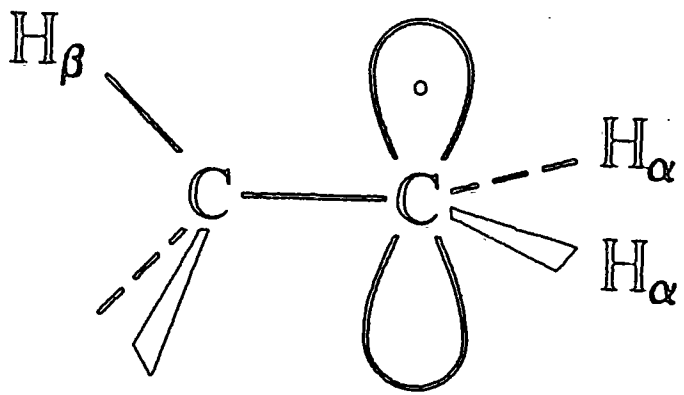

Figure 18. Hyperconjugation: the delocalization of the radical *p*-orbital with the β proton.(65)

Infrared Spectroscopy Used for Studying Asphalt Functional Groups

Infrared spectroscopy is a very useful tool and has been used for many years by asphalt chemists to study asphalt functional groups especially in the study of asphalt age-hardening.(9,11-13,15,16,39) As has already been discussed, age hardening has a deleterious affect on asphalt performance. Since oxidative aging is considered to be the most important cause of age hardening, it is crucial to characterize and understand the oxidative process.

Many asphalts from a variety of petroleum refineries have been used in IR studies. Asphalts that have been studied included the Thin Film Oven Test (TFOT) and/or the Pressure Oxygen Vessel (POV) aged asphalts, as well as those taken from core samples of actual road weathered asphalts. Figures 19 & 20 represent the mid-infrared spectra of an unaged asphalt and of samples of the same asphalt which has undergone several methods including the Thin Film Oxidation Test (TFOT) mentioned earlier. Except for changes in the two absorbance bands at 1700 cm^{-1} and 1050 cm^{-1}, there are virtually no changes in the spectra upon asphalt oxidative aging. The absorbance for the carbonyl stretch at 1700 cm^{-1} and the sulfoxide stretch at 1050 cm^{-1} seem to always increase in asphalt upon aging. Peterson *et al.* (12,15,16) identified sulfoxides and several types of carbonyl groups in the IR spectra of asphalt including dicarboxylic anhydrides, carboxylic acids, and ketones.(Figure 4)

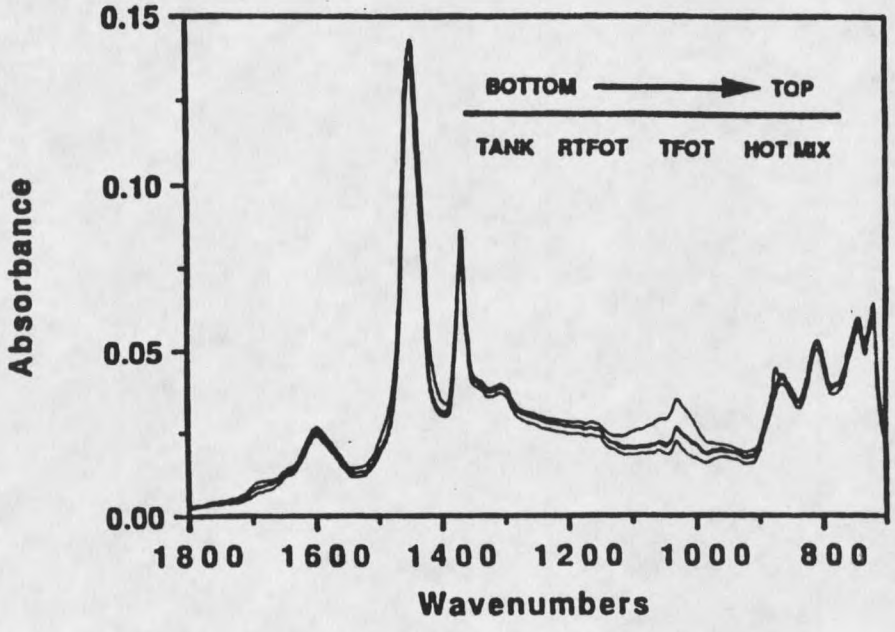

Figure 19. FT-IR carbonyl and sulfoxide aging spectra.(39)

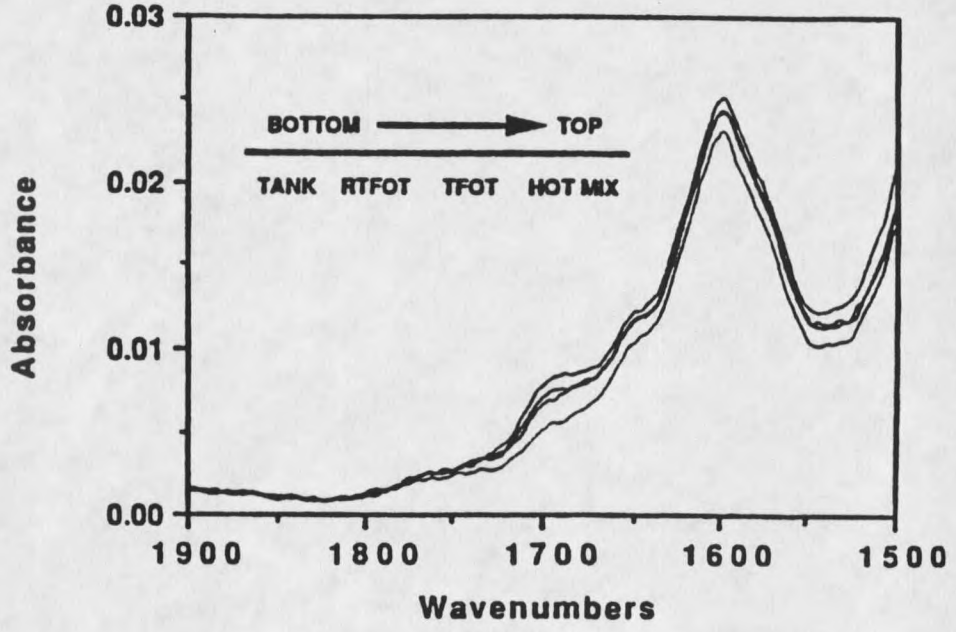

Figure 20. Close-up of the carbonyl (C=O) stretch at 1700 cm^{-1} for aging study.(39)

The IR O-H stretch band at 3500 cm^{-1} is extremely weak and broad for two reasons: first, phenols are present in low concentrations and aliphatic alcohols are practically non-existent in asphalt; second, the IR absorbance band is greatly broadened due to hydrogen bonding.(9)

Molecular Mass Distributions in Asphalt

It is known that asphalt is a complicated mixture of an enormous number of constituents with various chemical structures and molecular weights. However, asphalt has been fractionated into different mass ranges by many asphalt researchers over the years. Haley (40) used GPC in combination with Vapor Pressure Osmometry (VPO) and NMR to determine molecular weights of asphaltenes. He reported molecular weights of fractionated asphaltenes ranging from 780 to 1,350 Da. He also found that asphaltenes tend to associate in various solvents by strong intermolecular forces. The molecular weights obtained by VPO were thus larger ranging from 910 to 4,200 Da. However, these larger species could be broken apart by powerful solvents such as a mixture of dioxane and chloroform.

Farcasiu *et al.* (41) performed transalkylation reactions on bituminous resins. The alkyl substituents in the high molecular weight aromatic constituents of asphalts can be transferred to a small molecule such as benzene using a Friedel Crafts catalyst. Figure 21 illustrates the general

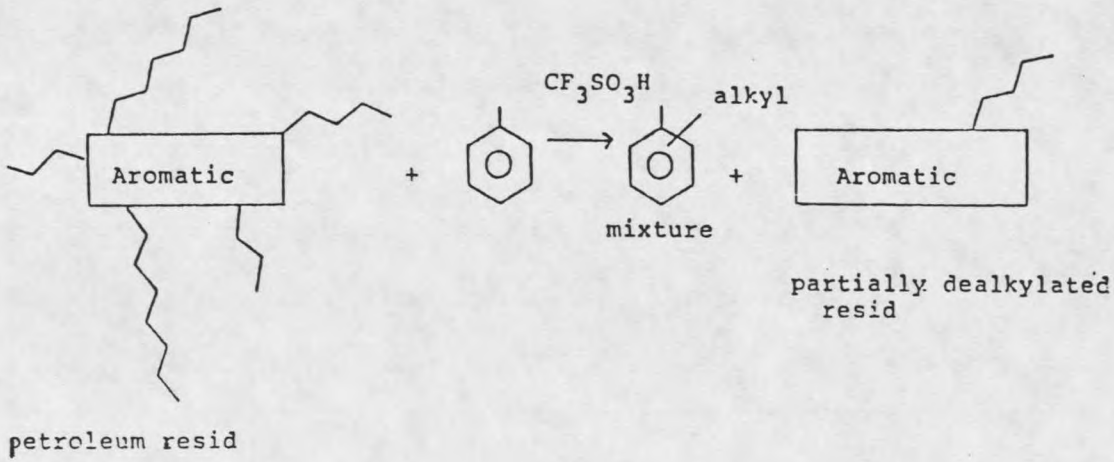

Figure 21. Transalkylation reaction.(41)

reaction scheme. Qualitative and quantitative product analysis was by Gas Chromatography-Mass Spectrometry (GC-MS). This investigation revealed structural and mass information of asphalt alkyl polyaromatic substituents such as alkyl chain length, ratio of normal/iso alkyl chains bonded to aromatic rings, and abundance of aromatic-CH_2-aromatic linkages. It was found that over 70% of the transalkylation products from petroleum residuals were monoalkylated o-xylenes consisting of normal and iso-alkyl groups ranging from 2 to 16 carbons. They also found that these alkyl chains are transferred without isomerization. 12 to 25 % of the product consisted of o-xylene-CH_2-o-xylene linkages.

Mass Spectrometry in Asphalt Research

GC Mass spectrometry has been used in the analysis of asphalt.(42,43) Field Ionization Mass Spectrometry (FI-MS) (44) has also been used to determine metal porphyrin structures in asphalt. And, with the advent of more sophisticated analytical instruments within the past 10 years, it seems promising that additional structural and mass information will be made available on asphalt through mass spectrometry.

Classical mass spectrometric methods such as Electron Impact MS (EI-MS), is of limited use when applied to compounds of high mass. The high energy used in EI breaks large molecules into fragments such that limited structural information is obtained. Also, EI requires that a sample has a

sufficient vapor pressure and thermal stability to be vaporized in the ion source. This severely limits the application of EI to high mass compounds such as petroleum residues (asphalt).

A revolutionary advancement in the mass spectrometric analysis of high mass molecular species came in the early 1980's with the development of Fast Atom Bombardment (FAB) (45) MS and Plasma Desorption MS (PDMS) (46). In 1988, two additional soft ionization techniques were introduced that were ideal for large molecules. They were Electrospray (ES) (47,48) and Matrix Assisted Laser Desorption Ionization (MALDI) (49).

Laser Desorption ionization is not a new technique; it has been used to generate ions in mass spectrometry since the 1960's.(49) A necessary condition for molecular ionization via laser irradiation is that the analyte absorbs at the laser wavelength. Lasers that emit in the UV or in the far IR are most commonly used. Another important consideration is that due to the possibility of thermal decomposition of the analyte caused by heat generated by the laser, the laser pulse must be short, between 1-100 ns.(49) With direct laser desorption only masses of up to about 1000 Da are desorbed as intact molecular ions.

Direct laser desorption mass spectrometry (LD-MS) has been used for coal analysis.(50-52) Sodium adduct ions and molecular ions have been shown to be the sole product ions in the laser desorption process of polyaromatic hydrocarbons (PAHs).(52) However in coals, sodium adduct ion formation

appears to be greatly diminished. The tendency to form sodium adduct ions in PAHs apparently decreases with increasing polyaromaticity.(52) More extensive work involving coal has revealed that carbon clusters are formed during laser desorption. Figure 22 shows the positive ion spectrum of high-mass carbon clusters in a semi-anthracite coal sample.

In brief, MALDI introduced the use of a matrix molecule to absorb the laser light thus making it a much softer ionization process. It was discovered by Karas, *et al.* (53) that by dispersing a sample in a highly absorbing solid matrix by co-crystallization upon solvent evaporation, it was possible to ionize and desorb very large molecules. The reason for this seems to be that the matrix acts to absorb excess laser energy and to distribute it evenly throughout the sample. The fact that the matrix dilutes the sample, which results in exposure of more of its surface area, increases the probability of producing intact molecular ions. However, it is not yet completely known why a matrix improves laser desorption.

While much work is currently being published that uses the MALDI technique there are no publications involving applications to asphalt. However, MALDI has been used to analyze coal and coal derived products. For example, John *et al.* (54) claim to have measured masses of up to 270,000 Da in coals using MALDI Time-of-Flight Mass Spectrometry (TOF-MS).

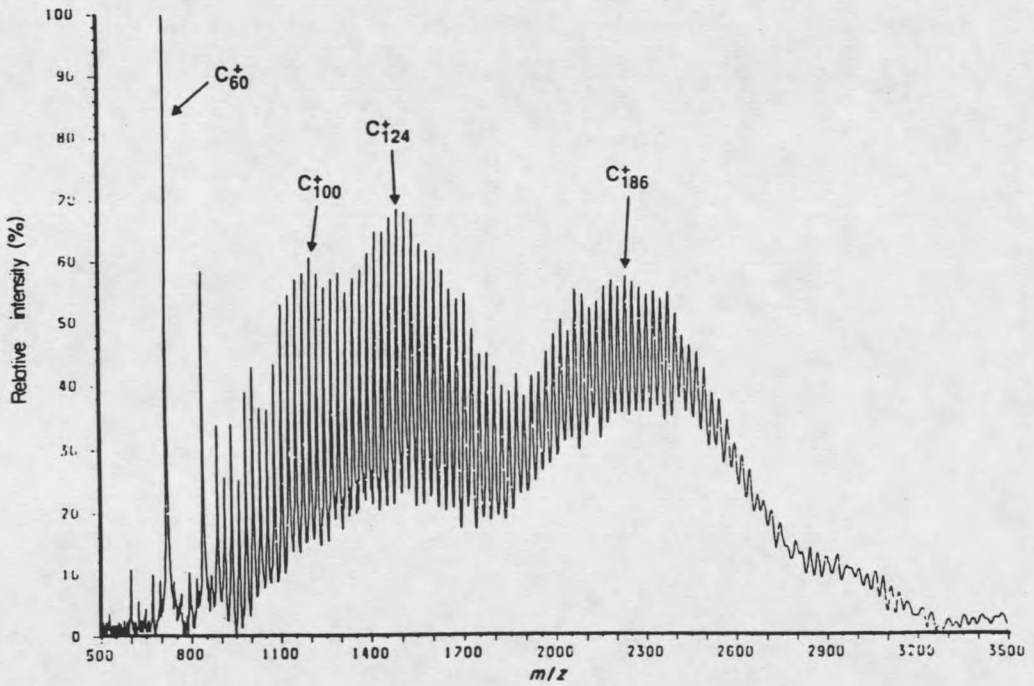

Figure 22. Positive ion mass spectrum of carbon clusters of a semi-anthracite coal.(52)

Gel Permeation Chromatography Fractionation and Laser Desorption Mass Spectrometry of Asphalt

The separation of asphalt into fractions with different molecular weights could be useful if used in combination with some of the newest mass spectrometric "soft" ionization techniques. As mentioned earlier GPC fractionation has been used on asphalts and asphaltenes for asphalt chemical analysis. GPC fractions have been used to determine percentage of, for example, aromatic, naphthenic, and paraffinic carbon; the number of ring systems per molecule; the average molecular size; and composition.(55) Approximate molecular weight distributions have also been determined by fractionation.(56,57)

GPC fractionation of asphalt has been coupled to several other methods for identification of structural features. These include pre-GPC centrifuging, Vapor Phase Osmometry (VPO), IR, and NMR. However, GPC doesn't seem to have been combined previously to laser desorption MS. In this work, GPC and LD has been combined and used to characterize asphalt fractions.

EXPERIMENTAL METHODS

List of Chemicals

Aldrich Chemicals:

- anisaldehyde
- carbazole, 96%
- chromium (III) acetylacetonate, 97%
- coronene, 99%
- cumene, 99%
- dihydroxybenzoic acid, 99%
- 3,5-dimethoxy-4-hydroxy-cinnamic acid (sinapinic acid), 98%
- 9,10-dimethylanthracene, 99%
- 2,6-dimethyl phenol, 99%
- dodecanone, 99.5%
- ethylbenzene, 99%
- 2-naphthol
- methyl iodide, 99%
- 3-picoline
- pyrene, 99%
- rubrene, 98%
- sodium hydride, 95% dispersion in mineral oil

Fisher Scientific:

- diethyl ether (distillied)
- hydrogen peroxide, 30%
- hydrogen chloride
- magnesium sulfate (anhydrous)
- potassium bromide (anhydrous)
- sodium bicarbonate
- tetrahydrofuran (Optima)
- toluene

J.T. Baker Chemical Co:

- benzoic acid
- phenol

Lancaster:

- 1-(2-naphthyl)ethanol
- 1,2,4,5-tetramethyl benzene, 98%

Chem Service:

- octanoic acid, 99.5%
- tetrahydronaphthalene

Cambridge Isotope Laboratories:

chloroform d, 99.8%
methyl-^{13}C iodide, ^{13}C 99%, stabilized with copper wire
tetrahydrofuran d_8, "100%", (D,99.95%)

Waters Associates:

polystyrene standards for GPC. M.W.=35,000;15,000;3,600; and 2,350

Sigma:

cytochrome c, 99%, from horseheart

Quantitative NaH/$^{13}CH_3I$ Methylation of Phenols in Asphalts via The Inverse Gated ^{13}C NMR Experiment

Instrumentation and Experimental Parameters

The experiments were performed on both a Bruker AC300 (for model compounds) and a Bruker AM500 (for asphalt samples) NMR spectrometer. The resolution and S/N was far superior when using the AM500 for acquiring asphalt ^{13}C spectra than when using the AC300 model. The AC300 was fitted with a 5 mm $^1H/^{13}C$ dual probe operating at 75.47 MHZ and the AM500 was fitted with a 5 mm broadband probe operating at 125 MHZ. The Inverse Gated NMR experiment was used with proton broadband decoupling without NOE enhancement. Instrument parameters were as follows:

PW ^{13}C 90°	AC300 = 7.6-8 μs AM500 = 4-5 μs
01 transmitter offset frequency	AC300 = 6137.164 Hz AM500 = 11036.52 Hz

02 decoupler offset frequency	AC300 = 4900 Hz AM500 = 8200 Hz
SI spectrum size	32,000 points
SW sweepwidth	AC300 = 17,856.147 Hz AM500 = 33,333.33 Hz
RD receiver delay	2 s
NS number of scans	8,000-15,000

Sample Preparation

Model Compound Chemical Preparation. Approximately 0.003 moles of each of the following model compounds were used: phenol, benzoic acid, 2,6-dimethyl phenol (2,6 DMP), octanoic acid, and 2-naphthol. The model compounds were then together placed in a 100 mL round bottom flask with 25 mL of THF. An excess of about 0.01 moles of NaH was then added to the flask. The solution was then allowed to stir under nitrogen for about 3 hr. An excess of CH_3I (about 0.02 moles) was then added to the flask with an additional 25 mL of THF. The reaction was then allowed to proceed for approximately 10 hr under a continual flow of nitrogen, and constant stirring, at ambient temperature. At this point, the THF was partially evaporated over warm water. The residual NaH and any product NaI salts were filtered. A saturated $NaHCO_3$ solution was then added (this would dissolve any remaining NaI as well as react with any remaining NaH).

The methylated products were then separated with diethyl ether and washed once with additional water. While using carboxylic acid models the

water layer was saved. The organic layer was dried over $MgSO_4$ and filtered. The ether was then evaporated under vacuum at room temperature. All of the product was then pipetted into an NMR tube with 1 mL of $CDCl_3$ for NMR analysis.

To the aqueous layer, concentrated HCl was added dropwise until the pH was sufficiently acidic. This converted any carboxylate salt to carboxylic acid. The acid was then extracted twice with diethyl ether, dried over $MgSO_4$, filtered, and dried in a vacuum at room temperature. A portion of the product was placed in an NMR tube, dissolved in 1mL of $CDCl_3$ to obtain both ^1H and ^{13}C NMR spectra.

Asphalt and Model Compound Preparation using Simplified Chemistry. Approximately 90 mg of each asphalt sample was weighed in a tared NMR tube. Fifteen mg of Cr(III) acetylacetonate ($Cr(acac)_3$) was also added as a relaxation agent. Next, a 0.5 mL ampule containing 99.95% d_8 THF was unsealed and the contents were pipetted into the NMR tube containing the asphalt and $Cr(acac)_3$. The tube was capped and agitated until the solids were completely dissolved. Twenty five µL of 45% $^{13}CH_3I$ in CCl_4 was then injected into the NMR tube.

Twenty five µL of toluene was always added to use as an internal NMR integration standard. Approximately 30 µg of NaH was finally added to the NMR tube. The reaction was then allowed to proceed for about 2 hr at room

temperature with the tube lid off due to the evolution of hydrogen. The tube was then capped and placed in the NMR probe to acquire a ^{13}C spectrum.

The same method as described above was employed for methylating the model compounds (2,6 DMP and 2-naphthol) in the NMR tube however, normal CH_3I was always used and $Cr(acac)_3$ was never used.

Two-Dimensional NMR Experiment for Assignment of Benzylic Protons in Asphalt

Instrumentation and Experimental Parameters

All two-dimensional inverse COLOC spectra were obtained using a Bruker AC300 NMR spectrometer fitted with a 5 mm inverse probe. The experimental parameters were as follows:

The pulse widths (P1, P2, and P3) were always measured prior to an experiment for all samples. The values listed are very close however. Several inverse COLOC experiments were run to adjust for the D4 delay for optimization.

P1 ^{1}H 90°	4.5 µs
P2 ^{1}H 180°	9 µs
P3 ^{13}C 90°	7.75 µs
01 decoupler offset frequency	4642.48 Hz
02 transmitter offset frequency	4123.03 Hz
SW1 ^{13}C spectral width	6038.647 Hz 0-160 ppm
SW2 ^{1}H spectral width	1501.502 Hz 0-5 ppm
Delays:	
D0	3 µs

D1=1-5xT_H	2 s
D2=1/2$^1J_{CH}$	
where $^1J_{CH}$=144.9 Hz	3.45 ms
D4=1/2$^2J_{CH}$	
where $^2J_{CH}$=10 Hz	50 ms
SF synthesizer frequency	300.13 MHZ
SFO synthesizer frequency offset	75.47 MHZ
SI1 carbon spectrum size	128 points
SI2 proton spectrum size	1024 points
NS number of scans/experiment	432
NE number of experiments	60

The duration of each experiment was approximately 17 hr.

Sample Preparation

Oxidation of SHRP Asphalt AAA-1 Using H_2O_2. A 0.53 g sample of AAA-1 was weighed out, placed in a 100 mL round bottomed flask, and dissolved in 50 mL of THF. Then 5 mL of hydrogen peroxide (H_2O_2) was pipetted into the flask. This mixture was left to stir at room temperature for approximately 17 hr. Excess H_2O_2 was then extracted three times, first with a saturated aqueous $NaHCO_3$ solution, and the last two times with deionized water. The THF/asphalt solution was then dried over $MgSO_4$, filtered, and the THF was vacuum evaporated.

Preparation of Asphalt Samples for COLOC Experiment. Sample size for ^2J coupling experiment was 96 mg asphalt dissolved in 0.3 mL deuterated chloroform ($CDCl_3$). Samples were placed in thin-walled 5 mm O.D. NMR

tubes. 9,10-dimethylanthracene (9,10 DMA) was used as a benzylic proton reference standard at 3.1 ppm in the ^1H spectrum. The concentration of the 9,10 DMA was 8.9 mg/0.4 mL $CDCl_3$ (4.17 moles/0.4 mL) dissolved within a coaxial NMR tube and inserted into the NMR tube containing the asphalt. The tubes were capped and sealed with Parafilm.

Fourier-Transform Infrared Analysis of Carbonyls in Asphalt using KBr/Asphalt Pellet Procedure

Instrumentation and Experimental Parameters

All infrared absorbance spectra were taken on a Bruker IFS25 fourier-transform IR spectrometer fitted with a Globar (silicon carbide rod) 100-5000 cm^{-1} IR laser, a Deuterated Triglycine Sulfate (DTGS) detector, and a KBr beam splitter (useful range: 400-4800 cm^{-1}). The resolution was at 2 wavenumbers. The scanning frequency was set from 400-2000 cm^{-1}. The samples were scanned 16 times per experiment. The carbonyl Integration range was from 1675-1753 cm^{-1}. Carbonyl concentrations were all reported in moles carbonyl/g asphalt (moles C=O/g).

Sample Preparation

The sample preparation was very similar to that used by Glover, *et al.*(11) The one exception was that it was not necessary to freeze the asphalt prior to mixing with the KBr powder. Pre-freezing did little to help keep the asphalt sufficiently brittle and hard for very long after the onset of mixing. A standard curve for quantifying the C=O absorbance band was derived by preparing a series of standards with increasing concentrations of cyclododecanone in KBr.

Fractionation of Selected Asphalts Using High Pressure Gel Permeation Liquid Chromatography

Instrumentation and Experimental Parameters

The hardware used for the GPC experiments included the following components:

Rheodyne model 7125 syringe loading sample injector fitted with a 100 µL sample injector loop.
Waters Associates chromatography pump model 6000A. Operating range: 0-6000 psi.
Jordi GPC column filled with 1000 Å polystyrene beads.
Hewlitt Packard model 1040A UV-VIS diode array detector with a deuterium lamp source. Detection at eight selected wavelengths: 440, 410, 380, 340, 280, 254, 230, and 210 nm.
Phase Sep direct reading digital display flowmeter with reading range between 0.1-10 mL/min.

Hewlitt Packard
Hard drive model 9153C040
Computer model 9000 series 300
Video color monitor model 98561A
Keyboard
Think Jet printer model 2225A
HB-IB interface card model HP98624A
HPLC Chem Station software.

For each experiment, the flowrate was always set at 0.900 mL/min. This flowrate had been previously optimized by Jennings, *et al.*(25) A typical column pressure was 2000 psi. The absorbance was recorded at 3520 ms sampling intervals for 42 minutes.

Sample Preparation

Gel Permeation Chromatography (GPC) is based on the differential permeation of the various molecular species into matrices of defined pore size. As the sample traverses the column, the small compounds permeate the matrix pores to a greater degree than the larger components, and are retained longer. Elution order, for similar compound types, is a function of molecular weight, the largest materials eluting first, and the smallest last. For example, linear synthetic molecules would have different elution times than globular proteins of similar weight. For this reason, it was necessary to prepare a mass calibration curve using standard compounds of known molecular weight. Four polystyrene samples of molecular weights: 35,000; 15,000; 3,600; and 2350 were chosen for the high mass range calibration. They were diluted to

10% (w/v) in THF. In addition, seven organic compounds similar to those found in asphalt were used for the low mass range calibration. They included: 1,2,4,5-tetramethyl benzene (mw. 134), carbazole (mw. 167), benzo[a]pyrene (mw. 252), 1-(2-naphthyl)ethanol (mw. 172), coronene (mw. 300), 1-methyl-3,4-diphenanthrene (mw. 342), and rubrene (mw. 532.69). The dilutions made of these samples ranged from 0.12 - 5% (w/v). The dilute solutions made were of the polyaromatic compounds because they were better chromophores at 254 nm.

All asphalt samples were dissolved in THF and diluted to 0.5% (w/v). One hundred µL of this dilution was loaded into the sample loop and then injected into the GPC flow. Fractions were collected in 20 mL glass vials. Five fractions were collected per run during 5-8 minute intervals which translates to approximately 4.5 to 7.2 mL per fraction. This procedure was repeated three times per asphalt. Like fractions were then combined and the THF was then allowed to air evaporate. The vials were then capped.

Laser Desorption Mass Spectrometry of Asphalt

Instrumentation and Experimental Parameters

The Laser Desorption MS experiments were run on a reflecting Perseptive Biosystems/Vestec benchtop instrument. The time-of-flight mass

spectrometer has a 1.3 m vertical flight tube. The experiments were performed in linear mode only. The accelerating voltage was set at 20 kV. The ion source pressure ranged from approximately $1x10^{-6}$ to $1x10^{-7}$ torr. All spectra were obtained in positive ion mode only. The Savitsky-Golay order statistical analysis was applied to smooth out noise in the resulting spectra. A 337 nm nitrogen laser was used for desorption. The vacuum system was equipped with two turbomolecular pumps. The analyzer/detector was a secondary electron multiplier. All spectra were downloaded into Gramms/386 version 3.0 software for calibration and plotting.

Mass calibration was internal when using standards. However, a two point external calibration was made for asphalt samples. The +2 charge state of cytochrome c (horseheart, MW=12,360) was used for the high mass calibration point at 6,180 Da. Sodium was always used for the low mass calibration point.

Sample Preparation

The calibration mixture was prepared by first dissolving 1 mg of cytochrome c in 1mL of a 70:30 ratio of H_2O:acetonitrile mix. One µL of this mixture was then placed on the laser desorption sample plate along with 1µL of a saturated aqueous solution of sinapinic acid matrix.

When still using the MALDI technique for asphalt, 1 µL of a saturated

solution of 10 mg of dihydroxybenzoic acid dissolved in 1 mL of a 90% ethanol:10% H_2O mix was used as the matrix. This was then mixed with 1 µL of asphalt in THF on the laser desorption sample plate. When no longer using a matrix for laser desorption, either pure asphalt was directly deposited onto the sample plate or 1µL of a solution of asphalt in THF was pipetted onto the plate. The THF was always allowed to evaporate before inserting the plate into the instrument. Laser desorption of standards i.e. pyrene, carbazole, and coronene was also accomplished without the use of a matrix. The mixtures consisted of the concentrations listed in Table 2.

Table 2. Concentrations of model compounds and asphalt used for determining LD ion processes.

Sample Mixture	Concentration in THF
coronene	2 mg/mL
carbazole 1) and 2)	1) 2 mg/mL and 2) 1.7mg/mL
pyrene	2 mg/mL
NaCl	2.6 mg/mL
SHRP AAD-1 asphalt	6 mg/mL
pyrene:carbazole 2:asphalt	1:1:1 of the above dilutions
coronene:carbazole:asphalt	1:1:1 of the above dilutions
coronene:NaCl	1:1 of the above dilutions
coronene:NaCl:asphalt	1:1:1 of the above dilutions

RESULTS AND DISCUSSION

NaH/CH_3I Methylation and NMR Quantitation of Phenols in Asphalt

General Discussion

As discussed in the Introduction, phenols probably contribute to asphalt self-assembly through hydrogen bonding. In addition, phenols may facilitate aromatic electrophilic substitution under the appropriate conditions. One of several possible sites for phenol assisted electrophilic substitution to occur would be at the asphalt/aggregate interface. Aggregate material may contain many different types of ionic species that could be involved in the aromatic substitution of asphalt molecules.(10) Such changes would not neccessarily result in "poor" pavement performance, but there is the possibility, as with asphalt chemical autoxidation, that any chemical change in asphalt is detrimental. Irreversible chemical changes may well alter the preexisting balanced molecular composition that makes asphalt such a superior paving material.

Because the phenolic group is likely to contribute both to chemical changes in asphalt, and to be involved in asphalt self-assembly, a method that could reliably quantify phenol in asphalt would be important. As explained in

the Introduction, NMR is a promising method for quantifying phenols in asphalt, however, they must first be methylated. The Phase Transfer Methylation (PTM) method (3,33,58) that has been previously used for phenol quantification in asphalt by NMR involved several problems. First, the PTM method not only converted phenols to methyl ethers but it methylated carboxylic acids, imines and thiols in asphalt as well.(3) Second, the PTM chemical procedure was time consuming (3) and not practical for processing many asphalt samples. Figure 23 shows several NMR spectra of PTM methylated asphalts. The phenol peaks at 60 and 55 ppm are very broad and, in fact, difficult to integrate. The shoulder on the left side of the ^{13}C methylated carboxylic acid peak could not be assigned and contributed to the difficulty of integrating the peak. The need for finding a specific and reliable method for phenol quantification was great. Here we will demonstrate the application of a novel method for specific and simple phenol methylation that uses sodium hydride and methyl iodide (NaH and CH_3I). The NaH/CH_3I methylation of phenols (37,38) proved to be a significant improvement over the PTM method.

NaH/CH_3I Methylation of Model Compounds

Phenol Specificity The NaH/CH_3I method, as described in the Experimental section, was first tested on model compounds. The objective was to optimize experimental paramenters as well as to determine any limitations of

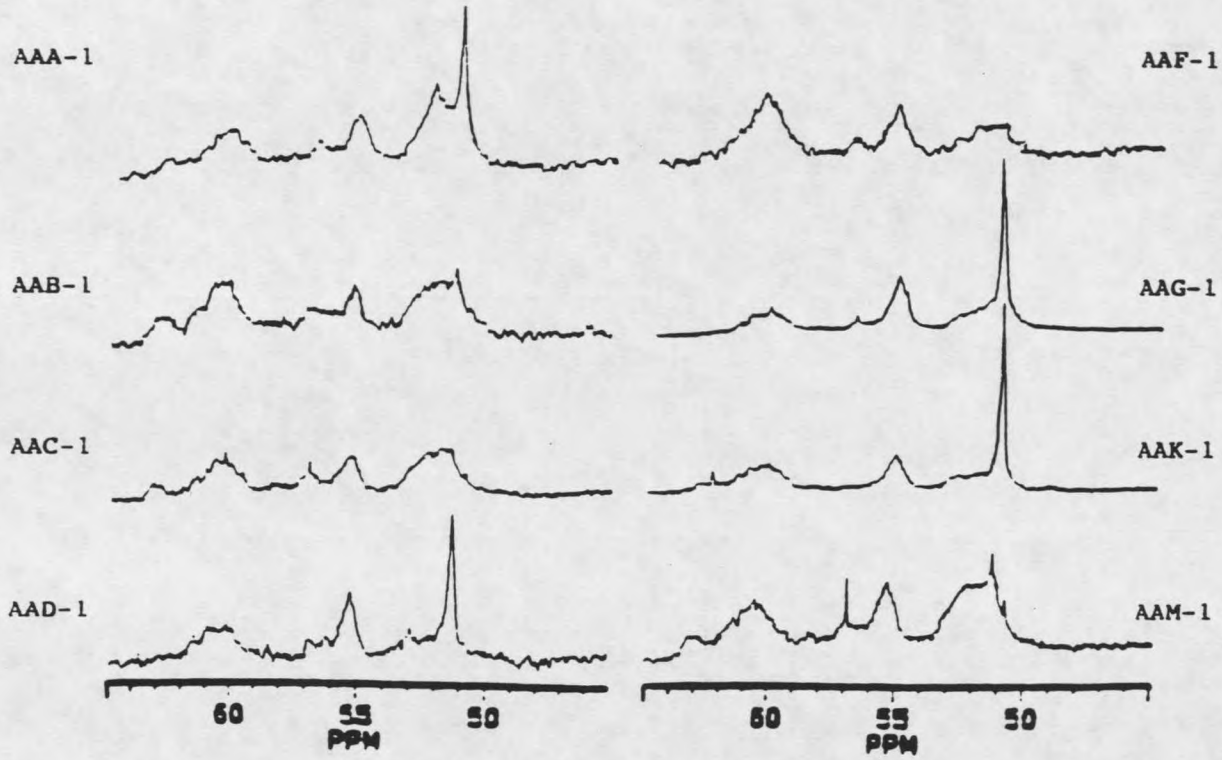

Figure 23. Old spectra of the Phase Transfer Methylation previously used to quantify phenols in asphalt.(3)

this method.

The model compounds initially chosen to test the NaH/CH_3I method were phenol and benzoic acid. Benzoic acid was included to confirm the literature reports that the method is specific for phenols.(37,38) The results of this experiment can be seen in Figure 24 which shows both the ^1H (24a) and the ^{13}C (24b) NMR spectrum. The methylated phenol peaks at about 1.5 ppm in Figure 24a and 55 ppm in Figure 24b are each labeled by number 1. There is no evidence of any peak for methylated benzoic acid. If the benzoic acid had been methylated, both a methoxy ^1H NMR peak at about 2 ppm in Figure 24a and a methoxy ^{13}C peak at about 51 ppm in Figure 24b would have been present. Figure 25a shows the ^1H NMR spectrum of the recovered benzoic acid that had been extracted from the methylated phenol solution. Figure 25b shows the ^1H spectrum of pure benzoic acid in chloroform ($CDCl_3$). A comparison of the spectra shows that the peak at about 12.5 ppm in 25a was indeed due to the recovered benzoic acid proton. This constitutes additional proof that the benzoic acid had not been converted to its respective methyl ester.

The NaH/CH_3I methylation method did indeed appear to be phenol specific. However, as an extra precaution, the experiment was repeated using additional model compounds. The next series of model compounds included: 2,6-dimethylphenol, used as an example of a hindered phenol; phenol, used as an example of a non-hindered phenol; benzoic acid; and octanoic acid. The ^1H

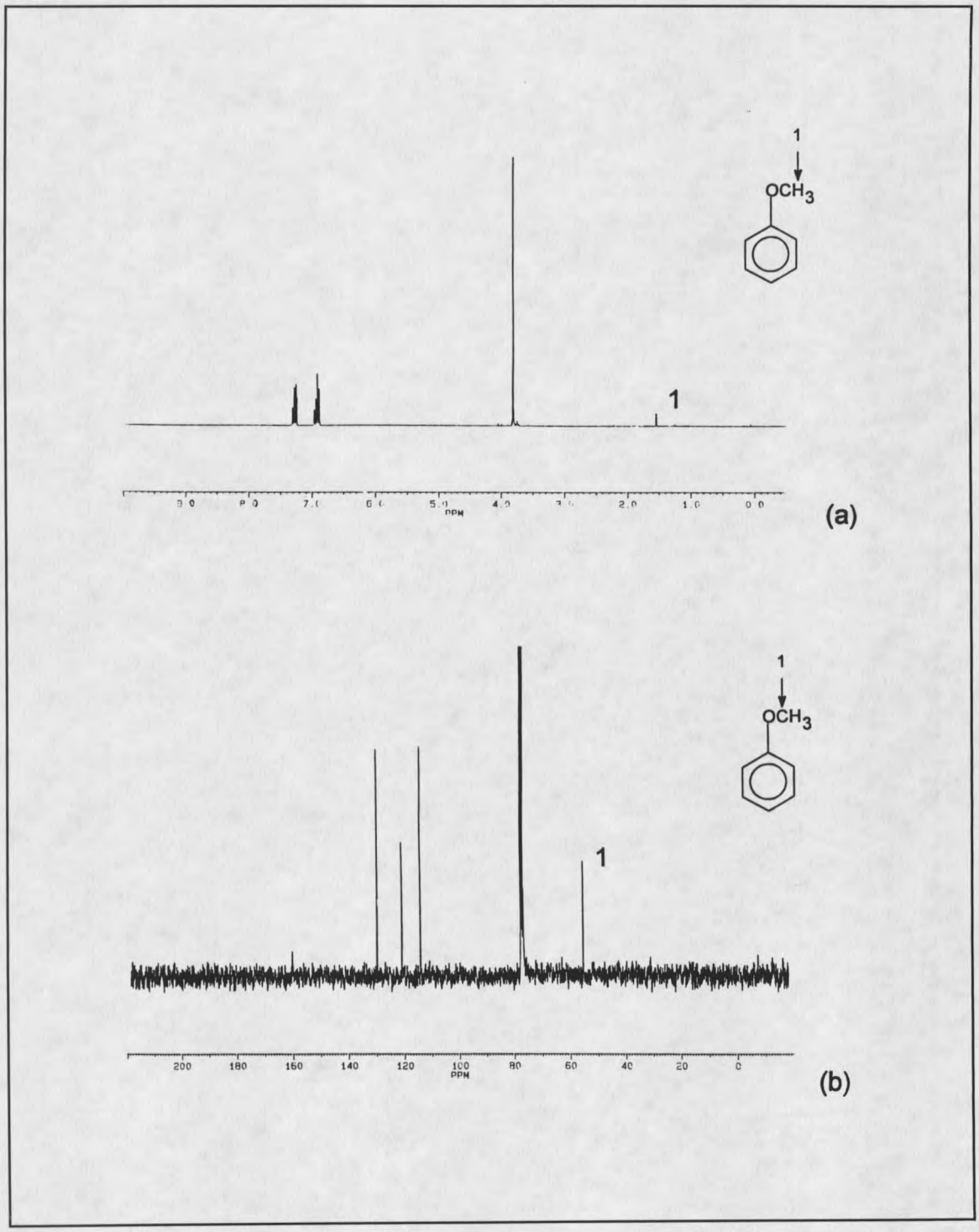

Figure 24. a) ^{1}H NMR spectrum of methylated phenol. b) Corresponding ^{13}C NMR spectrum of the same methylated phenol. The benzoic acid was not methylated as evinced by the absence of its methylated product in either spectrum.

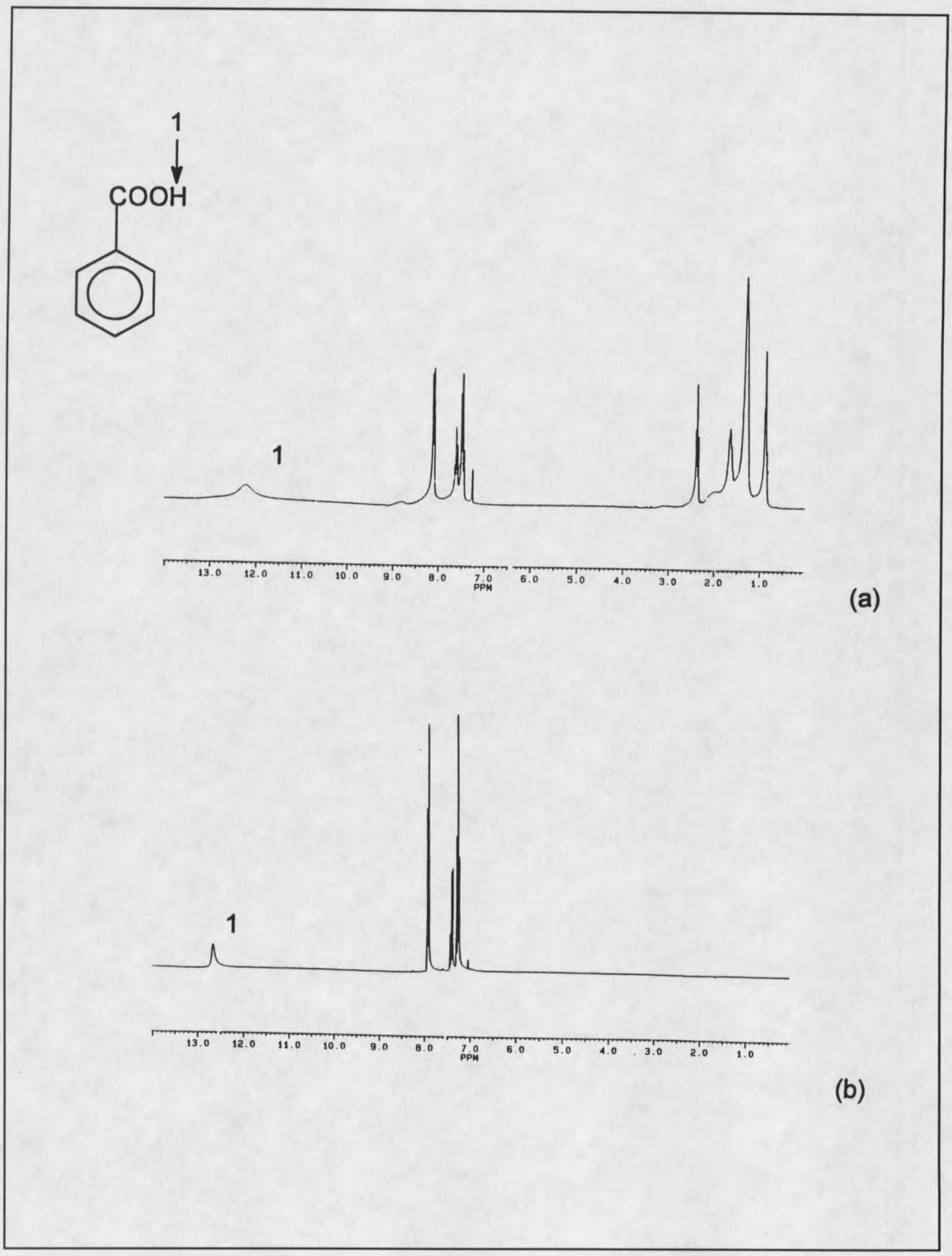

Figure 25. a) ^{1}H NMR spectrum of the recovered unreacted benzoic acid. b) The ^{1}H NMR spectrum of pure benzoic acid.

and the ^{13}C spectra in Figure 26 show peaks marked by 1 and 2. These peaks are due only to methylated phenol (methoxy benzene) and 2,6-dimethyl-phenol (2,6-dimethylmethoxy-benzene). Neither of the acids had been methylated. The general conclusion of these results was that the NaH/CH_3I method was promising for phenol specific methylation in asphalt.

Quantitative Measurements Experiments were performed to determine whether or not the NaH/CH_3I methylation method was quantitative. The model compounds, phenol, 2,6-dimethyl-phenol (2,6 DMP), benzoic acid, and octanoic acid were used for this experiment. The primary standard was a 25% solution of deuterated tetramethyl silane (TMS) in d_6 acetone, sealed in a coaxial NMR tube. The TMS solution had been used previously for the PTM method. This standard was specially prepared by Cambridge Isotope Company. In the event that the coaxial tube was broken, a new standard would have to be purchased. For both economic and time reasons, it was decided that an alternate standard would be tested against the TMS standard. A known volume of toluene was mixed in with the methylated model compounds in the NMR tube. Toluene was chosed because it was readily available, affordable, and its methyl ^{13}C NMR peak at 21 ppm was sufficiently upfield from the methoxy ^{13}C peaks to allow easy integration.

As mentioned above, the only methylated products observed by NMR were methoxy-benzene and 2,6-dimethylmethoxy-benzene. Table 3 shows the

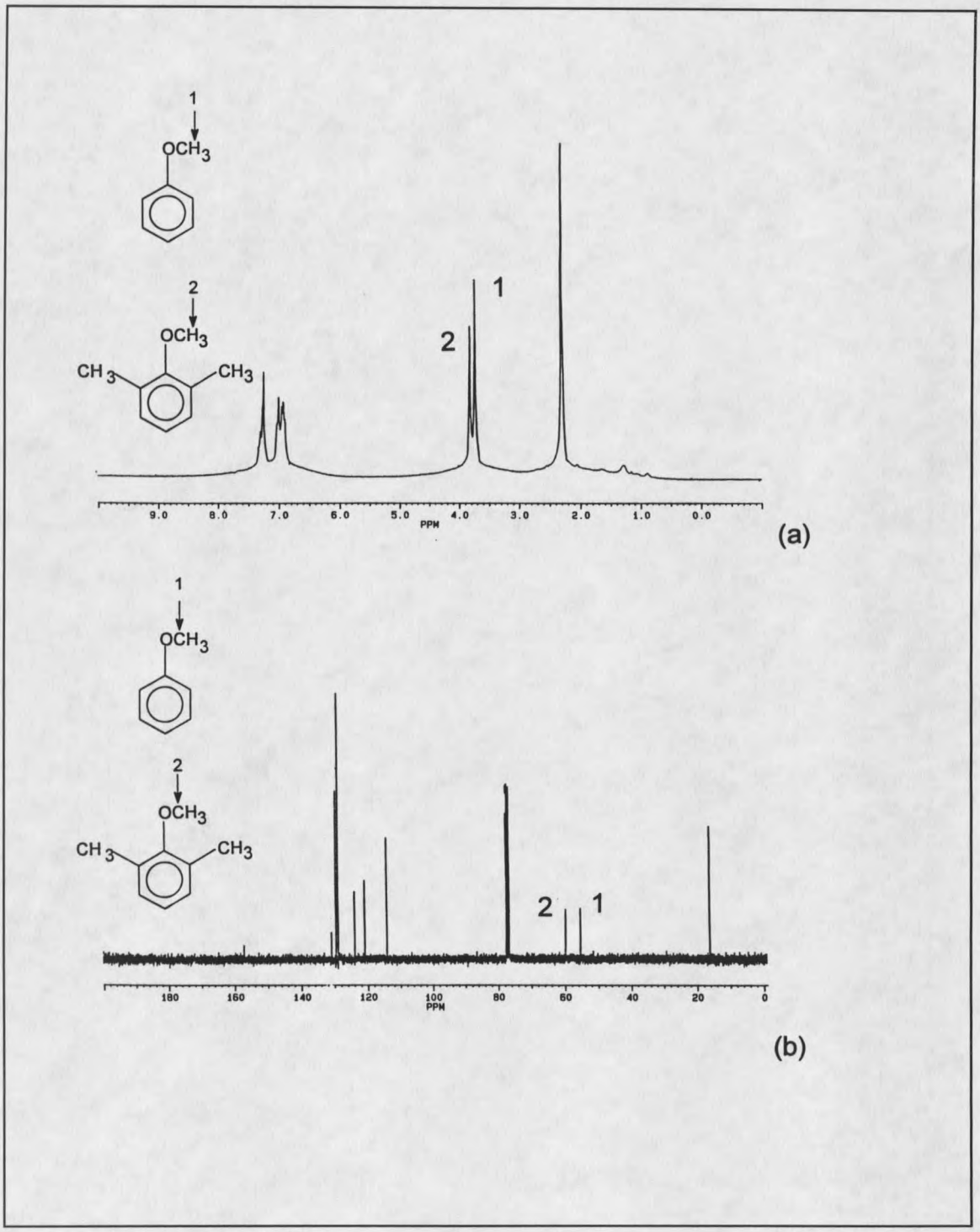

Figure 26. a) ^{1}H NMR spectrum of methylated phenol (methoxybenzene) and 2,6-dimethylphenol (2,6-dimethylmethoxybenzene). b) The corresponding ^{13}C NMR spectrum of the above mentioned products. Both the octanoic and benzoic acids have not been methylated.

yield data from the methylations using the two integration standards. A comparison shows that the two integration standards gave comparable yield values. However, the yields were low which did not coincide with the fairly high yields reported in the literature.(37,38) Hence, two possible reasons for

Table 3. Data comparing two integration standards for phenol quantification using the NaH/CH_3I methylation method.

Standard	Starting Material Weight(g)		Percent Methylated Yield	
	Phenol	2,6 DMP	Phenol	2,6 DMP
25% TMS	0.28	0.36	25	41
Toluene	0.28	0.36	29	41

the apparent low recovery were considered. First, the loss of product could have been due to losses that occured during the chemical separations performed after the completion of the methylation reaction, as described in the Experimental section. Second, the NMR experimental parameters could have been incorrectly chosen. One explanation of the second case type involves the T_1 relaxation time. The symbol T_1 represents the spin-lattice relaxation time (this relaxation occurs by the loss of energy from the excited nuclear spins to the surrounding molecular lattice). This is the time constant for the excited nuclear spin system to reach longitudinal equilibrium after being exposed to a RF pulse. To ensure complete relaxation of nuclear spin states, instrumental delays between excitation pulses are normally set to $5 \times T_1$. In this experiment,

the delay between exitation pulses was set at 50 s. If this delay time is too short, then the next excitation pulse will occur before complete relaxation of the excited nuclear spins giving NMR signals whose peak areas are too small. Upon integration against a standard, the measured concentration will be too low. Anisaldehyde, which contains a methoxy carbon, was used as the model compound to determine the methoxy ^{13}C T_1. Figure 27 shows the results from the NMR inversion recovery experiment used to determine T_1 for the anisaldehyde methoxy carbon. The peak of interest is indicated by the arrow marked 1 at about 56 ppm in the top spectrum in Figure 27. The experiment showed that T_1 = 5.34 s for the methoxy carbon in anisaldehyde. Therefore, $5xT_1$ = 26.7 s was well within the normally used delay time of 50 s.

It seemed as if the origin of the low recovery was either due to the loss of product during the chemical "clean-up" process after the methylation reaction was complete or to the possibility that the method was not quantitative.

The NaH/CH_3I methylation experiment was repeated on additional model systems to determine which of the two remaining possible reasons for the low recovery. The yields were again measured by NMR again using 2,6-dimethyl phenol and 2-naphthol as the model compounds. Toluene was used as an internal integration standard. Table 4 shows the percent yield of methylated product from three separate methylations. The yields that were calculated appear high, however, one must consider that there is a NMR error range between +/- 5-10%.

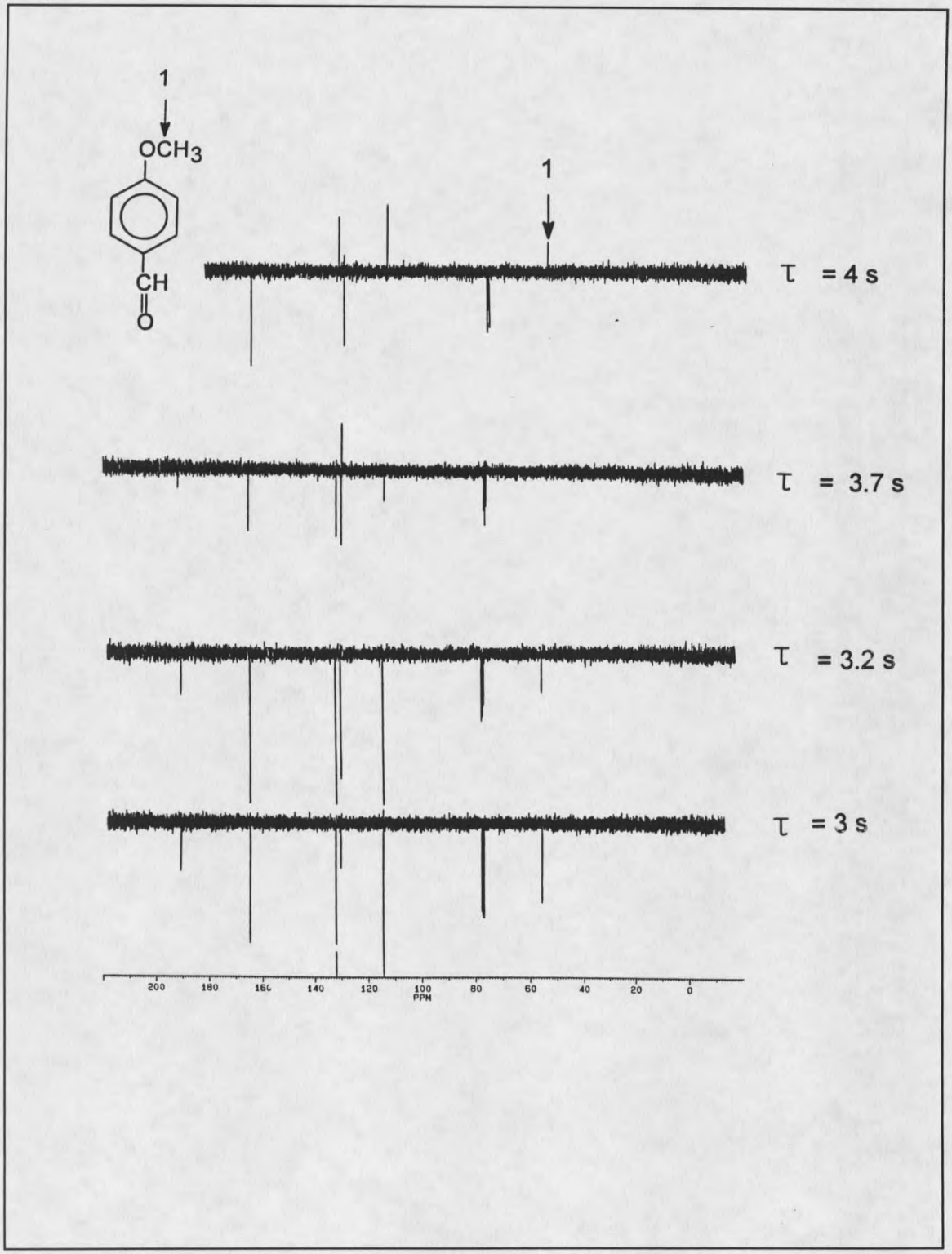

Figure 27. Determination of the methoxy carbon T_1 value for anisaldehyde using the inversion recovery NMR method.

Table 4. Percent yield of methylated model compounds.

Run	Percent Yield of Methylated Phenol (%)	
	2,6-dimethylmethoxy-benzene	2-methoxynaphthalene
1	102	98
2	110	95
3	90.4	99.6

Methylation Using ^{13}C Enriched Methyl Iodide for Low Phenol Concentrations It is known from previous methylations of phenols in asphalt that they exist in low concentrations, at approximately $1x10^{-5}$ mol/g asphalt.(3) For the model compounds, methyl iodide with the natural isotopic abundances of ^{13}C (1.1%) had been used for the NaH/CH_3I method. If one were to use unenriched CH_3I on asphalt, however, the combined effects of the low ^{13}C natural abundance of 1.1% and the low phenol functional group concentration in asphalt would result in the ^{13}C methoxy NMR signal to be lost in the noise. Therefore, 99% ^{13}C enriched methyl iodide was used in subsequent experiments. But, before applying the NaH/CH_3I method to asphalt, a solution containing low concentrations of 2-naphthol and 2,6-dimethyl phenol in THF was prepared. The total concentration of phenol functional groups used was approximately that found in asphalt. The methylation experiment was performed in the same manner as before. Figure 28 shows that the methoxy ^{13}C NMR peak increased substantially over the other peaks in the spectrum

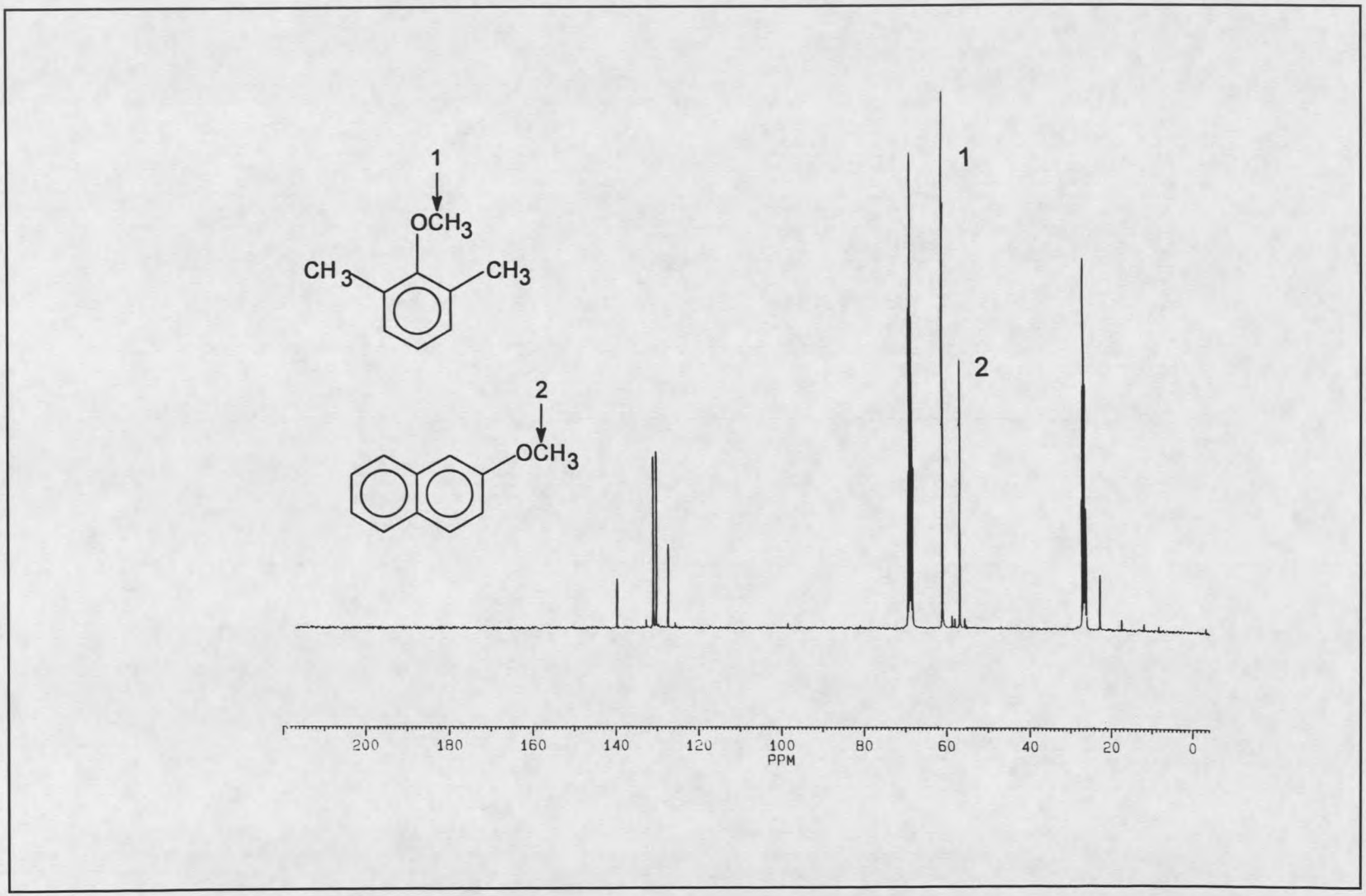

Figure 28. ^{13}C NMR spectrum of methoxybenzene and 2-methoxynaphthalene using ^{13}C enriched methyl iodide.

upon use of the enriched methyl iodide as can be seen by the peaks marked 1 and 2. The calculated percent yield is shown in Table 5. The yields are seen to be marginally lower than previously obtained. However, this could well have been due to the inaccuracy caused by weighing very small quantities of sample.

It is well to mention here that the peak intensities of the aromatic carbons in Figure 28 appear too high as compared to the peak intensities of the ^{13}C enriched methoxy peaks. By appearance, the intensity of the methoxy peaks should be much greater considering that they are enriched. However, this discrepancy has not been investigated and should be if further work is to be accomplished in this area..

Table 5. Yields for methylating low concentrations of model phenols using 99% ^{13}C enriched methyl iodide.

Starting Material	Percent Methylated Yield [a]	Original Mass (g) of Starting Material	Moles of Phenol in Starting Material
2-naphthol	85	0.0028	9.02×10^{-6}
2,6 DMP	92	0.0013	2.29×10^{-5}

a) Calculations were made against 1.8×10^{-4} moles of toluene standard.

NaH/CH_3I Methylation of Asphalt

The Use of a Relaxation Agent Carbon atoms within asphalt tend to have extremely long T_1 relaxation times.(59,60) The combined effect of low

phenol concentration in asphalt and long ^{13}C T_1's, is to decrease the likelihood of obtaining a strong ^{13}C NMR signal. Using ^{13}C enriched methyl iodide is expected to only partially solve the sensitivity problem. However, addition of a paramagnetic species like $Cr(acac)_3$ to samples such as asphalt greatly reduces ^{13}C T_1 relaxation times. Figure 29 compares two spectra of methylated asphalts. Figure 29a is the NMR spectrum of the asphalt to which no $Cr(acac)_3$ had been added where the only two peaks evident belong to aliphaltic carbons. Even though ^{13}C enriched methyl iodide was used on the asphalt in Figure 29a, one still cannot observe any corresponding methoxy carbon signals. Figure 29b shows the NMR spectrum of the same asphalt to which $Cr(acac)_3$ had been added. One can now observe more peaks including the hindered phenol group peak labeled 1 and the non-hindered phenol group peak labeled 2.

Upon studying the spectrum in Figure 29b one observes that the resolution and the signal to noise (S/N) ratio is very low, especially in the region of interest between 50 and 61 ppm which could have much to do with the magnetic field of the spectrometer used. The ^{13}C alphalt spectrum in Figure 29 had been acquired on a Bruker AC300 spectrometer. It was decided that a higher field instrument would be used for spectral acquisition, namely, a Bruker AM500. The increase in the S/N ratio when using magnets of increasing field strength can be seen as a consequence of the energy transition between nuclear spin states after having been exposed to an RF field. This transition energy is shown in Figure 30 and given by the equation:

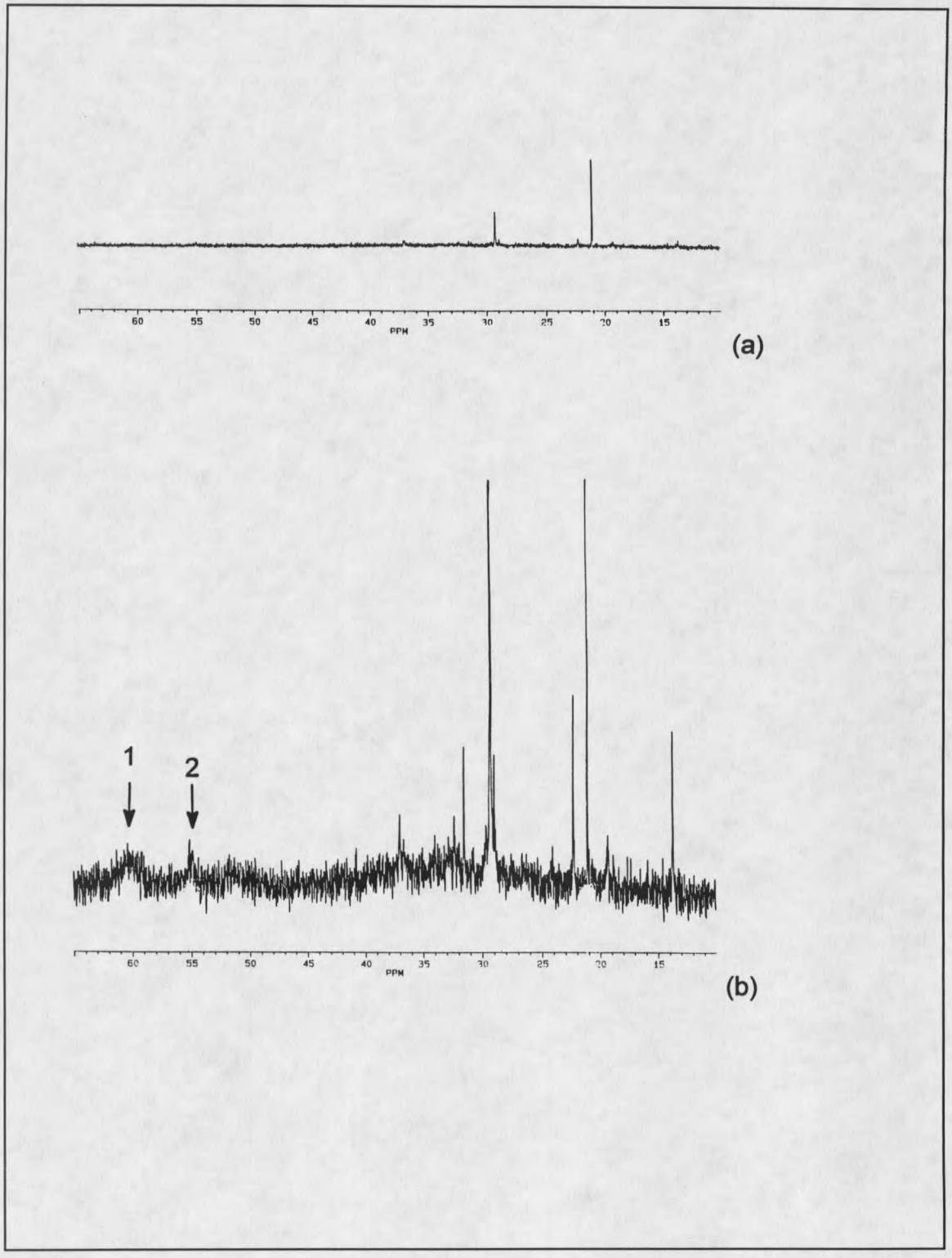

Figure 29. a) ^{13}C NMR spectrum of a methylated asphalt without $Cr(acac)_3$. b) ^{13}C NMR spectrum of a methylated asphalt with $Cr(acac)_3$.

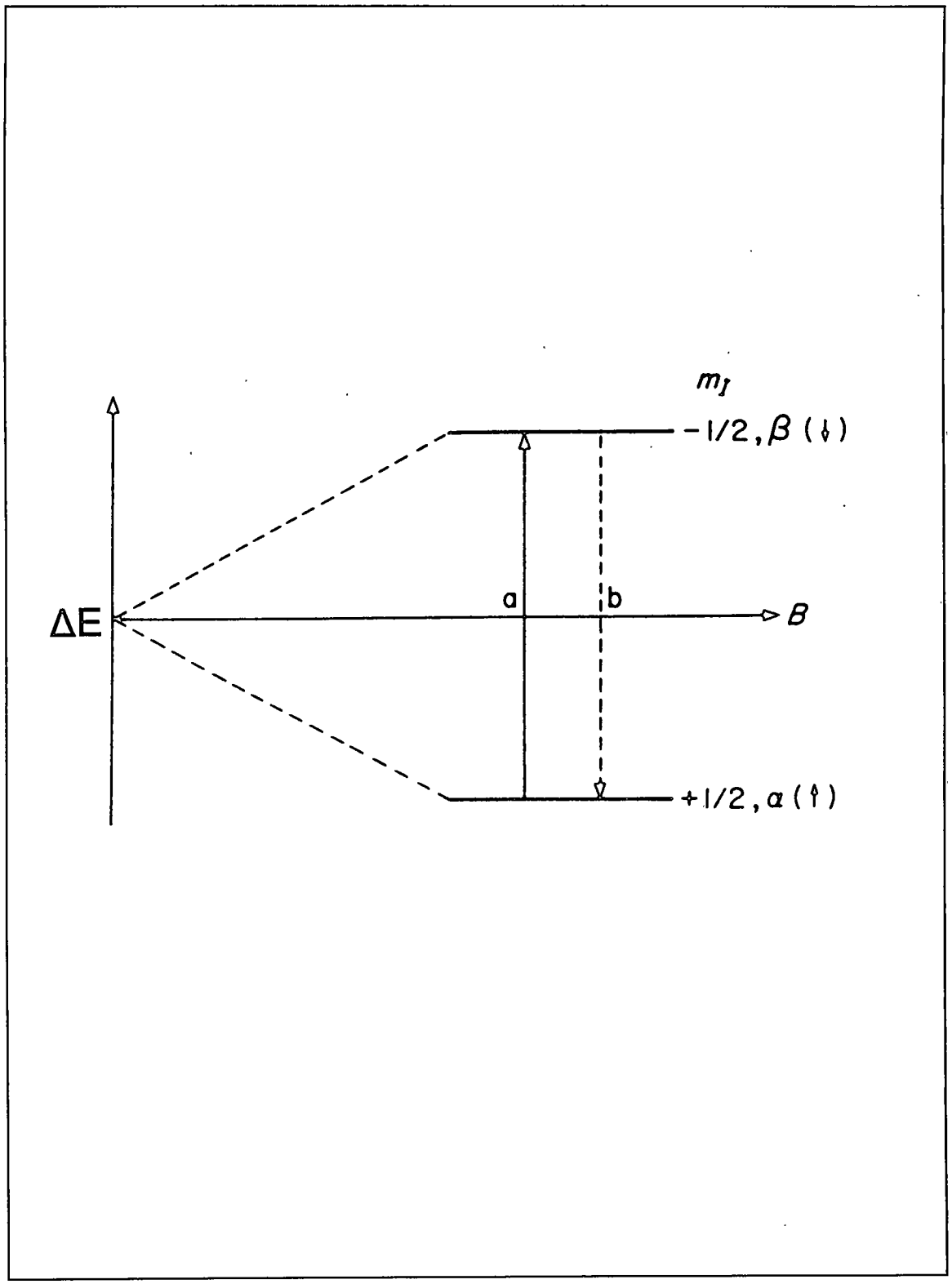

Figure 30. Energy levels and transitions for a nucleus in a magnetic field *B*.(60)

$$\Delta E = \gamma hB/2\pi \quad (60)$$

where γ is the gyromagnetic ratio and *B* is the of the applied RF field. As the magnitude of RF field is increased, the transition energy, ΔE, between spin orientations increases. This increase directly affects the Boltzmann nuclear spin population distribution, N_α and N_β shown in the following equation:

$$N_\beta/N_\alpha = \exp(-h\nu/kT) \quad (60)$$

At thermal equilibrium, N_α and N_β are degenerate (equal). However, in an applied magnetic field, these populations become unequal with $N_\beta < N_\alpha$ giving a net absorbtion of energy resulting in an NMR signal. As ΔE widens, more of the spin population will remain in the lower energy N_α orientation. And, the greater the difference between the N_α and N_β spin populations, the greater the NMR signal intensity.

Simplifying the Chemistry As seen above, the NaH/CH_3I method showed great promise as a selective method giving high methylation yields for phenol group analysis in asphalt. However, if one were to accomplish phenol group methylation for any series of asphalt samples where time constraints are imposed, the chemistry required to perform the NaH/CH_3I must be simplified and shortened. It was decided to attempt this method in a single "pot", the NMR tube. However, before attempting the simplified version of this method on asphalt, it was performed using the two previously used model compounds: 2-naphthol and 2,6-dimethyl phenol. Because the methylation was being

performed in the NMR tube itself, a suitable solvent was needed that could serve both as a good reaction medium and as a deuterated solvent for the NMR experiment. For this reason d_8 THF was chosen. This seemed an ideal solvent because both of the THF NMR ^{13}C multiplets are spectrally removed from the other peaks of interest. Table 6 gives the ^{13}C chemical shift values. Figure 31 shows the ^{13}C spectrum of this mixure where the peaks marked 1 and 2 show the methoxy carbon peaks of 2,6-dimethylmethoxy-benzene and 2-methoxy-naphthalene. The d_8 THF multiplets are marked by arrow 3 and the toluene peak is marked by arrow 4.

Table 6. ^{13}C chemical shift values for the Inverse Gated integratable NMR experiment.

Compound	^{13}C Chemical Shifts (ppm)
d_8 Tetrahydrofuran	25.8, 67.9 (quintets)
Toluene (methyl carbon)	22.7
2-Methoxy-naphthalene (methoxy carbon)	56.9
2,6-Dimethyl-methoxybenzene (methoxy carbon)	60.8

One-Step Methylation of Asphalt The NaH/CH_3I one-step methylation procedure was now applied to a series of experimental asphalts from the Strategic Highway Research Program (SHRP). (See Appendix for background information on the SHRP asphalts.) These asphalts included:

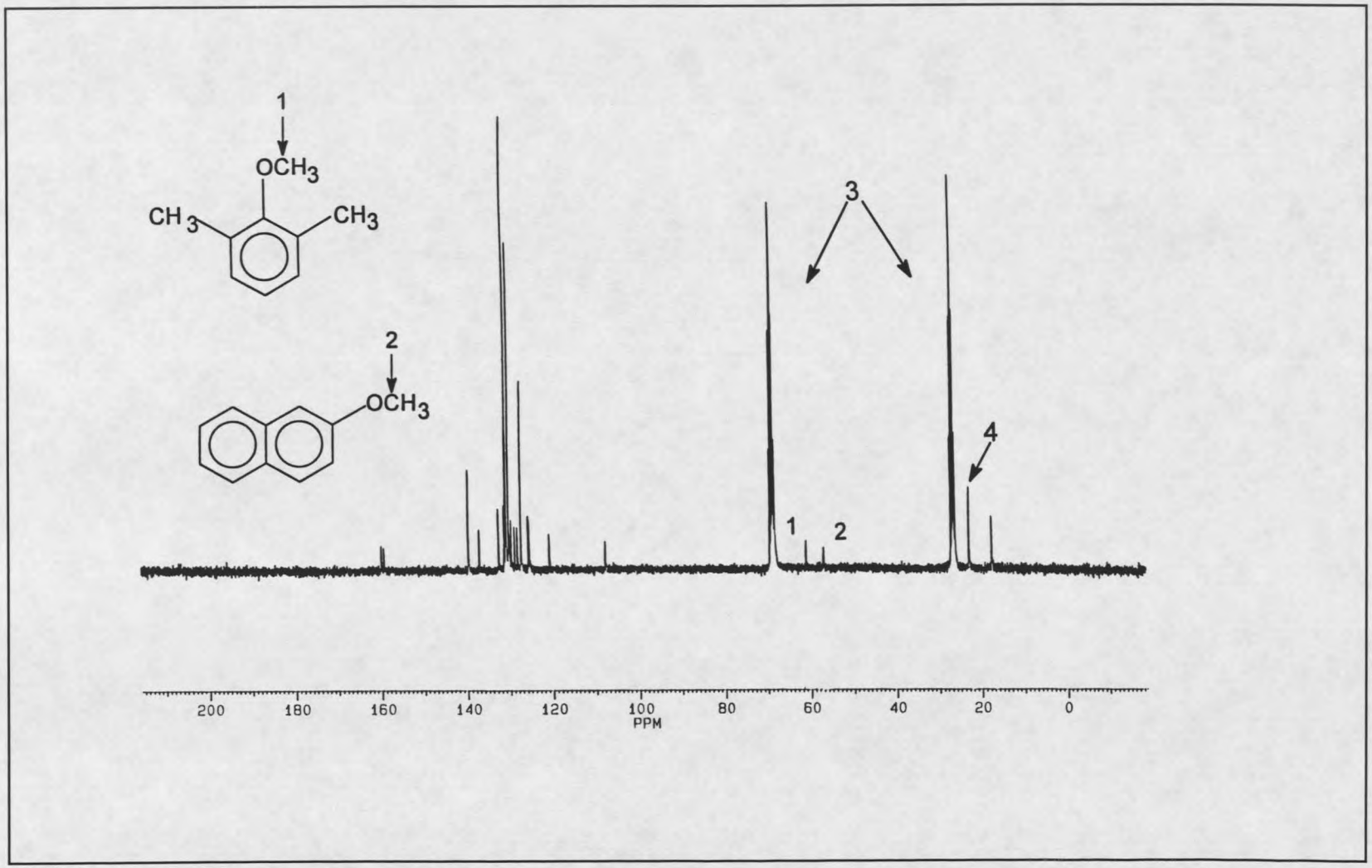

Figure 31. ^{13}C NMR spectrum of the methoxy carbons in methylated 2,6 dimethylphenol and 2-hydroxynaphthalene after using the simplified methylation procedure.

AAA-1, AAB-1, AAC-1, AAD-1, AAF-1, AAG-1, AAK-1, and AAM-1. An example spectrum of the result can be seen in Figure 32a. It shows the methoxy region of the ^{13}C NMR spectrum of asphalt AAM-1. The peak due to methylated hindered phenol groups in asphalt which resonate between approximately 61 and 63.3 ppm is designated by arrow 1. Arrow 2 points to the broad peak due to methylated non-hindered phenol functional groups between about 55.5 and 57.9 ppm. And, the peak marked by arrow 3 can only be attributed to methylated carboxylic acids. This third peak was a result of the one-step chemistry process and was a development not previously observed. One possible explanation that could account for the appearance of the methylated carboxylic acids in asphalt was that not only was a large excess of methylating agent added to ensure the completion of the reaction, the excess was left in the asphalt solution for about two hours reaction time plus eight additional hours during the NMR spectral acquisiton. This apparently was sufficient time for at least partial methylation of carboxylic acids. This reaction phenomenon has apparently not been reported previously in the literature.(37,38) A probable explanation is that previous experiments on model compounds were carried out under stochiometric conditions.(37,38) Since this methylation reaction preferentially methylates phenols, all of the methyl iodide would be consumed by the phenols, leaving no reagents for the apparently slow methylation of carboxylic acids. One should note that this, by no means, constitutes a proven method that should be used for methylating carboxylic

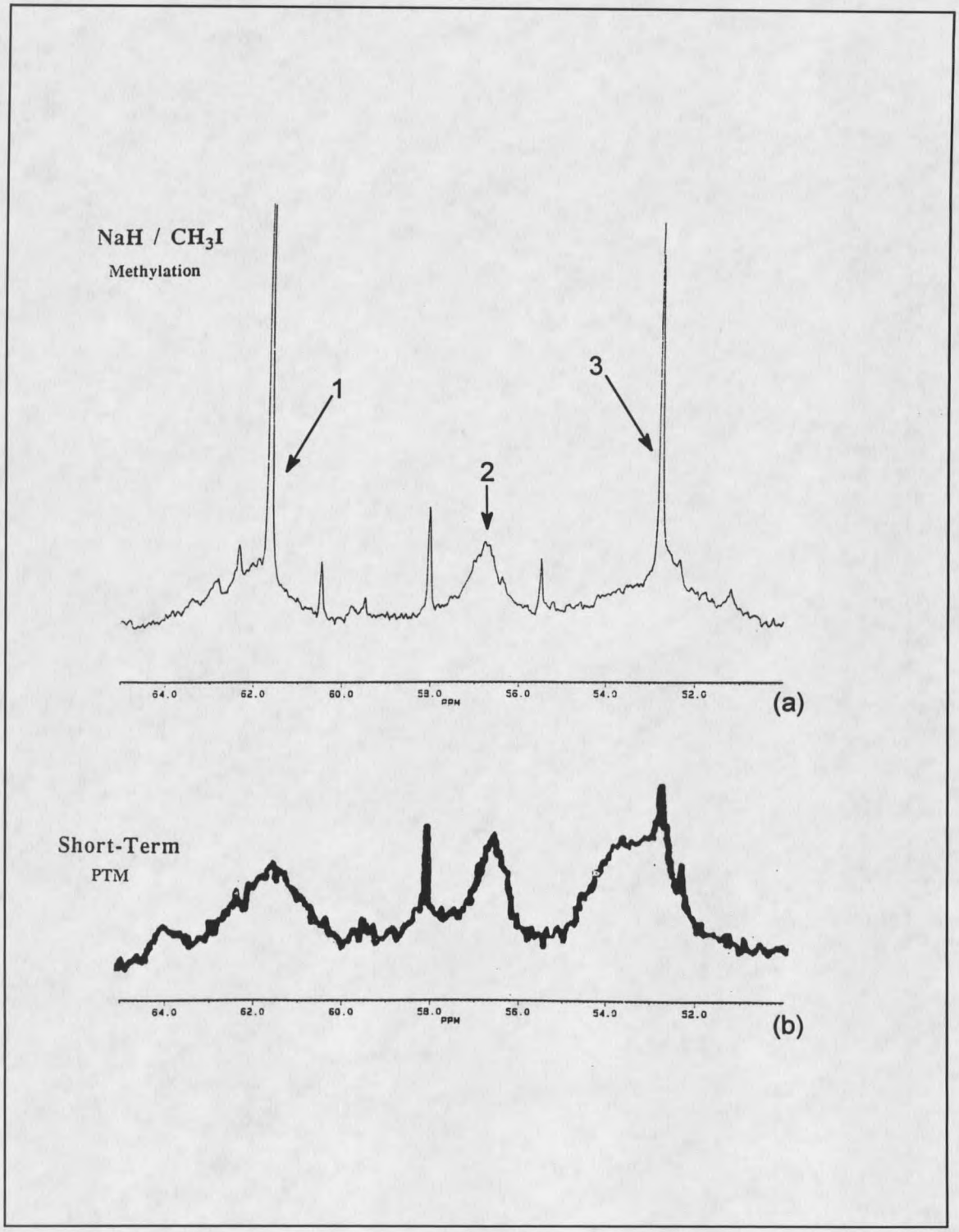

Figure 32. Comparison of the methoxy region of the ^{13}C NMR spectrum of an asphalt using (a) the NaH/CH_3I methylation method and (b) the old Phase-Transfer-Methylation.

acids.

The unidentified unresolved peak that overlapped downfield of the methylated carboxylic acid peak that was always present when using the PTM method did not appear when using the NaH/CH_3I method. To see the difference, compare Figure 32a (arrow 3) with the same region in Figure 32b. By comparing the peaks labeled 1 and 2 in Figure 32a of the NaH/CH_3I methylation to their respective positions in Figure 32b of the PTM methylation, it is clear that the NaH/CH_3I methylation results in a much "cleaner" spectrum with significantly better resolution. Additional peaks appeared as well that were not seen previously when using the PTM method. One of the most interesting "new" peaks was the sharp peak shown by arrow 1 in Figure 32a whose chemical shift was within the spectral range of the methylated hindered phenols at about 63.6 ppm. The fact that this peak is so sharp indicates a phenol group attached to a small molecule. This is not surprising given the evidence obtained from Laser Desorption Mass Spectroscopy (LD-MS) of asphalts discussed in detail in that section. Briefly, asphalt does contain many small molecules which could very possibly include small phenolic molecules. As shown in the LD-MS section, there is evidence of the presence of 9-hydroxyanthracene in most of the asphalt samples that were observed through the LD-MS technique. This is a speculation that could be subject for further research and not pursued in this dissertation. The identity of the unlabeled peaks in Figure 32 are unknown, however, their chemical shifts do not overlap

with those shifts belonging to the phenols in asphalt.

Figure 33 shows the ^{13}C methoxy region of the NMR spectra of the eight NaH/CH_3I methylated SHRP asphalts. One can see from Figure 33 that both S/N and resolution is much improved over that obtained after using the PTM method (Figure 23). The "mysterious" peak at 63.6 ppm is present in all of these samples. There are also other small peaks protruding from the hindered region that had not been previously seen. There is also some evidence of this occuring in the non-hindered peak region. Also seen is the methylated carboxylic acid peak at about 52.5 ppm. Table 7 compares the data obtained by both the PTM and the NaH/CH_3I methods.

It is seen in Table 7 that consistently higher concentrations for hindered phenols were measured when using the NaH/CH_3I method. One explanation may be that a specific phenol in asphalt is being methylated to a higher degree than when using the PTM method *i.e.* 9-hydroxyanthracene. There also appears to be a higher concentration of hindered phenols than non-hindered phenols in these asphalts which seems logical. Because of the polyaromatic nature of asphalt molecules, it would seem that there would be fewer non-hindered positions available, and phenol groups in asphalt would more likely have at least one substituted ortho position.

In conclusion, the NaH/CH_3I methodology used on asphalt is simple and reproducible with good S/N and superior resolution to that obtained with the PTM method. It appears to give NMR resonances that are specific for

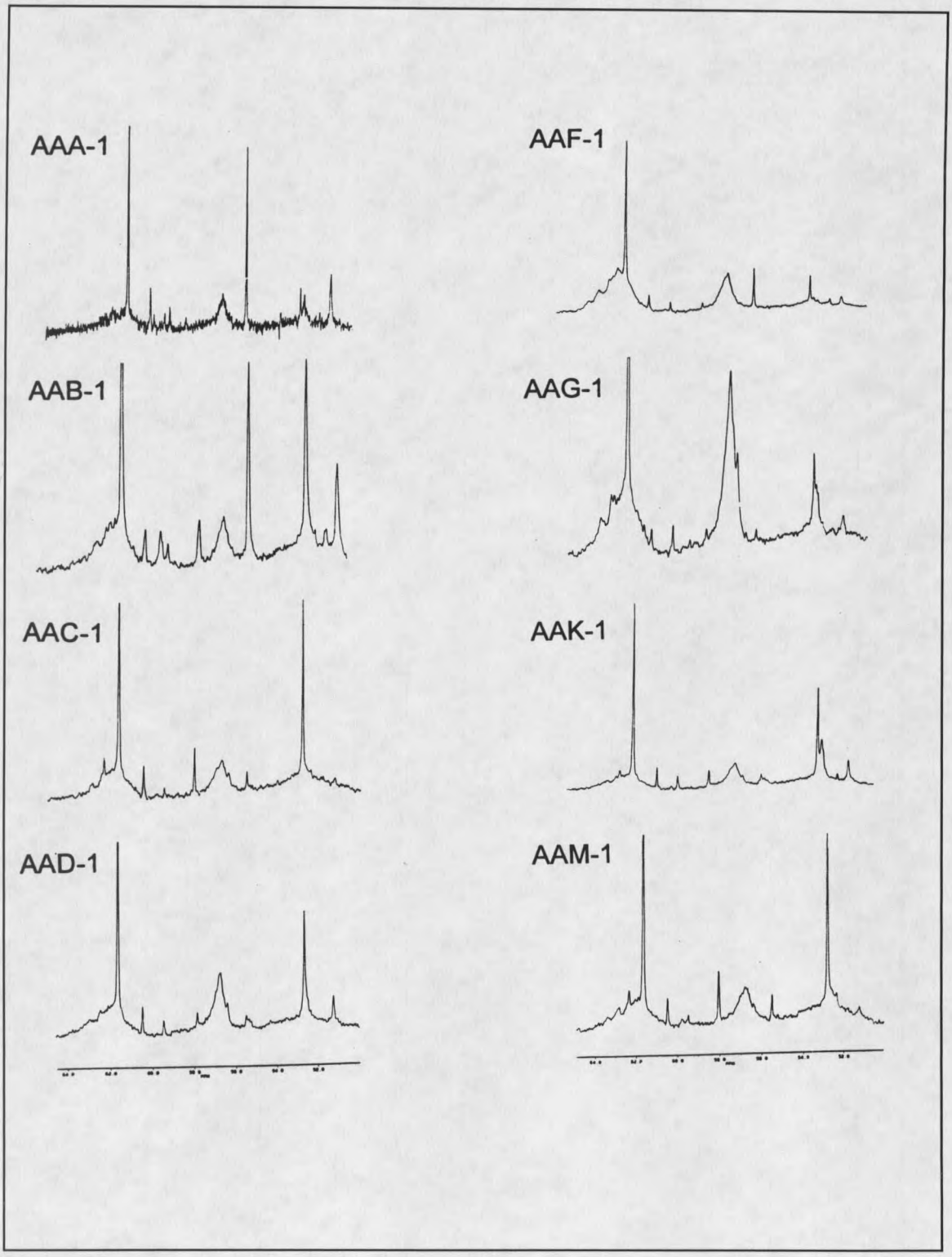

Figure 33. Methoxy regions of the ^{13}C NMR spectra of the NaH/CH_3I methylated SHRP asphalts.

individual phenols. Overall, the NaH/CH_3I method is a substantial improvement over the previously employed STPTM method for characterizing phenols.

Table 7. Comparison of calculated concentrations by two methylation methods reported in 10^{-5} mol phenol/g asphalt.

SHRP Asphalt	Short-Term Phase Transfer Methylation (PTM)		NaH/CH_3I Methylation	
	ASP-OH*[a]	ASP-OH [b]	ASP-OH*[a]	ASP-OH [b]
AAA-1	3.5	2.5	5.2	2.1
AAB-1	4.2	3.1	4.3	2.0
AAC-1	1.8	1.7	6.2	3.1
AAD-1	2.2	2.2	6.3	2.8
AAF-1	6.3	3.2	7.9	4.2
AAG-1	4.2	5.5	9.3	5.7
AAK-1	2.5	1.5	5.3	3.0
AAM-1	3.5	2.8	4.3	2.2

a = hindered phenols; *i.e.*, phenols that are substituted on one or both ortho positions.
b = non-hindered phenols: *i.e.*, phenols that have no ortho substitution.
ASP = asphalt.

Determination of Benzylic Carbon Oxidation in Asphalt Utilizing the COLOC 2D NMR Experiment

General Discussion

As discussed in the Introduction, benzylic aliphatic carbons are thought to be primary sites for autoxidation (free-radical oxidation) in asphalt. Upon this free-radical oxidation, benzylic ketones are formed.(3) These are among the major polar functionalities that appear only in age weathered asphalt and are not detected in non-aged asphalt.(16) It has been observed that the carbonyl absorbance invariably increases in the IR spectra of all age-hardened, cracked asphalt pavements, and ketones and carboxylic acid formation is said to be the cause. Benzylic aldehydes have not been observed in age-weathered asphalt pavements, which is probably due to the fact that methyl free-radical intermediate carbons are stabilized by hyperconjugation, hence making them less reactive towards autoxidation. The appearance of the IR carbonyl absorbance in aged asphalt is proof that chemical changes that have occured. However, IR spectroscopy does not specifically identify the exact source of the ketone absorbance. But, benzylic ketones are suspected to be major contributors to it. To investigate this possibility, the inverse COLOC (Heteronuclear Shift Correlation Spectroscopy via Long-Range Couplings) 2D

NMR experiment has been employed to observe whether or not benzylic carbons have oxidized during laboratory and road aging of asphalt.

Identification of Benzylic Protons via the COLOC NMR Experiment

Finding the quaternary benzylic carbonyl carbon resonance peak in the ^{13}C NMR 1D spectrum of an asphalt is not possible. This is in part due to its long T_1 relaxation time. Even when using a relaxation agent, such as $Cr(acac)_3$, the peak is not observed. In addition to having long T_1 relaxation times, carbonyl carbons are very dilute in asphalt even after aging. The problem is further compounded by the fact that the NMR active ^{13}C isotope has a natural abundance of only 1.1%. This isotope is not particularly NMR sensitive. For the two above mentioned reasons, using 1D ^{13}C NMR is not a practical option for the observation of benzylic carbonyl carbon in aged asphalt pavements.

One would then naturally assume that benzylic protons could be quantified before and after aging using ^1H NMR spectroscopy. Protons are relatively easy to detect because they have short T_1 relaxation times, and the natural abundance of the ^1H is 99.98%. The proton has the highest NMR sensitivity of all known NMR active isotopes with the exception of tritium (^3H). However, as shown in Figure 8 in the Introduction, direct spectral identification of benzylic protons is impossible. This is due to the presence of other protons

in asphalt whose NMR resonant frequencies occur within 2-3 ppm, the same spectral region as that of benzylic protons. This results in extensive peak overlap. Amine protons, i.e. R-NH_2 and R-NHR', are examples of protons in asphalt whose resonant peaks appear between 2-5 ppm (60) which overlaps the benzylic proton chemical shift region.

Although the 1D NMR approach to the problem was not feasable, indirect observation of the benzylic carbon in asphalt was possible by using the 2D COLOC NMR experiment.(59) The COLOC experiment allows the $^2J_{CH}$ coupling between benzylic protons and the quaternary aromatic carbons alpha to the benzylic carbons in asphalt to be observed in the form of cross peaks in the 2D spectrum. J coupling arises from the fact that the alignment of the nuclear spin with respect to an applied external magnetic (RF) field of an NMR active nucleus will influence the nuclear spin of a neighboring NMR active nucleus, thus splitting its NMR signal. This influence is transferred mainly through sigma bonds and the magnitude of this influence is expressed as the coupling constant, J, in cycles per second or Hz. The number of bonds intervening the two coupled nuclei can be expressed as n in ^nJ. Therefore, ^2J is coupling through two bonds. Hence, to explain a complex operation in a very elementary fashion: For the 2D NMR COLOC pulse experiment, this $^2J_{CH}$ coupling constant is converted to seconds. This time constant is then included in the NMR pulse sequence as a delay time between RF pulses. This delay allows the time required for the quaternary carbon/ benzylic proton coupling to

evolve. On asphalt, this method was first used by Jennings *et al.* (33) They obtained 2D spectra which showed benzylic coupling cross peaks. However, these were preliminary results and not pursued in greater depth at this time. In this work, the COLOC method has been expanded and, as a result, it has been shown that benzylic protons disappear upon asphalt road aging.

Determining Benzylic ^{1}H and ^{13}C NMR Chemical Shifts

The NMR chemical shift of the three types of benzylic protons i.e. methyl ($-CH_3$), methylene ($-CH_2$), and methine (-CH), were determined by using selected model compounds. Toluene, 3-picoline, ethylbenzene, tetrahydronaphthalene (THN), cumene, and 9,10-dimethylanthracene were selected for this purpose. In each case, the deuterated solvent used was chloroform ($CDCl_3$). NMR proton spectra were acquired for each individual compound; for a mixture of these compounds; and for each again individually, however spiked into an asphalt (SHRP AAG-1). Table 8 gives the chemical shifts of the benzylic protons of these model compounds. One can also see that there is little effect on the chemical shift of these protons in each of the three chemical environments.

Once the chemical shift of the benzylic protons were known for the model compounds, a COLOC experiment was performed on a mixture of all the compounds except 9,10-dimethylanthracene (9,10 DMA). ^{13}C NMR spectra

were also obtained for these standards to determine the chemical shifts of the

Table 8. Benzylic proton chemical shifts of selected model compounds.

Model Compound	Chemical Shift (ppm)		
	With SHRP AAD-1 in $CDCl_3$	As a Mixture in $CDCl_3$	Individually in $CDCl_3$
Toluene	2.337	2.293	2.310
3-Picoline	2.301	2.408	2.297
Ethylbenzene [a]	2.638	2.710	2.634
THN* [a]	2.751	2.831	2.752
Cumene [a]	2.890	2.967	2.900
9,10 DMA	3.066	NA	3.095

* THN = Tetrahydronaphthalene.
a = Shift value chosen as the center of a multiplet.

quaternary aromatic carbons substituted by the benzylic aliphaltic carbons. Both the ^{13}C and the ^{1}H shifts were used to locate the cross peaks in the 2D COLOC spectrum of the model compounds. The data are summarized in Table 9.

Not only were these chemical shifts used to approximate the location of the $^{2}J_{CH}$ benzylic coupling cross peaks, but a test COLOC experiment using model compounds was needed to adjust instrument parameters.

Table 9. ^{13}C and ^{1}H chemical shifts that correspond to the $^{2}J_{CH}$ coupled COLOC benzylic cross peaks.

Compound	^{2}J Coupled Aromatic Carbon (ppm)	Benzylic Proton (ppm)
Cumene	148.8	2.97
Ethyl benzene	144.2	2.71
Tetrahydronaphthalene	136.9	2.83
3-picoline	133.1	2.41
Toluene	137.7	2.29

Determining COLOC $^{2}J_{CH}$ Coupling Cross Peaks

Figures 34, 35, and 36 show the ^{1}H, the ^{13}C, and the 2D COLOC spectra of the model compounds listed in Table 9. Figures 34, and 35 are self-explanatory. The benzylic proton and the quaternary aromatic carbon peak of each model compound has been labeled. Figure 36 shows the 2D COLOC spectrum of the model mixture. The y-axis to the left of the 2D spectrum shows the 1D ^{13}C NMR spectrum of the model compound mixture. The x-axis at the top of the 2D spectrum shows the 1D ^{1}H NMR spectrum of the model compound mixture. The $^{2}J_{CH}$ and the $^{3}J_{CH}$ benzylic proton coupling cross peaks are circled. The $^{3}J_{CH}$ coupling crosspeaks are due to the spin-spin couplings between the benzylic protons and the aromatic carbons that are adjacent to the $^{2}J_{CH}$ coupled quaternary aromatic carbons. This is referred to as $^{3}J_{CH}$

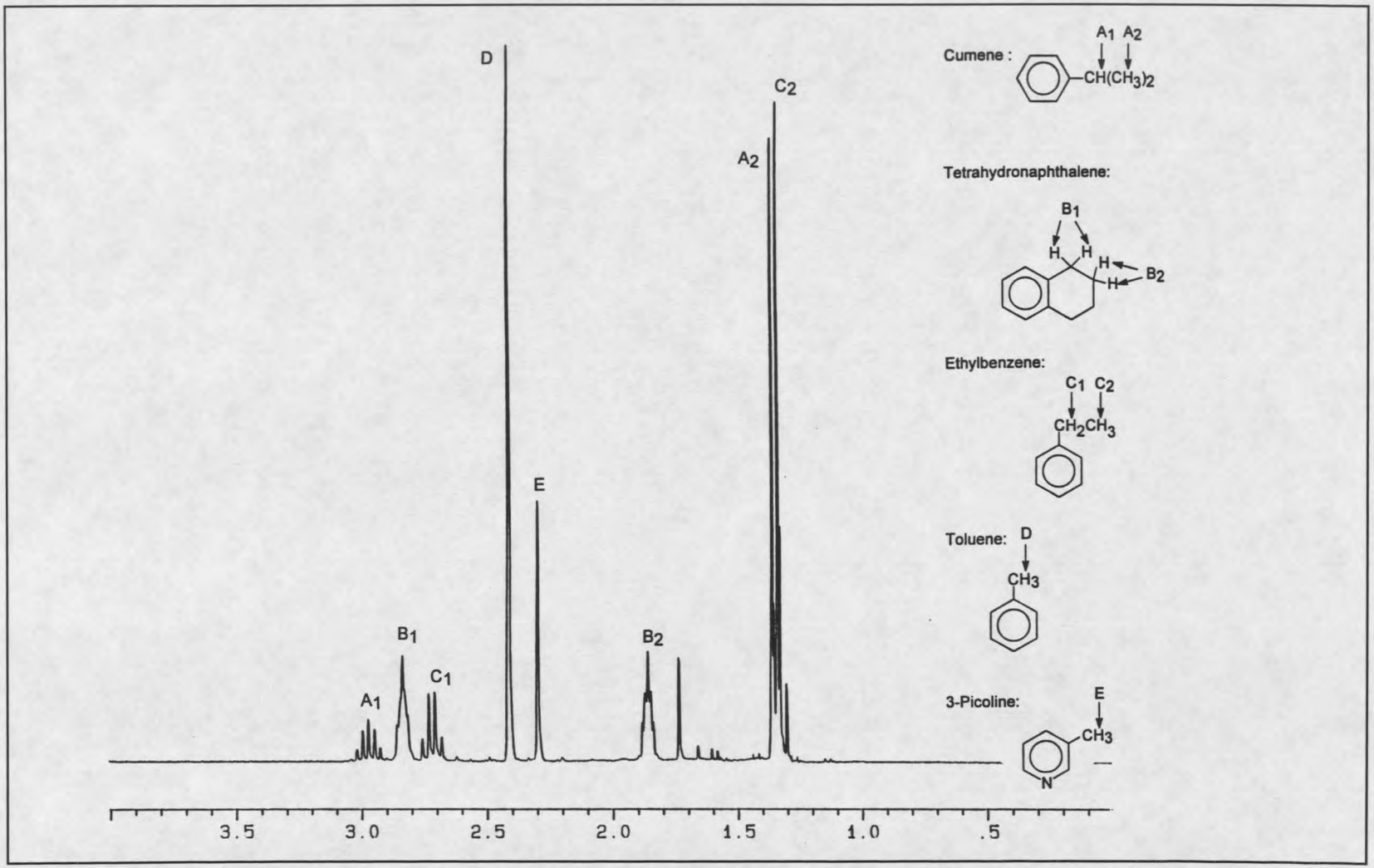

Figure 34. The ^{1}H NMR spectrum of the model compound mixture: cumene, tetrahydronaphthalene, ethylbenzene, toluene, and 3-picoline.

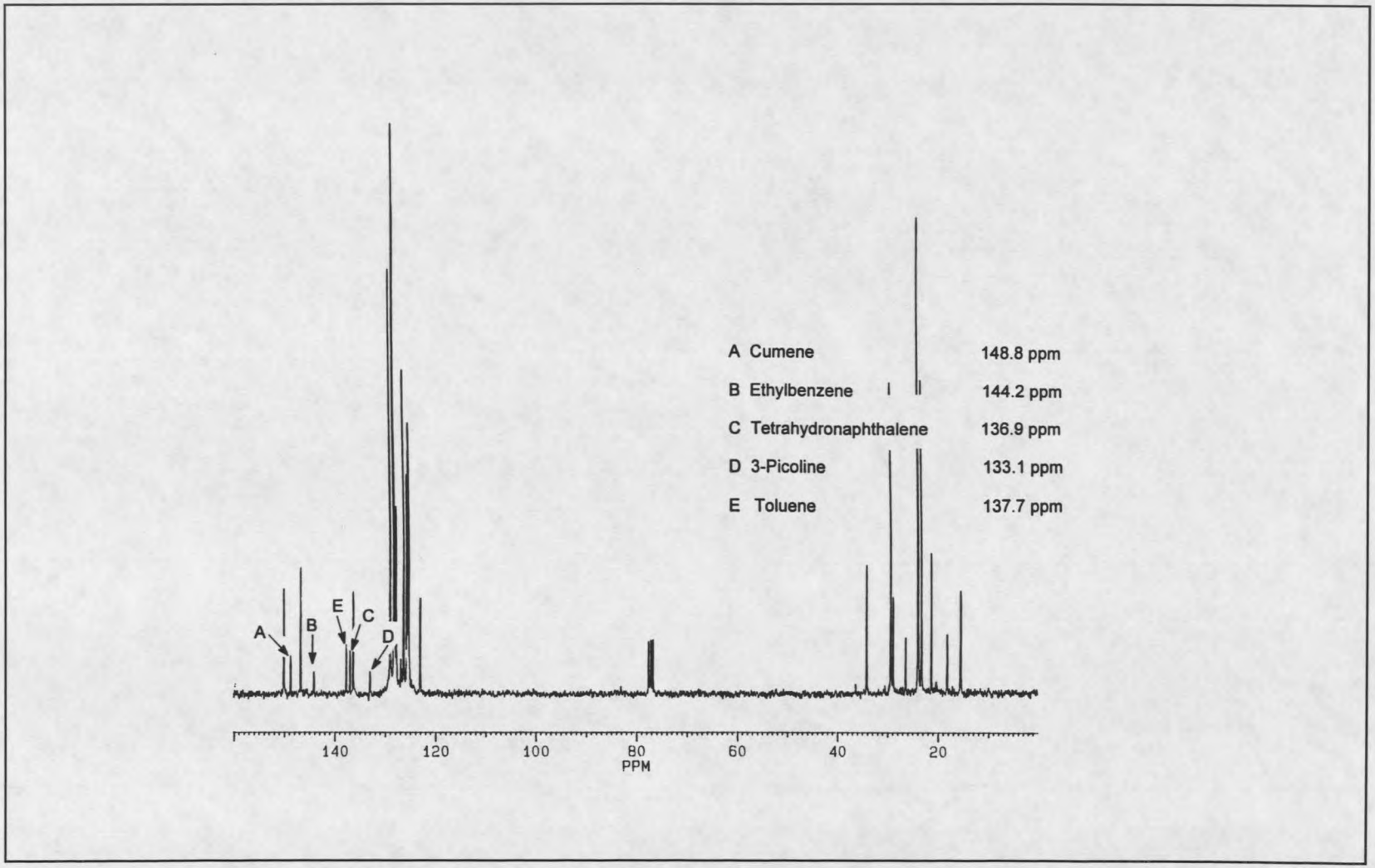

Figure 35. ^{13}C NMR spectrum of the model mixture showing the chemical shift of the quaternary aromatic carbons that are ^{2}J coupled with the benzylic protons in each of these compounds.

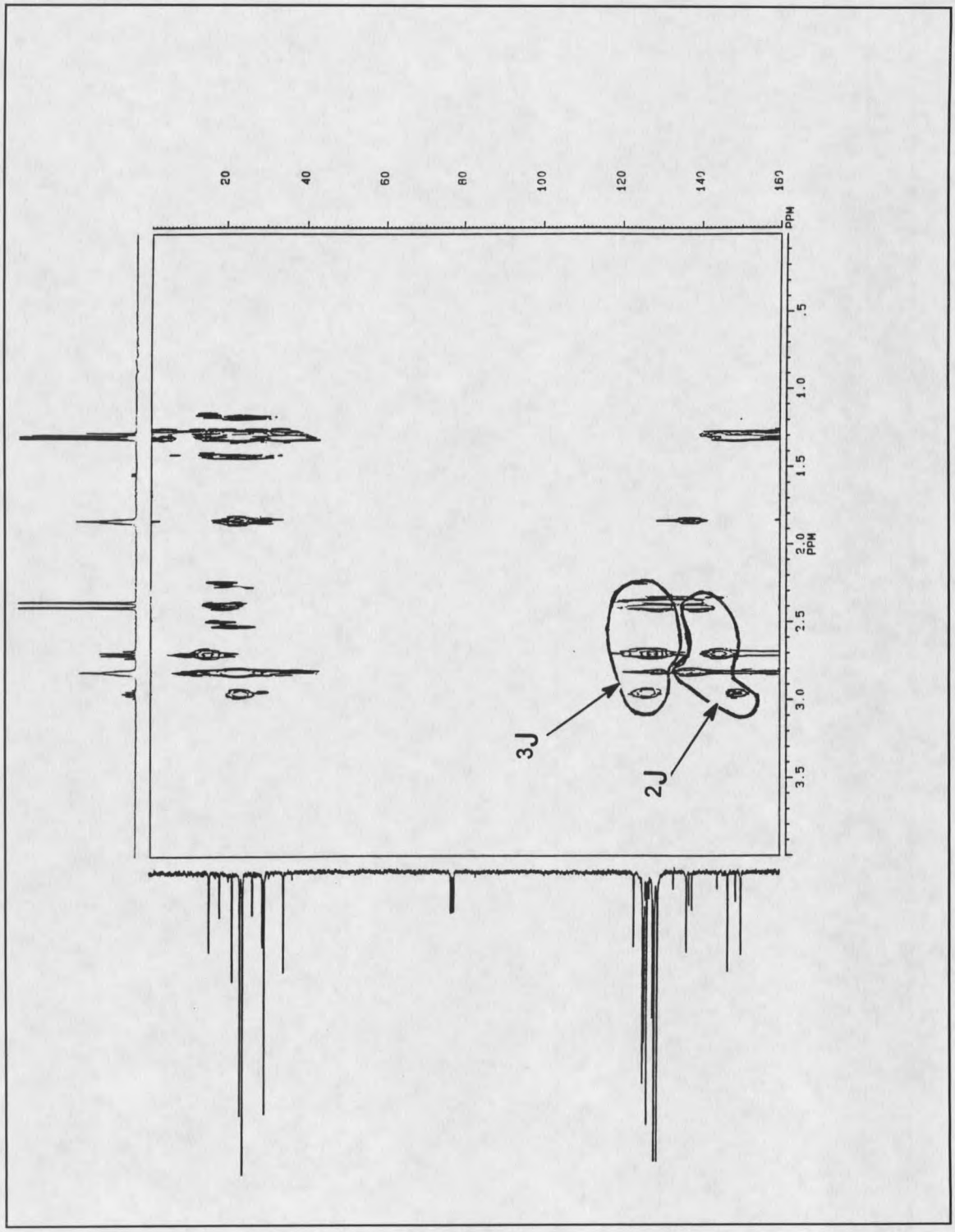

Figure 36. COLOC spectrum of the model mixture: toluene, 3-picoline, ethylbenzene, tetrahydronaphthalene, and cumene. ^{2}J and ^{3}J benzylic coupling cross peaks have been circled.

coupling because there are three intervening bonds between the two coupled nuclei.

This information turned out to be valuable because $^{2}J_{CH}$ and $^{3}J_{CH}$ benzylic coupling cross peaks were always present in the COLOC spectra of asphalt samples. However, until actually applying the COLOC experiment to a model system it was not known which of these cross peaks were due to benzylic proton asphalt $^{2}J_{CH}$ coupling. Figure 36 also shows other cross peaks whose coordinates are located in the region between 5 and 40 ppm along the ^{13}C axis and between 1 and 3.2 ppm along the ^{1}H axis. Although these peaks are not labeled, they are due to the aliphaltic/aliphaltic $^{2}J_{CH}$ and $^{3}J_{CH}$ coupled nuclei in asphalt and are not important to this work.

Comparison Between COLOC Spectra of Aged versus Unaged Asphalts

By locating the benzylic proton and the quaternary aromatic carbon chemical shifts to identify the $^{2}J_{CH}$ and $^{3}J_{CH}$ cross peaks in the COLOC spectrum of a model system made it easier to understand the COLOC spectrum of an asphalt.

Figure 37 shows the $^{2}J_{CH}$ and the $^{3}J_{CH}$ benzylic coupling cross peaks as well as the three benzylic proton shifts corresponding to methyl (at 2.31ppm), methylene (at 2.51ppm), and methyne (at 2.7ppm) in an asphalt sample.

Also seen in Figure 37 are the aliphaltic/aliphaltic $^{2}J_{CH}$ and $^{3}J_{CH}$ cross

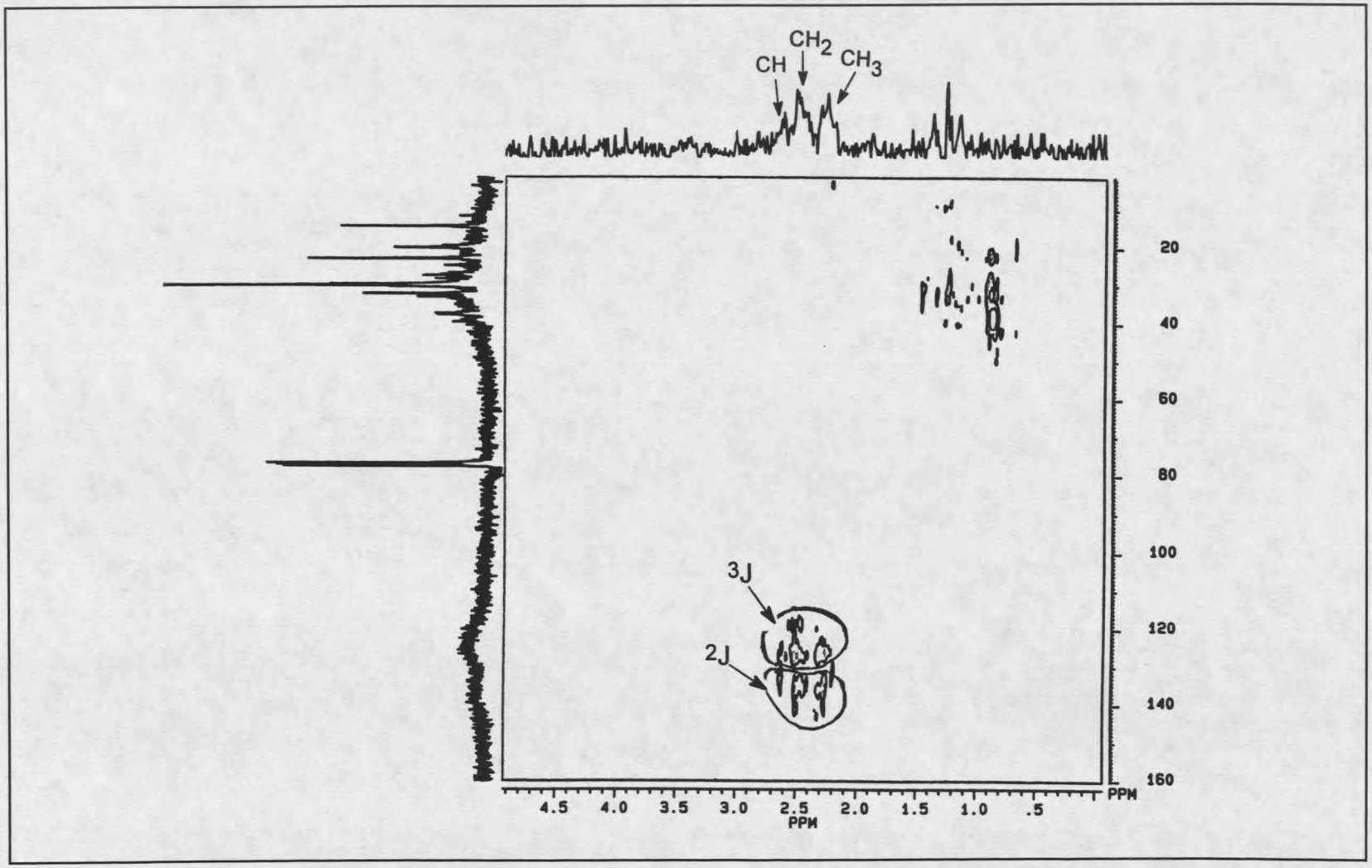

Figure 37. ^{2}J and ^{3}J couplings are shown in an asphalt sample as well as the benzylic CH, CH_2, and CH_3 ^{1}H chemical shifts.

peaks in the upper right-hand corner of the 2D spectrum. This spectrum is typical for all those of asphalt. No cross peaks, other than the ones shown in Figure 37, are ever seen which supports the premiss that asphalts are comprised mostly of polyaromatic hydrocarbons bearing aliphaltic substituents. Hence, aromatic/benzylic and aliphaltic/aliphaltic $^{2}J_{CH}$ and $^{3}J_{CH}$ coupling cross peaks are then the only ones expected in the COLOC spectra of asphalt.

Asphalt samples were chosen to observe any changes in the benzylic cross peaks upon aging. The asphalt samples chosen for this experiment where selected from a series of experimental asphalts previously used in an extensive nationwide study, the Strategic Highway Research Program (SHRP).(Appendix) The following asphalt samples were selected: AAA-1, AAB-1, AAC-1, AAD-1, AAF-1, AAG-1, AAK-1, and AAM-1. In addition, Western Research Institute (WRI), Laramie, Wyoming, provided laboratory aged SHRP asphalts. The aging technique used was the combined Thin Film Oxygen(TFO)/Pressure Oxygen Vessel (POV) method described in the Introduction.

The resulting 2D spectra (not shown here) did not neccessarily show that the WRI aged asphalts contained fewer benzylic protons than the unaged samples. The TFO/POV laboratory aging methods are supposed to mimic the actual road aging of asphalt. And, if it is true that road aging oxidizes benzylic carbons in asphalt via autoxidation (3), then one would have expected to observe a decrease in, or even the disappearance of aromatic quaternary

carbon/ benzylic proton $^2J_{CH}$ cross peaks after the TFO/POV aging. However, the opposite trend was observed in some of the aged samples where all of the $^2J_{CH}$ benzylic cross peaks increased in intensity. In other cases, methylene benzylic ^1H cross peaks increased in intensity whereas methyl benzylic ^1H cross peaks decreased in intensity upon aging. Perhaps the TFO/POV aging methods did not provide the proper conditions to promote benzylic carbon autoxidation in asphalt. In order to support the premise that autoxidation occurs at the benzylic carbon site in asphalt (3), an experiment was performed using hydrogen peroxide (H_2O_2) as the oxidant and SHRP AAA-1 as the benzylic carbon containing asphalt. The results of this experiment would be used as a contrast for comparison with the SHRP TFO/POV aged asphalt COLOC results. If H_2O_2 could oxidize benzylic carbons in asphalt, then the above stated premise would be more convincing.

Figures 38, 39, and 40 show the 2D COLOC spectra of AAA-1 (unaged), AAA-1 (TFO/POV), and AAA-1 (H_2O_2 oxidized) asphalts, respectively. In Figure 39 of TFO/POV aged AAA-1, it can be seen that the benzylic $^2J_{CH}$ coupling cross peak intesities have increased as compared to those of unaged AAA-1 shown in Figure 38. In contrast, as shown in Figure 40, the $^2J_{CH}$ benzylic coupling cross peaks have decreased in overall intensity in H_2O_2 oxidized AAA-1. Yet, one can still see $^2J_{CH}$ cross peaks associated with the methyl groups supporting the fact that methyl benzylic protons are the most difficult to oxidize because of the stability of the free-radical intermediate by hyperconjugation.

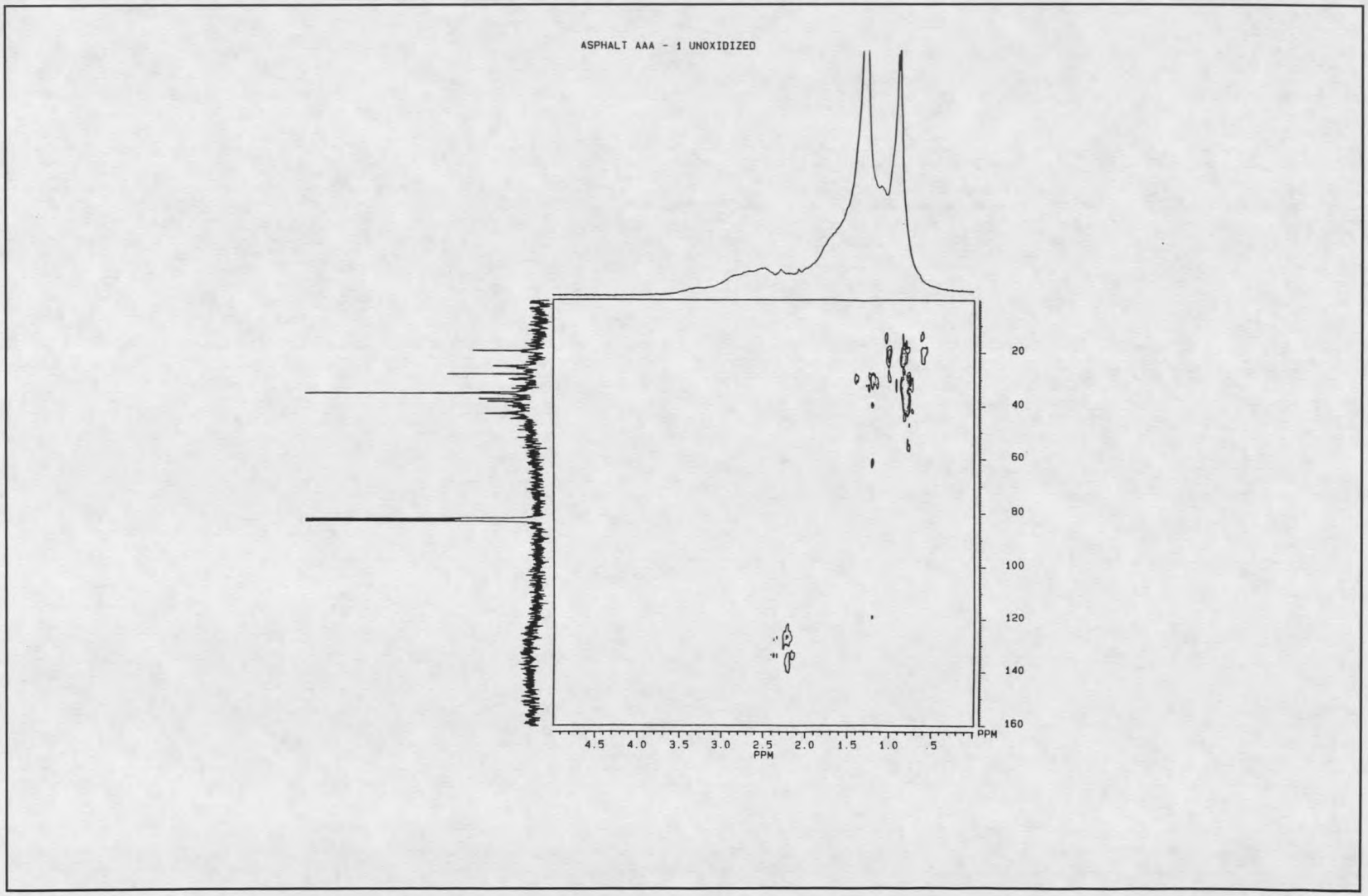

Figure 38. COLOC 2D spectrum of unaged SHRP asphalt AAA-1.

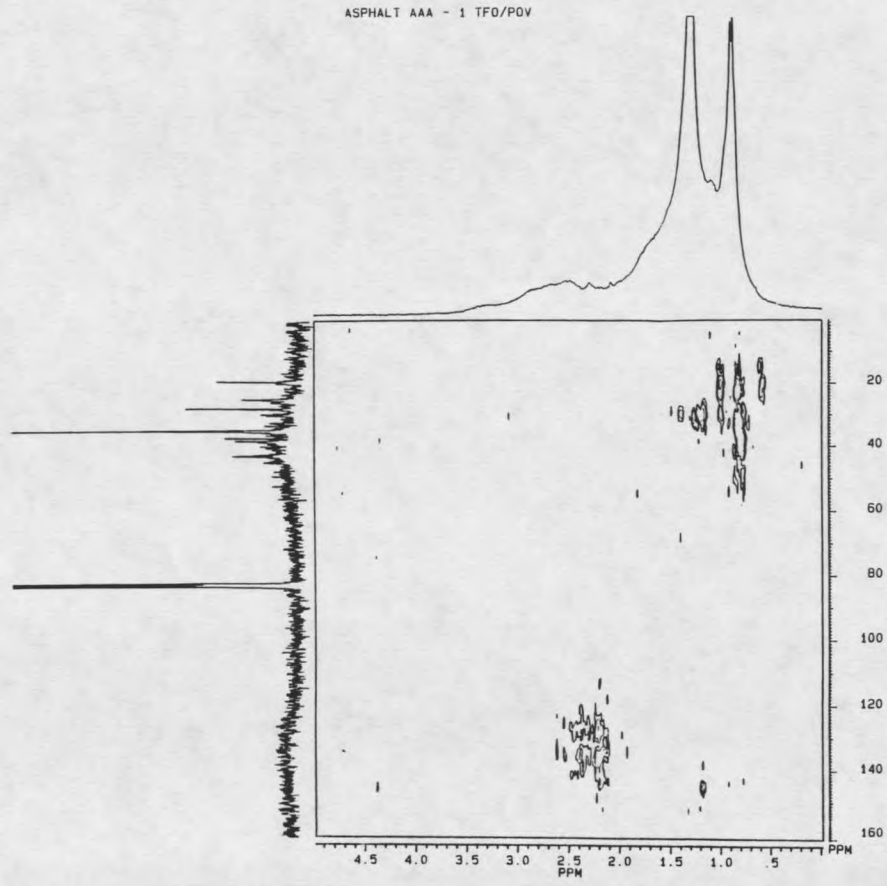

Figure 39. COLOC 2D spectrum of TFO/POV aged SHRP asphalt AAA-1.

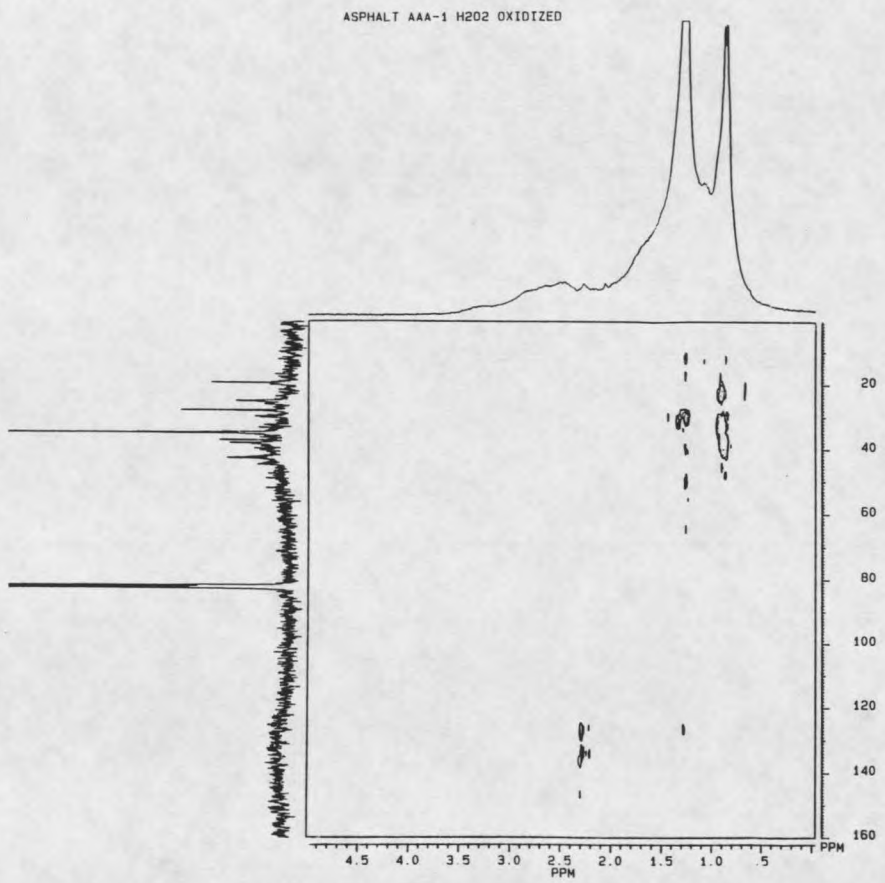

Figure 40. COLOC 2D spectrum of H_2O_2 treated SHRP asphalt AAA-1.

IR spectra of AAA-1, AAA-1 (TFO/POV), and AAA-1 (H_2O_2 oxidized) asphalts were obtained in order to show that carbonyls were formed during the H_2O_2 experiment. If so, one would expect to observe a corresponding increase of the carbonyl stretch absorbance for asphalt at 1700cm^{-1} in the infrared spectrum. Figure 41 shows superimposed IR spectra of the carbonyl stretch region of the three AAA-1 samples. It is seen that the carbonyl stretch absorbance progressively increases from low absorbance in AAA-1 unaged (labeled 1) to a maximum absorbance in H_2O_2 oxidized AAA-1 asphalt (labeled 3). These observations do not explain the mechanism of the formation nor the type of carbonyls formed in asphalt, however the combined results of the disappearance of the benzylic $^2J_{CH}$ coupling cross peaks plus the marked increase of carbonyl IR absorbance upon the H_2O_2 oxidation suggests that benzylic carbons in asphalt can be oxidized, if only partially, under certain conditions. This is not to say that the H_2O_2 method mimicked actual road aging, but it did support the fact that the WRI laboratory aging method was too mild to completely oxidize benzylic carbons in asphalt.

Gel Permeation Chromatograms were obtained for AAA-1, AAA-1 (TFO/POV), and AAA-1 (H_2O_2 oxidized) asphalt samples to observe differences between them. Figure 42 shows their superimposed chromatograms detected at 230 nm wavelength. One can see a steady increase in the intensity of the Large Molecular Size (LMS) region (between 15-20 min) starting from AAA-1 unaged (labeled 1) to AAA-1 TFO/POV (labeled 2) up to a maximum in AAA-1

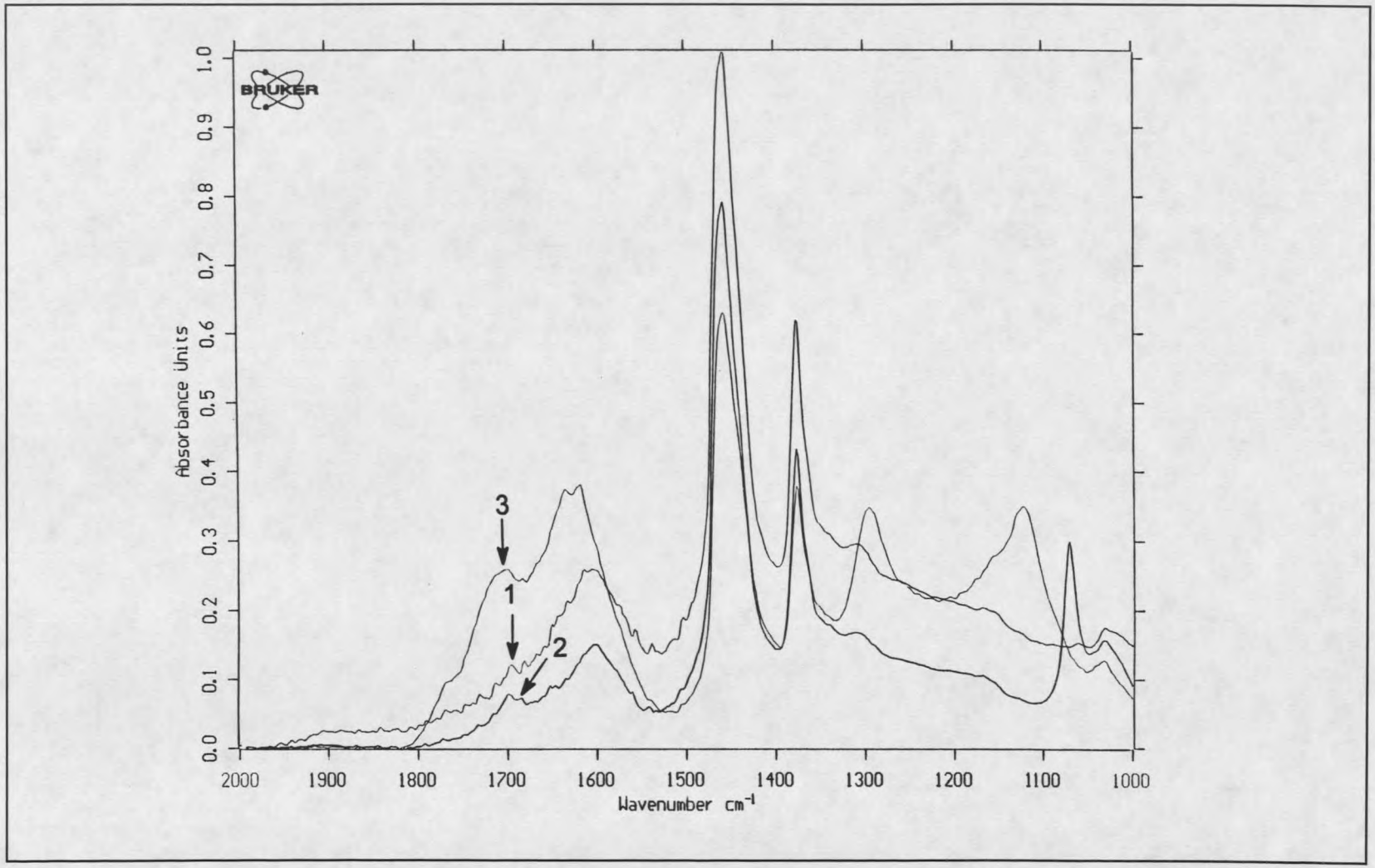

Figure 41. Three superimposed IR spectra showing the emergence of the carbonyl stretch from 1) AAA-1 unaged to 2) AAA-1 TFO/POV aged to 3) AAA-1 H_2O_2 oxidized SHRP asphalt.

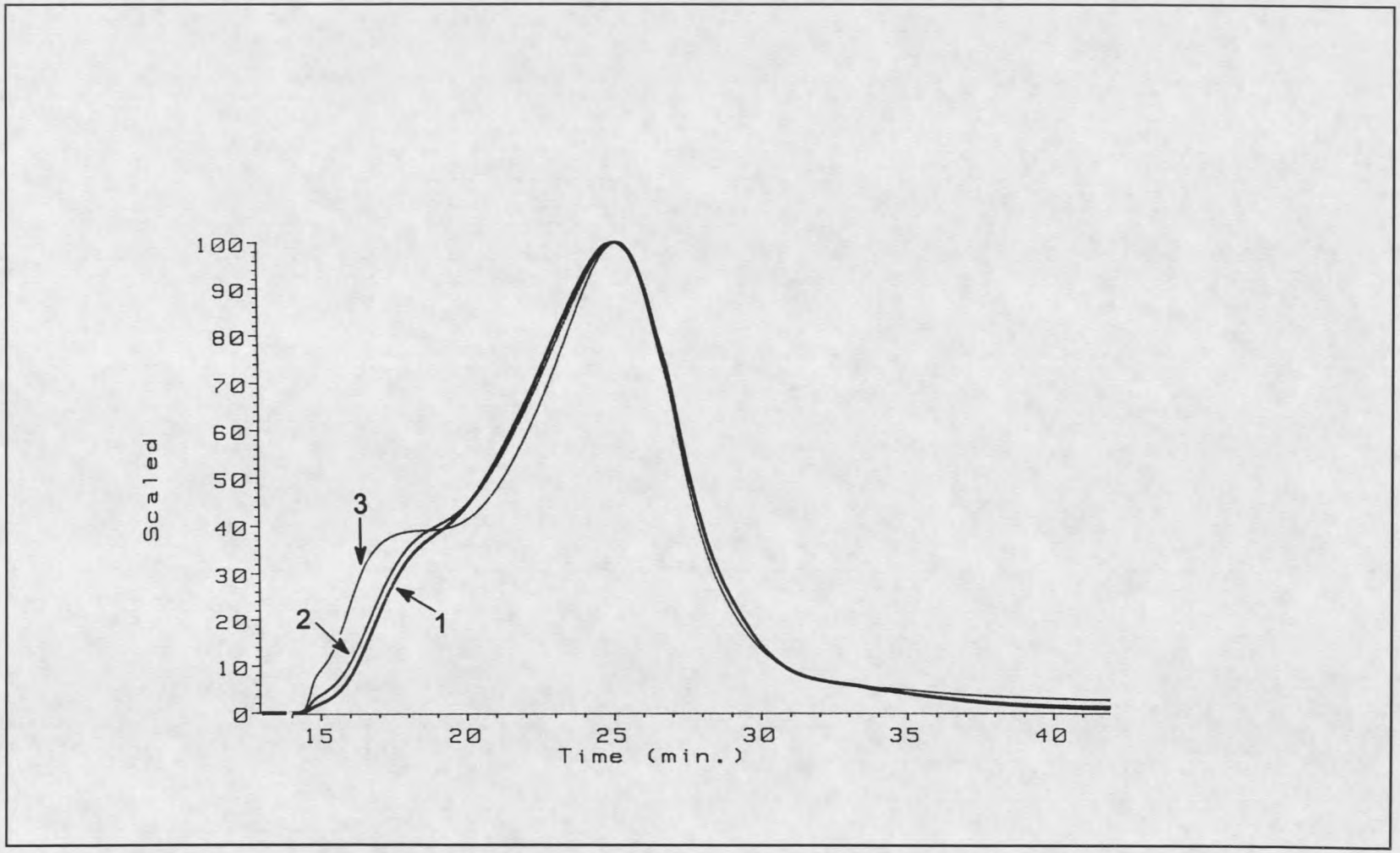

Figure 42. Three superimposed Gel Permeation Chromatographs shown at 230 nm detection of 1) AAA-1 unaged to 2) AAA-1 TFO/POV aged to 3) AAA-1 H_2O_2 oxidized SHRP asphalt. The Large Molecular Size (LMS) region is shown to increase progressively.

H_2O_2 oxidized (labeled 3). This trend supports the idea that self-assembly of asphalt molecules increases upon the production of more polar functional groups which in turn are manifestations of aging. This result is also consistent with the premise that benzylic carbons in asphalt are oxidizable.

Relative Quantitation of Benzylic Protons

Due to the complex nature of 2D NMR experiments, which do not remove interferences such as Nuclear Overhausser Effects (NOEs), It was doubtful that the exact concentration of benzylic protons could be calculated using the COLOC technique. NOEs have a non-quantitative effect on NMR peaks. Nonetheless, an experiment was carried out to prove whether or not benzylic protons could indeed be quantified. A solution made of known concentrations of two benzylic proton bearing model compounds was pipetted into an NMR tube. The two compounds were 9,10-dimethylanthracene and 2,6-dimethylphenol. Figure 43 shows the resulting COLOC spectrum. By extrapolating down into the 2D spectrum from the peak labeled A for the benzylic protons of 9,10 DMA, one can locate its corresponding benzylic $^2J_{CH}$ cross peak. And, by proceeding in the same fashion as above with the peak labeled B for the benzylic protons in 2,6 DMP, one will locate its corresponding benzylic $^2J_{CH}$ crosspeak. The benzylic proton 1D peak A was used to attempt to back calculate the concentration of benzylic protons in peak B. This

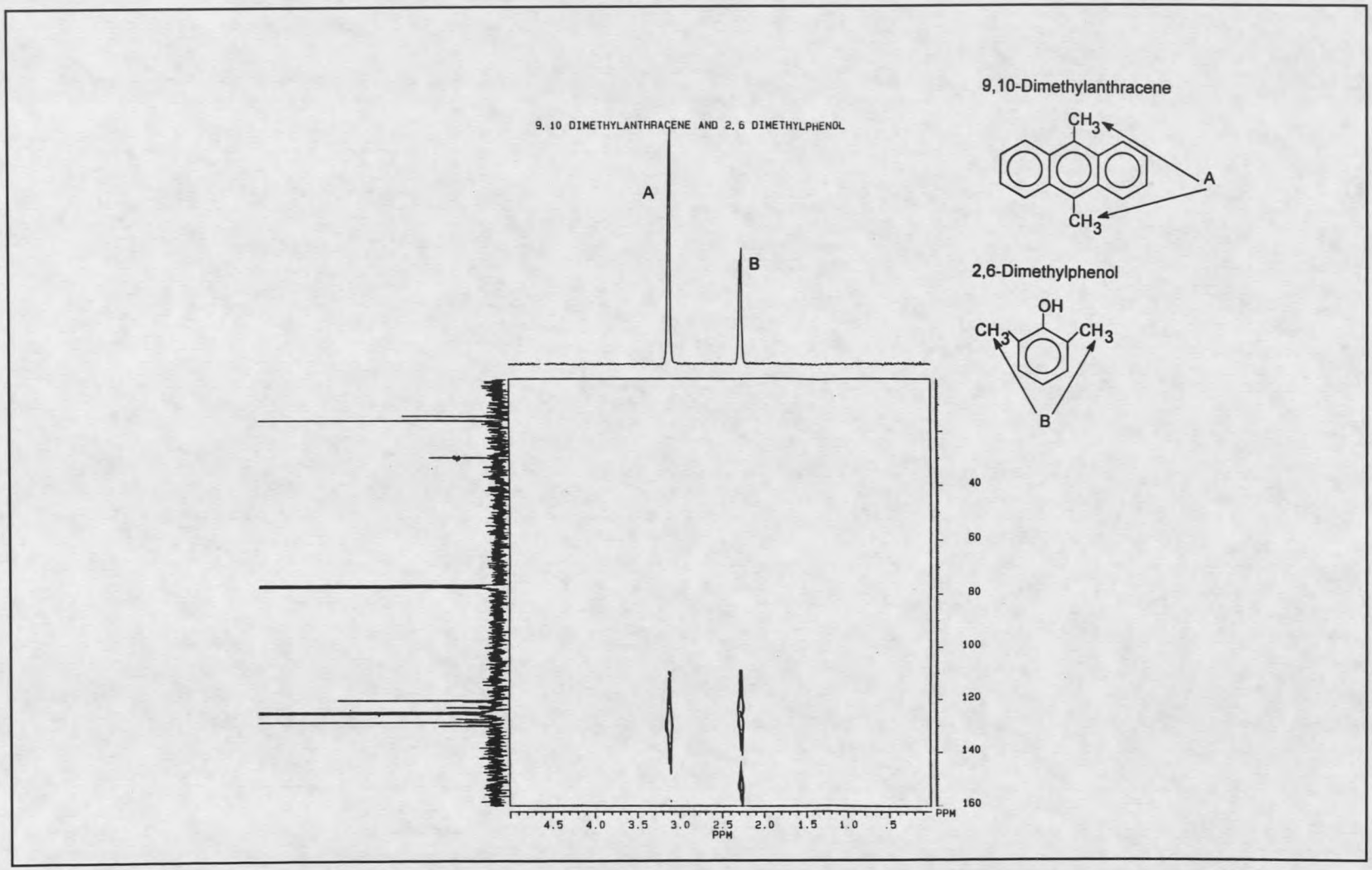

Figure 43. COLOC spectrum showing the ^{2}J couplings of the benzylic protons to the quaternary aromatic carbons of 9,10-dimethylanthracene and 2,6-dimethylphenol.

calculated value was then compared to the "true" value. Unfortunately, the calculated value for 2,6 DMP was 56% less than the true value. Indeed, the error here was large. However, having established that actual benzylic proton concentration could not be calculated using a standard was not a complete deterrent. There was still an alternative solution. A standard benzylic proton peak could still be used, not as a quantitative standard, but as a standard that could be employed as a constant to compare relative differences between the benzylic proton peak area of unaged versus aged asphalts. It was decided that 9,10 DMA, whose benzylic proton peak is at 3.12 ppm, would be used as the relative standard because its chemical shift is sufficiently down-field from those in asphalt to not interfere by overlapping with them. An indirect method for observing the effects that road aging has on the benzylic proton peak area in asphalt COLOCs was now possible. The benzylic protons were measured by obtaining the ratio of the benzylic proton peak area of the 9,10 DMA to the peak area of the benzylic protons in both unaged and aged asphalt samples. If, for example, this peak ratio value decreased upon aging, then one could assume a decrease of benzylic protons. The proton 1D peak projections from the COLOC experiments were used for this.

To demonstrate that the relative standard method could be used to compare two separate 2D experiments, the COLOC experiment was repeated using the same sample (AAG-1 TFO/POV with 9,10 DMA). However, both experiments were carried out using different NMR probes: an inverse probe,

and a broadband probe. Essentially, one should be able to run the COLOC experiment on both probes. The only difference that should be observed between the two experiments would be a loss of S/N when using the normal broadband probe due to the reversed positions of the proton and the broadband coils around the probe. In the inverse probe, the proton coil is located closer to the sample. And, by being closer, the sensitivity to ^{1}H NMR signals is enhanced. If the ratios were duplicated by repeating the COLOC experiment using a different probe of lower sensitivity, then this would be reassurance that the use of a relative standard was a valid methodology for relative quantitation. After running the COLOC experiment on the same sample twice, using the two probes, the peak area ratios of the 1D proton projections of the 9,10 DMA and the AAG-1(TFO/POV) were compared. Table 10 lists the benzylic proton peak ratios and the S/N ratios obtained from both probes.

Table 10. COLOC validation test using both a broadband and an inverse probe.

Probe Used	AAG-1(TFO/POV) to 9,10 DMA Peak ratio	Signal to Noise Ratio S/N
Inverse	2.93	16.525
Broadband	3.00	6.650

The S/N of the proton projection obtained when using the normal broadband was roughly 40% of that obtained when using the inverse probe. Nonetheless, the ratio of the integrations, differing by only 2.3%, is sufficiently

close to validate the reasoning that; if the results were reproducible using a different probe, then conversely, one could certainly make relative quantitative comparisons by repeating the experiment using the same probe.

Relative Quantitation of Benzylic Protons in Asphalt A series of COLOC experiments were run using the SHRP unaged and TFO/POV aged asphalts using the 9,10 DMA internal benzylic proton relative standard. The samples used were those designated as: AAA-1, AAB-1, AAC-1, AAD-1, AAF-1, AAG-1, AAK-1, and AAM-1. A COLOC was also taken of the previously hydrogen peroxide (H_2O_2) AAA-1 treated sample. In addition, COLOCs were obtained for an actual road aged asphalt and its unaged counterpart. This particular asphalt was among a series of asphalts which were used to pave experimental road test sections near Big Timber, Montana. This experiment was conducted by Jennings *et al.* (61). Twenty asphalt pavement test sections were included in this highway test experiment. Four sections contained one each of four asphalts from various refineries and one section contained a blend of two Montana asphalts. Twelve sections contained one of the four original asphalts mixed with one each of the following additives: fly ash, hydrated lime, or a chemical antistripping agent. The last three sections contained one of the original asphalts mixed with a commercial manganese compound (Chemcrete), mixed with carbon black, and the same asphalt of a different hardness.

Core samples were taken yearly from 1983 to 1986. The asphalt was

then removed from the aggregate by dissolving it in THF and studied using Gel Permeation Chromatography (GPC). The number of transverse cracks and ruts in each test section were also counted yearly and comparisons of the actual physical data versus the GPC data were applied towards determining the variances of asphalt pavement durability depending upon the asphalt source and/or its additive.

The road aged Big Timber asphalt sample that was used for the COLOC experiment was chosen based upon two reasons. First, the cores were each split in half resulting in a lower and an upper half. The top half was the core segment that had been exposed to more oxygen, and UV light. Oxygen is a necessary reactant in autoxidation and UV light is a potential autoxidation initiator. Second, the greatest physical degradation was observed in the last core samples taken in 1986. Therefore, it was decided to run a COLOC experiment using the top half of the core taken in the last year of sampling. The Big Timber asphalt sample that was chosen for this experiment exhibited the most severe cracking (TG18). A COLOC was also taken of its unaged counterpart (T18). Also chosen was a non road aged sample of this asphalt mixed with Chemcrete. Chemcrete is known to contain MnO_2 which is a very strong oxidant and could very possibly oxidize benzylic carbons without the assistance of road weathering.

The results are shown in Table 11 which shows that the SHRP asphalts again, gave mixed results when comparing the unaged versus the TFO/POV

aged samples. Plus or minus percent changes in peak area ratios are reported, in parentheses, next to the aged ratio data in Table 11. Most of the SHRP asphalts showed an increase in benzylic protons upon the WRI aging process and only two others (AAB-1 and AAM-1) showed a decrease. However, the AAA-1 H_2O_2 treated sample showed a substantial decrease of 41% in benzylic proton peak area. However, a considerable decrease of 25% in the benzylic protons was observed in the TG18 core sample. And an even more notable benzylic proton decrease of 41% was observed in the Chemcrete mixture.

IR spectra were obtained for all of the asphalts used in the COLOC study to compare the increase in the concentration of the carbonyl functional group upon both laboratory and road aging. A standard curve was made shown in Figure 44 using cyclododecanone to calculate the concentration of carbonyl per gram of asphalt (Table 11). There was an increase in the carbonyl concentration after both the laboratory and the road aging as well in the T18/Chemcrete mix. However, the most noticeable increases occurred in AAA-1(H_2O_2 treated), the TG18 core sample, and the Chemcrete mixture. The IR data shows that the carbonyl concentration does indeed increase after both laboratory and road aging but, this is not necessarily due to the autoxidation of benzylic carbons as shown by the COLOC data from the TFO/POV aged asphalts. Therefore, it appeared that the TFO/POV laboratory aging method did not support the accepted theory that asphalt aging oxidizes benzylic

Table 11. COLOC ^1H peak projection integration values for benzylic protons and carbonyl concentrations from IR data.

Asphalt	Aging	Peak Area Asphalt/9,10 DMA[a]	Carbonyl Conc. Mole C=O/g Asphalt
AAA-1	Unaged	2.80	2.86×10^{-6}
	TFO/POV Aged	3.04(+8.6%)	7.00×10^{-5}
	H_2O_2 Treated	1.15(-41%)	3.09×10^{-4}
AAB-1	Unaged	1.87	2.86×10^{-4}
	TFO/POV Aged	1.17(-37.4%)	3.2×10^{-4}
AAC-1	Unaged	1.76	1.11×10^{-4}
	TFO/POV Aged	1.99(+13.1%)	4.16×10^{-4}
AAD-1	Unaged	1.99	2.09×10^{-4}
	TFO/POV	2.30(+15.6%)	8.41×10^{-4}
AAF-1	Unaged	1.37	1.51×10^{-4}
	TFO/POV Aged	1.59(+16.1%)	3.39×10^{-4}
AAG-1	Unaged	2.24	2.99×10^{-4}
	TFO/POV Aged	2.93(+30.1%)	5.64×10^{-4}
AAK-1	Unaged	2.02	1.88×10^{-4}
	TFO/POV Aged	2.84(+40.6%)	4.32×10^{-4}
AAM-1	Unaged	2.1	1.58×10^{-4}
	TFO/POV Aged	1.65(-21.4%)	3.64×10^{-4}
Big Timber	Unaged	3.2	6.66×10^{-5}
	TG18 Aged	2.4(-25%)	2.52×10^{-4}
	With Chemcrete	1.89(-41%)	3.61×10^{-4}

a) The values in parenthesis show the percent change of benzylic proton peak area after aging or after treatment with H_2O_2 or upon addition of Chemcrete.

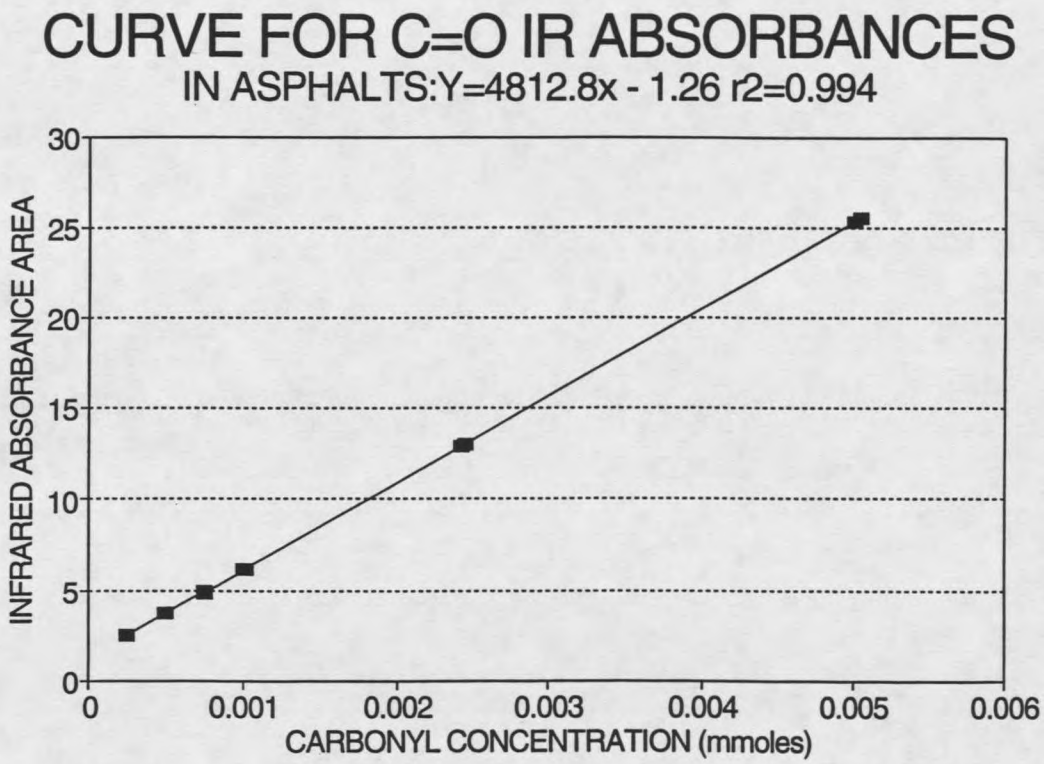

Figure 44. The dodecanone standard curve for the calibration of the IR carbonyl strech.

protons.

One possible explanation could be that the TFO/POV method does not actually mimic true combined short-term and long-term age weathering. Perhaps only partial oxidation occurred leaving asphalt molecules in various stages of oxidation. For example, Figure 45 shows some of the general reaction schemes that represent increases and decreases as well as changes in types of benzylic protons that could occur during TFO/POV aging.(3,22)

It is evident that although the TFO/POV method seems to cause chemical oxidation within asphalt, it does not neccessarily oxidize benzylic carbons. However, when exposed to strong oxidizing agents such as H_2O_2 and MnO_2 asphalt benzylic carbons appear to be oxidized. Actual road aging also appears to oxidize benzylic carbons, however to a lesser degree. It is difficult to determine the exact mechanism(s) by which asphalt benzylic carbons oxidize in either laboratory or road aged asphalts. This is especially true for road aged asphalts, where many indeterminant variables exist that could affect asphalt aging. However, what has been accomplished within the body of this work, is a unique methodology for observing real changes in the benzylic position after both the laboratory and road aging of asphalts.

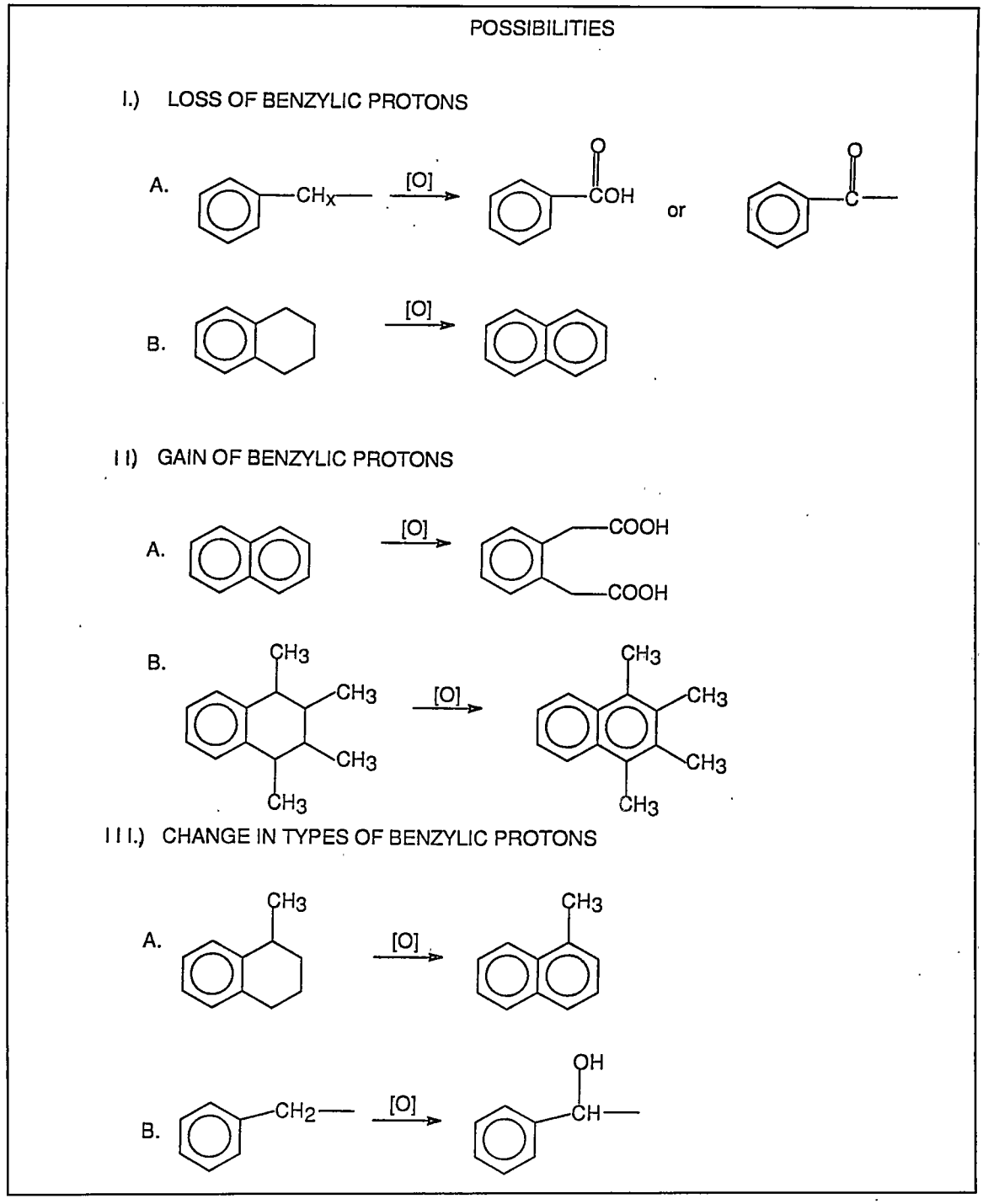

Figure 45. Simple model examples of possible products that could be forming upon the TFO/POV aging that might explain not only the disappearance of benzylic protons in the COLOC spectra, but an increase and/or change in the types of benzylic protons present in asphalt.

Laser Desorption Ionization Time-of-Flight Mass Spectrometry for Asphalt Characterization and Fingerprinting

General Discussion

In Matrix Assisted Laser Desorption Ionization Time-of-Flight Mass Spectrometry (MALDI/TOF MS), a solution containing both matrix and analyte is made. As the solvent evaporates, the analyte will co-crystalize with the matrix. As a result, the analyte molecules are surrounded by the solid matrix.(62) In order to isolate individual analyte molecules, the matrix is always used in considerable excess over the analyte from anywhere between 10^3 and 10^6 in excess. The exact role of the matrix is not completely known. However, it is clear that the aromatic matrix molecules are UV-absorbing and absorb sufficient laser energy for a successful desorption process. For mass analysis, Time-of-Flight (TOF) mass spectrometers are used. In TOF MS, all ions are accelerated to the same kinetic energy and made to travel in a vacuum, through a flight-tube of fixed length. Ions will travel at different velocities according to their mass to charge (m/z) ratio. Lighter ions will travel the distance more quickly than heavier ones. The flight time is directly proportional to the square root of the mass and can be calculated by using the following equation:

$$t = l(m/2KE)^{1/2}$$

where t is the drift time, l is the flight distance, m is the mass, and KE is the kinetic energy.

The MALDI TOF technique appears to be a novel approach for studying asphalt. The advantages of using MALDI TOF technology on asphalt seemed promising at the onset of this work. These advantages include:

> MALDI can analyze very large molecules with masses at least up to 400,000 Daltons (Da),
>
> MALDI TOF can simultaneously detect ions within the entire mass range in a sample,
>
> MALDI can analyze a wide variety of polymeric compounds.

The discovery of Laser Desorption, without a matrix, preceeds MALDI (62). The LD Ionization technique was also used in this study of asphalt, but was not considered as promising as MALDI mainly because of the claim that the LD method has an upper mass limit of only 1,000 Da.(52) Yet, the LD method has been successfully used to ionize molecules in coal (51), which are presumably much larger than 1,000 Da. Coal molecular masses up to 270,000 Da have been reported by John, *et al.*(54) Since molecules in coal are similar to those in asphalt, it was decided to also attempt the LD method on asphalt.

MALDI and Laser Desorption Ionization

Both the MALDI and LD ionization techniques were attempted on T18 unaged, TG18 road aged, and T18 H_2O_2 treated Big Timber asphalt.(61) For

the MALDI technique, dihydroxybenzoic acid (DHB) was selected as a suitable matrix for asphalt. DHB was chosen not only because it is aromatic, but because it is substituted with hydroxy and carboxylic acid groups. It has been well established that these two functional groups are found in asphalt. Thus, DHB would seem to be chemically similar to asphalt. The DHB matrix solution and the asphalt solution, prepared as described in the Experimental section, were co-deposited on the TOF sample plate. The solvents were then allowed to evaporate, leaving a solid solution of analyte molecules in matrix.

Asphalt samples were prepared for LD in two ways. In the first method, the asphalt was dissolved in THF, the solution was pipetted onto the sample plate, and the THF was allowed to evaporate. In the second method, the neat asphalt was deposited directly onto the sample plate. Figures 46, 47, and 48 show the MALDI and the LD mass spectra of T18, TG18, and H_2O_2 treated T18. The "neat" sample method was used for the LD spectra. The spectra using the THF dissolved method are not shown due to the fact that they were nearly identical to those obtained using the "neat" method.

General Spectral Features The mass spectra obtained using all three sample preparation techniques exhibited similar patterns. A typical LD spectral pattern for asphalt is exemplified by the T18 neat asphalt spectrum shown in Figure 46a. The mass range shown here is from 0 Da to 1,000 Da. In the low

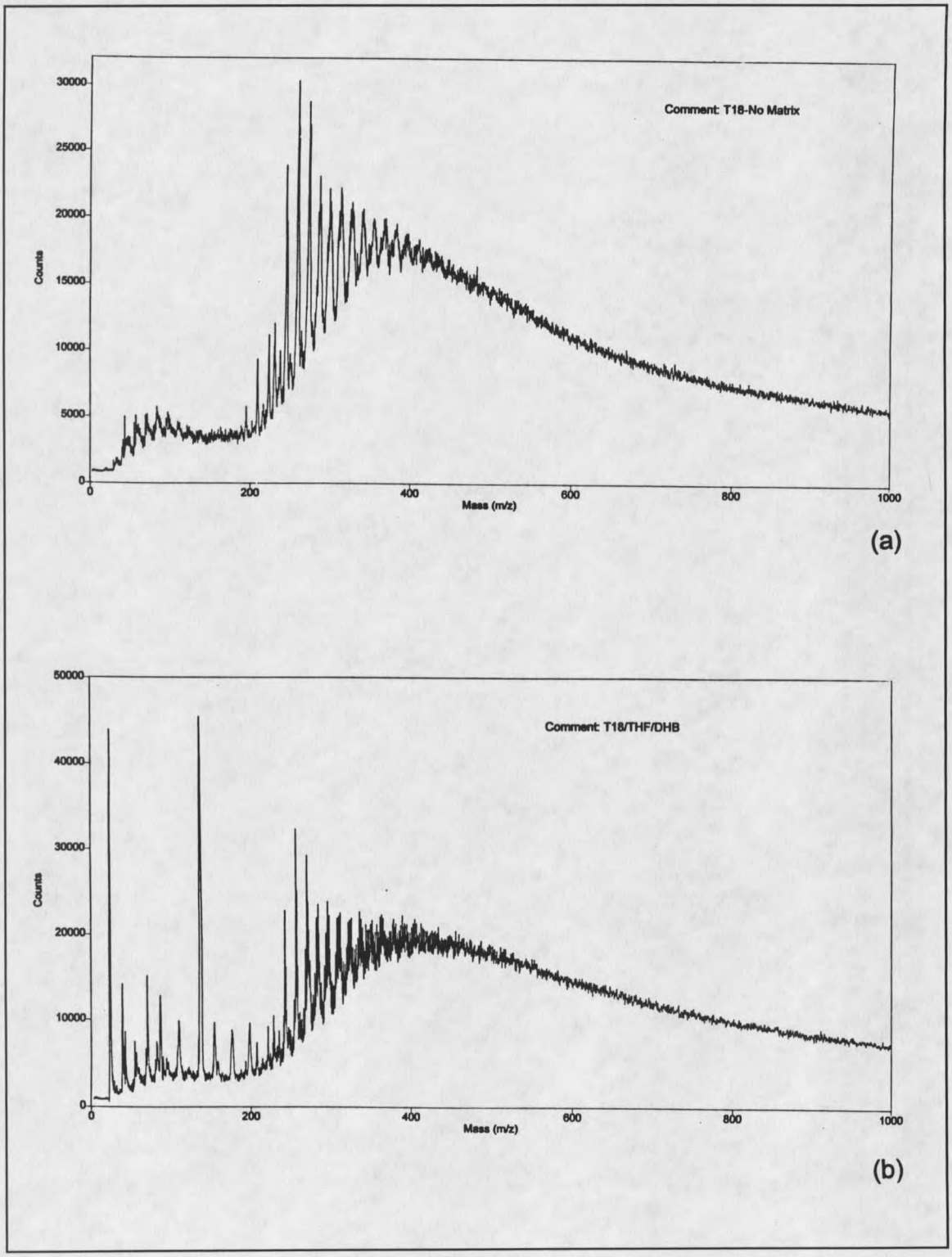

Figure 46. a.) LD spectrum of T18 without the use of a matrix molecule.
b.) LD spectrum of T18 using dihydroxybenzene matrix.

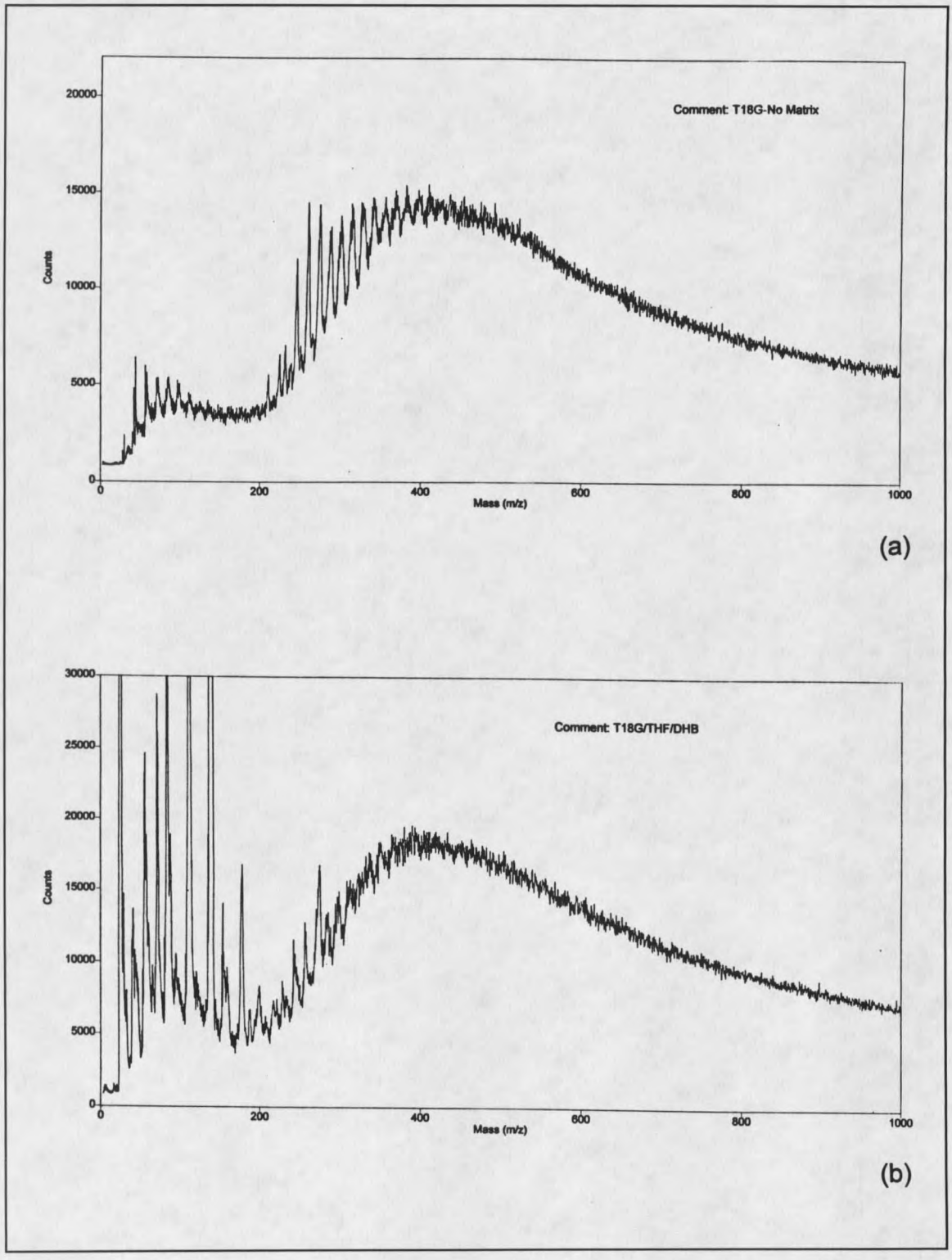

Figure 47. a.) LD spectrum of TG18 without the use of a matrix molecule.
b.) LD spectrum of TG18 using dihydroxybenzene matrix.

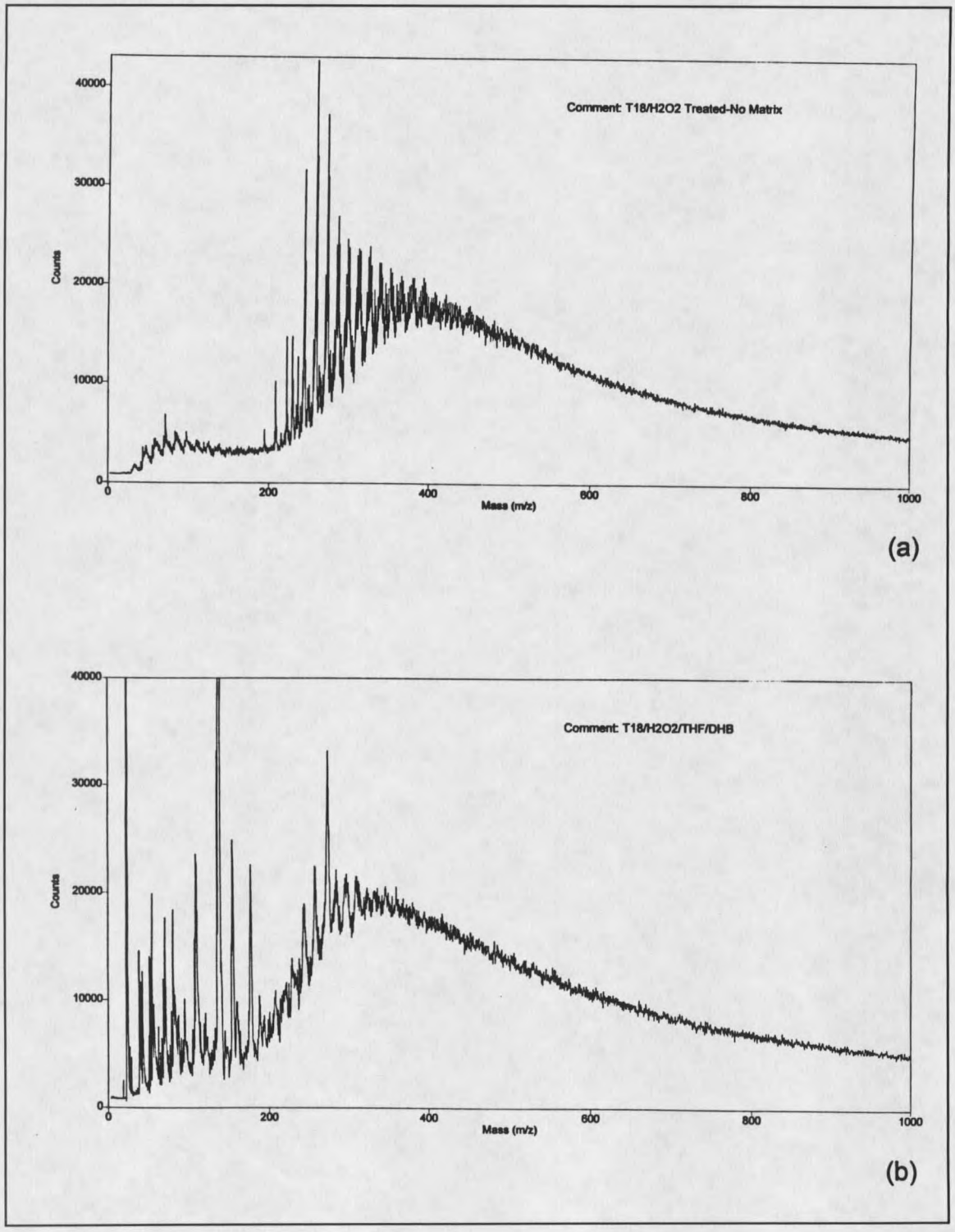

Figure 48. a.) LD spectrum of T18 (H_2O_2 treated) without the use of a matrix molecule. b.) LD spectrum of T18 (H_2O_2 treated) using dihydroxybenzene matrix.

mass range, from approximately 20 Da to 120 Da, one can see a broad, low intensity mass distribution out of which protrude several sharp peaks. An even broader mass distribution begins at about 200 Da, and it rises steeply from a low intensity to a maximum intensity at m_{max} at about 400 Da. The m_{max} value varies slightly between different asphalts. From m_{max}, the curve slopes downward with a lower gradient and flattens out at about 4,000 Da. The final feature in the LD spectrum is a pattern of sharp peaks which protrude out of the left shoulder of the broad mass distribution. This "peak progression" is shown in an expanded view from 190 to 390 Da in Figure 49. It is seen that the peaks are not completely resolved; there is considerable peak overlap.

What has just been described in terms of the whole asphalt LD spectral pattern will, from now on, be referred to as the typical "envelope" pattern.

Comparison between MALDI and LD It is of interest to compare the MALDI and the LD ionization techniques. One can see from the LD spectra in Figures 46a, 47a, and 48a that the mass resolution is superior to that obtained when using the MALDI technique in Figures 46b, 47b, and 48b. Not only is the mass resolution inferior in the MALDI spectra, but the many MALDI matrix peaks in the lower mass region interfere severely with the low mass curve that can be clearly seen in the LD spectra of typical asphalts. For instance, in the MALDI spectra, the peaks at 137 and 154 Da are due to the DHB matrix. There is also a very prominent sodium peak (23 Da) in all three MALDI spectra.

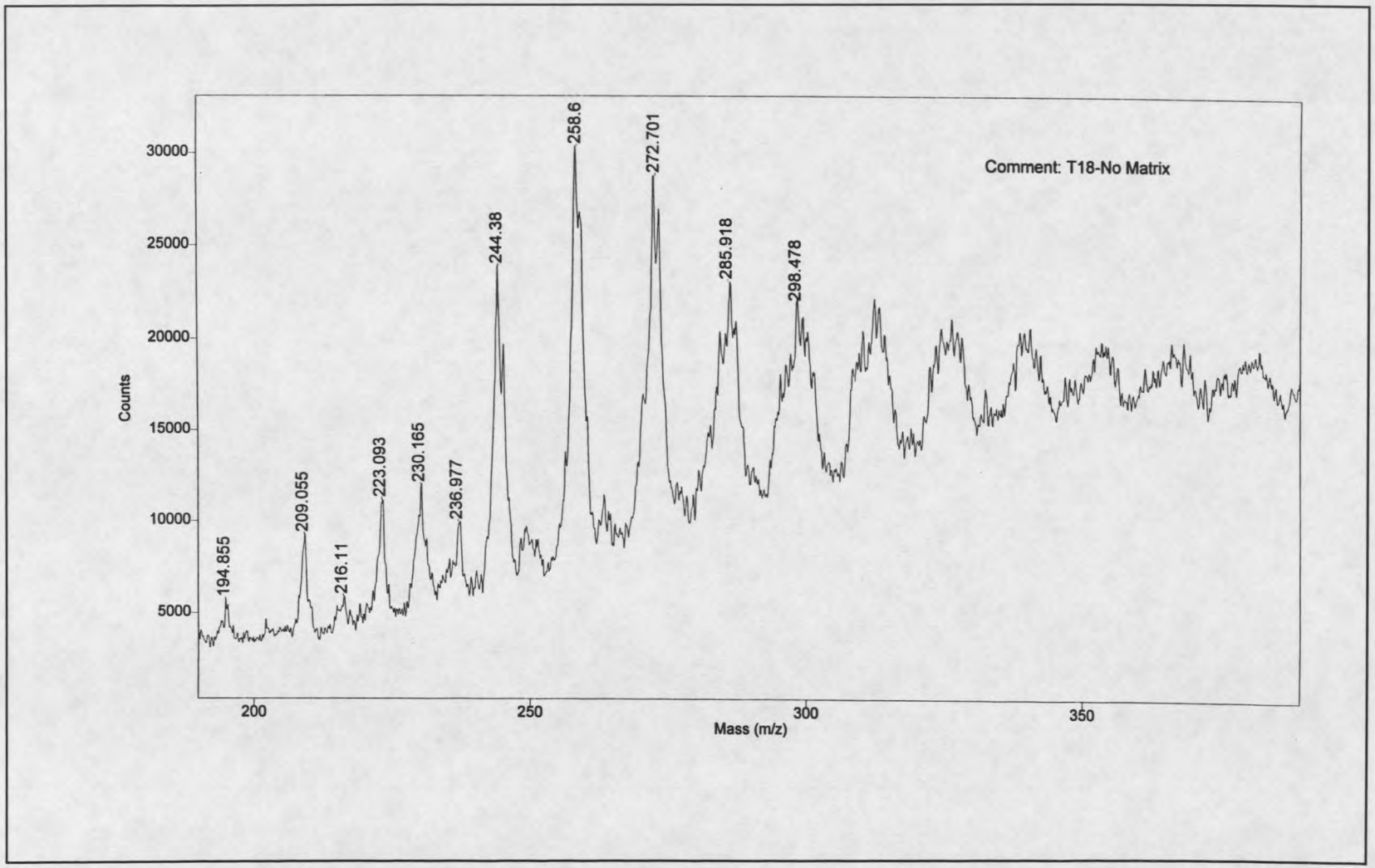

Figure 49. Magnified view of the LD spectrum of neat T18 asphalt showing the unresolved peaks off of the left side of the "broad" shoulder.

Another observation was the presence of abundant asphalt and MALDI matrix fragment ions in the low mass region, below 100 Da, in the MALDI spectra. The LD spectra showed a significantly lower abundance of fragment ions below 100 Da. These observations are surprising and interesting. MALDI is recognized to be a "softer" ionization technique than LD. In the case of asphalt, however, it appears that LD is softer than MALDI. Asphalt appears to serve as its own (liquid) matrix. One could term this "liquid MALDI". For these reasons, It was decided, that LD would be used for asphalt ionization. It can be seen that the two techniques give approximately the same mass distribution which is supportive evidence that these distributions are meaningful.

Ionization Processes in LD of Asphalt

Analyte ions are formed by three processes in laser desorption:

1. Cationization involving the formation of a sodium or potassium adduct ion of the analyte molecule M, $[M + Na]^+$, $[M + K]^+$.
2. Protonation of the analyte molecule M, $[M + H]^+$.
3. Electron abstraction forming the molecular ion, M^+.

In order to be able to interpret the LD mass spectra of asphalts, it is necessary to know which of these types of ions dominate the spectra. The problem of analyte ion formation was addressed in several ways. First, in order to determine whether any of the desorbed ion species was in the $[M + Na]^+$ state, coronene was doped with sodium chloride (NaCl). Also, a combination of

coronene and asphalt (AAD-1) was doped with NaCl. Figure 50 shows the LD mass spectrum of coronene doped with NaCl. The coronene molecular ion, M^+, is very intense, but there is no evidence of a coronene sodium adduct ion. Figure 51 compares the LD spectra of coronene spiked AAD-1 asphalt with and without added NaCl. The peak at 323 Da would have increased in intensity in Figure 51b if the sodium adduct ion of coronene was being desorbed. Indeed, no observable changes were seen in the mass spectrum of neat AAD-1 asphalt upon addition of NaCl. Carbazole, a nitrogen containing aromatic compound, was chosen to further investigate the ion formation processes. A mixture of coronene, carbazole, and AAD-1 asphalt was doped with NaCl, and, as shown in Figure 52, no sodium adduct $[M + Na]^+$ ions were observed. Instead, the major peaks were of coronene and carbazole molecular ions. Indeed, in all spiked asphalt spectra, the molecular ions dominated.

The conclusion was that the adduct $[M + Na]^+$ of small molecules in asphalt and small PAHs is not formed during LD. However, there was invariably a peak of much lower intensity at M + 1. Some, if not all of the M + 1 peak intensity was due to the isotope peaks of ^{13}C and ^{15}N in carbazole. However, some contribution to the M + 1 peak intensity was from the protonated molecular ion, $[M + H]^+$. To determine the isotope corrected abundance of $[M + H]^+$, an experiment was performed by spiking carbazole and pyrene into asphalt AAD-1. Equimolar amounts of 1.5×10^{-7} moles of carbazole

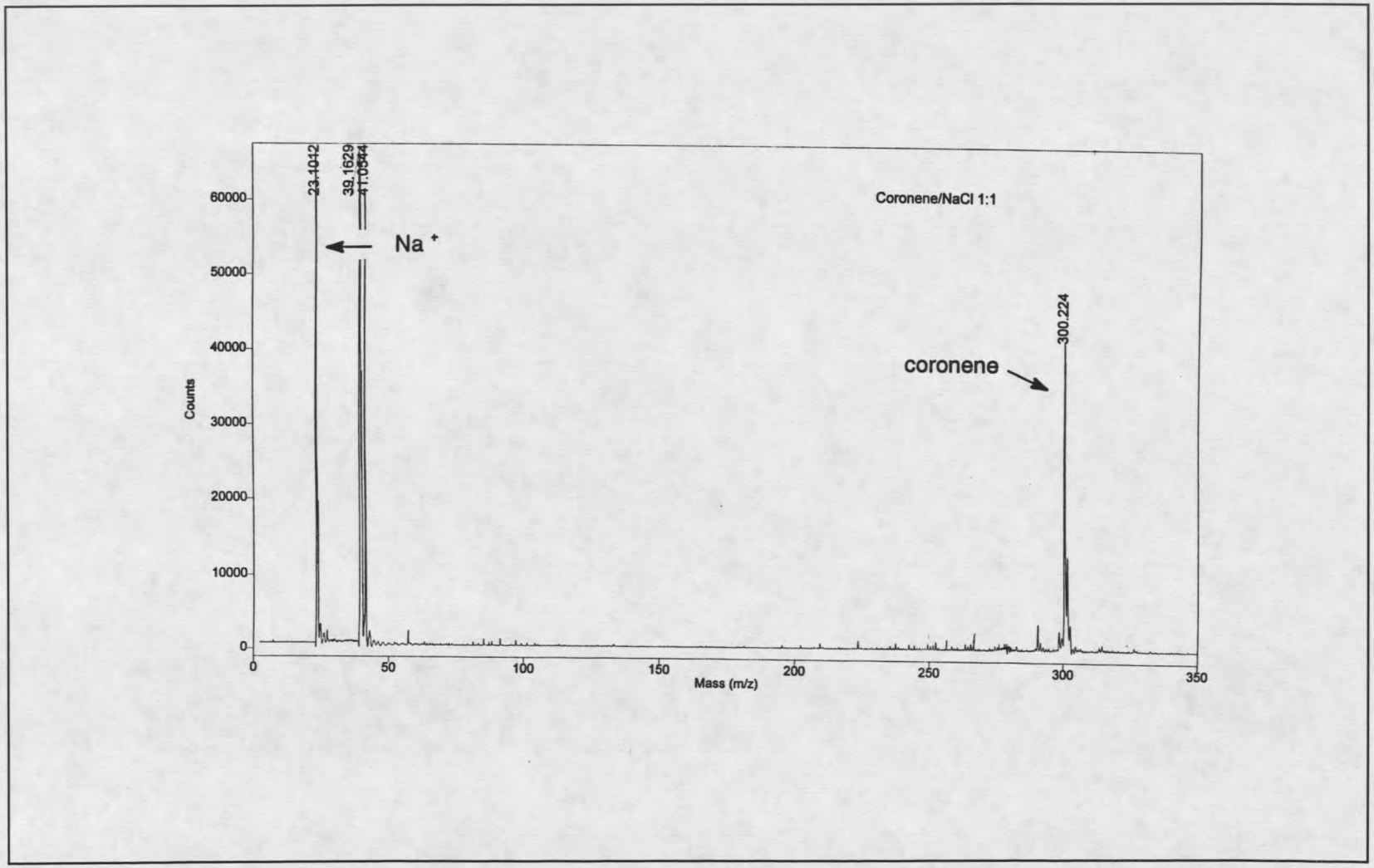

Figure 50. Coronene doped with sodium chloride (NaCl). There is no indication of a sodium adduct ion at 323 Da.

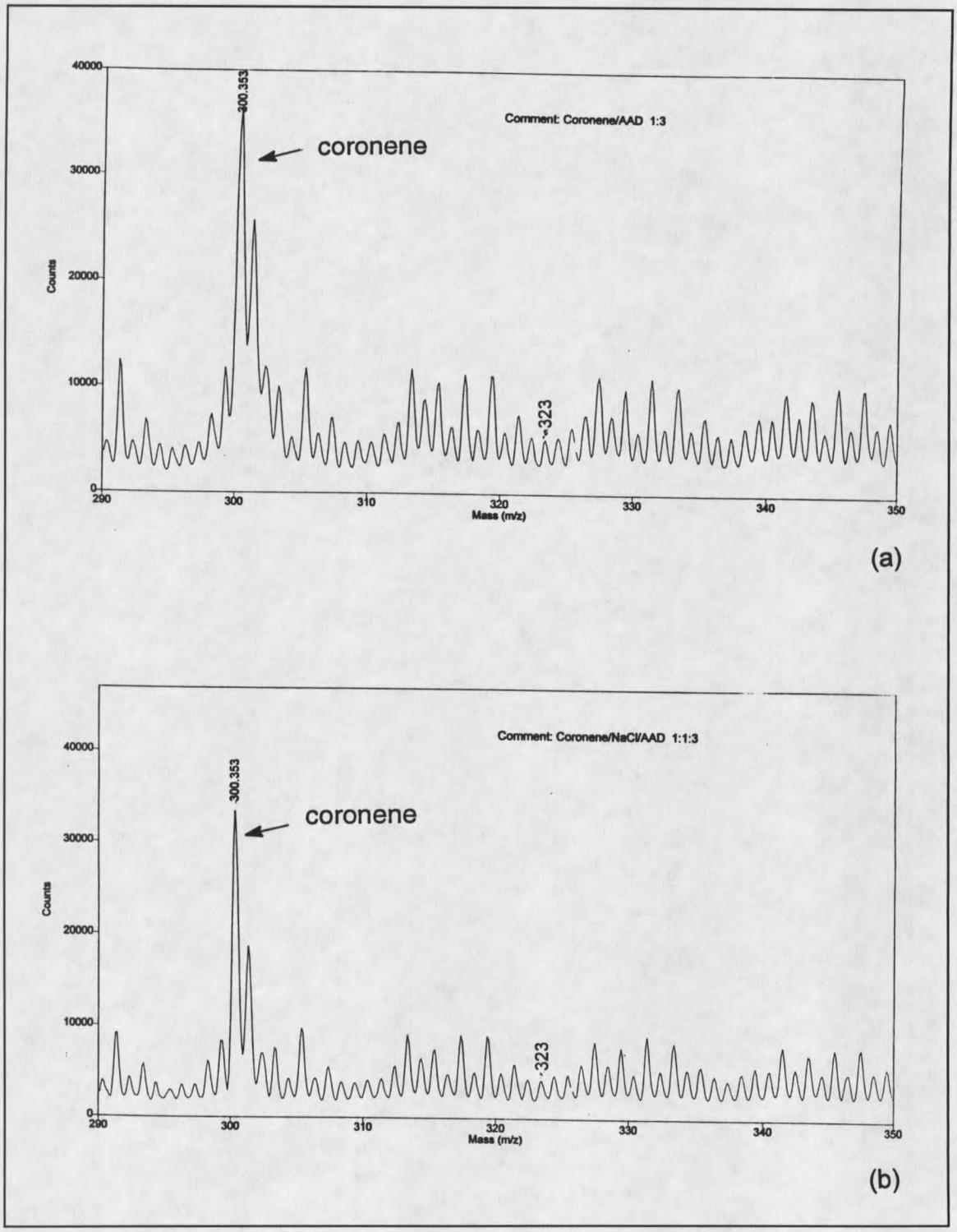

Figure 51. LD spectrum of a.) Asphalt AAD-1 spiked with coronene and b.) Asphalt AAD-1 spiked with coronene and doped with sodium chloride.

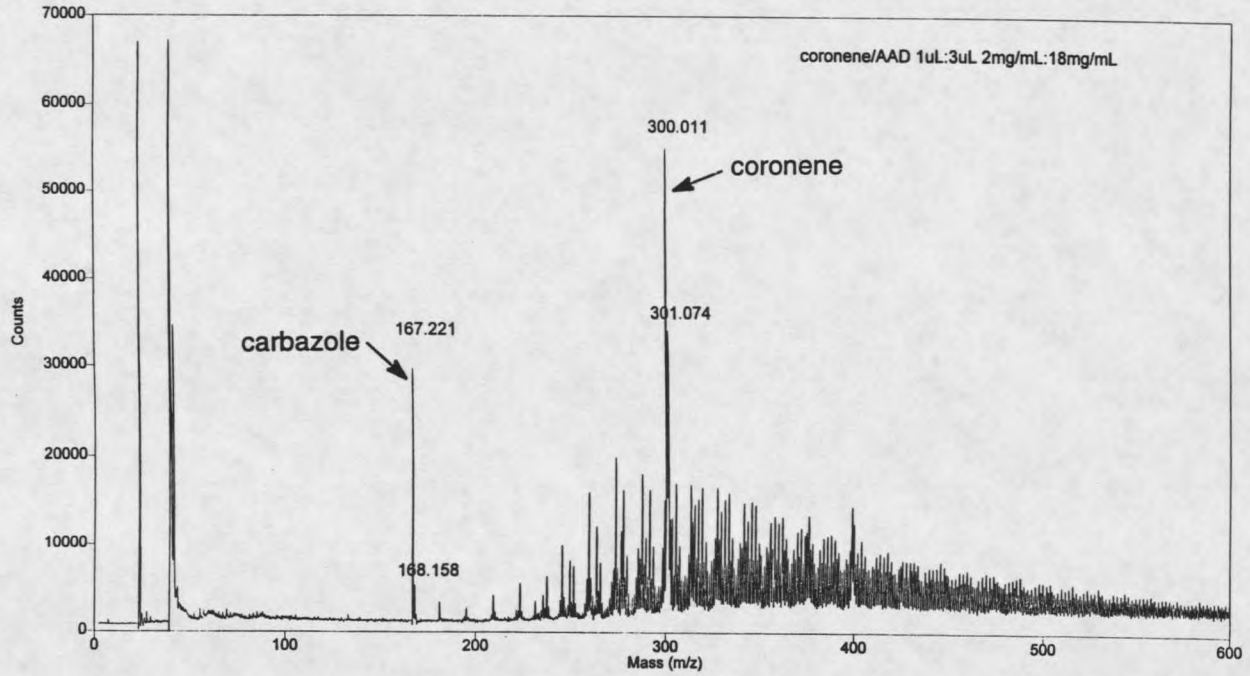

Figure 52. LD spectrum of AAD-1 spiked with coronene and carbazole and doped with sodium chloride. Sodium adduct ions did not form however, M^+ and $[M + H]^+$ ions did.

and pyrene were added to 1 µL of a 6 mg/mL THF solution of AAD-1. Figures 53a and b show the LD spectra, between 150 and 250 Da, of spiked and unspiked AAD-1 respectively. Figure 53b shows that AAD-1 did not contribute to the peaks at 167 Da (carbazole) or 202 Da (pyrene). Therefore, any contributions to the intensities of these peaks in the spiked asphalt spectrum in Figure 53a belong exclusively to the spiked compounds. The isotopic contributions were subtracted from the M + 1 peaks and the $[M + H]^+/M^+$ ratio was determined for both model compounds. The peak ratios are shown in Table 12. The $[M + H]^+/M^+$ ratio for the carbazole peak was found to be about 0.04. The $[M + H]^+/M^+$ ratio for pyrene was calculated to be approximately 0.0. However, this value involves substantial uncertainy because the peak intensity was low for the M peak and very low for the M + 1 peak, making direct measurements difficult. As for coronene (300 Da), whose LD spectrum is shown in Figure 50, the isotope corrected $[M + H]^+/M^+$ ratio was about 0.03. As shown in Table 12 carbazole has the highest proton affinity of the three compounds. It is therefore reasonable that the carbazole $[M + H]^+/M^+$ ratio should be the highest. The proton affinities of pyrene and coronene are very close and one might assume that a difference of 3% between the two ratios is large. However, this difference is not too significant. One must consider that these ratio values were taken from only one experiment. By repeating these experiments it was found that these ratios do center around 1-2% difference (results not shown).

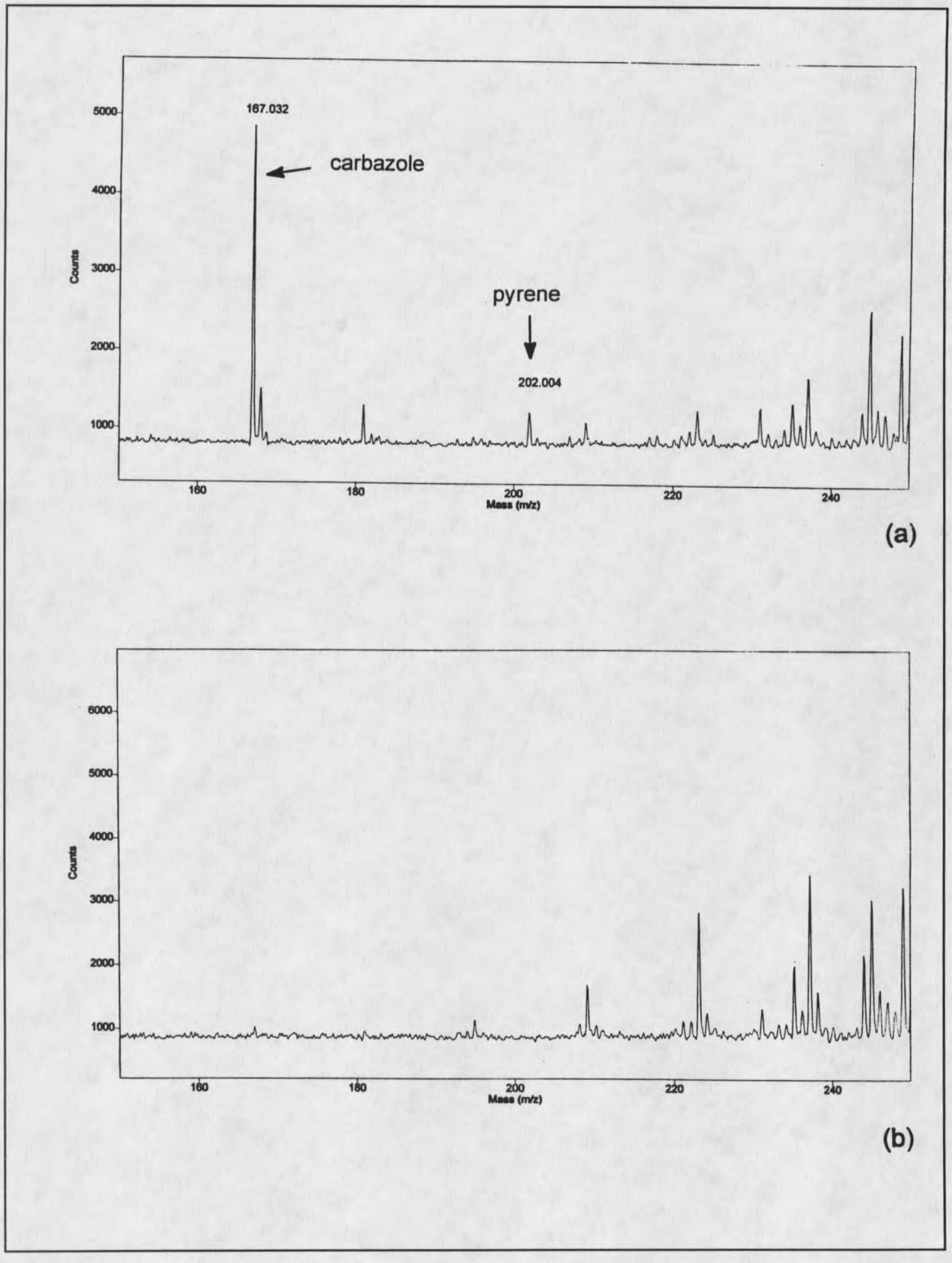

Figure 53. LD spectra of a.) AAD-1 spiked with carbazole and pyrene and b.) AAD-1 unspiked.

Table 12. LD ion species data for carbazole, pyrene, and coronene.

Model Compound	Structure	Proton Affinities (kcal/mol)	Peak Height (counts)		Peak Ratio
			M^+	$[M + H]^{+}$ [a]	$[M + H]^+/M^+$
carbazole	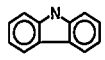	220(est.)[b]	4,060	151	0.04
pyrene		206.1	403	0	0.0
coronene		205.1	40,400	1,140	0.03

a) Adjusted for ^{15}N (0.42%) and ^{13}C (1.1%) isotopic contributions.
b) Estimated value using similar compounds for comparison.

Based on the spiking experiments, it was concluded that the predominant ion species in laser desorption of asphalts was the M^+ molecular ion. However, it is clearly possible that for some compounds, the abundance of protonated molecules is significantly higher. It can be surmised that, in the asphalt matrix, charge transfer in the form of the following reaction is occurring during the desorption event:

$$B^+ + M \text{ -------} > M^+ + B$$

Where B and M are molecules in asphalt. This reaction will only occur if the ionization potential of M is less than that of B.(63)

In Figure 53a it can be observed that the carbazole M^+ peak is 10 times larger than the pyrene peak although equimolar amounts the two compounds were present. Based on this observation, one might assume the ionization

energy for carbazole to be less than for pyrene; however, this is not the case. The ionization potential for carbazole is 7.57 eV as opposed to 7.43 eV for pyrene.(64) A possible explanation for the high carbazole abundance is as follows. The charge transfer reactions occur during laser desorption, not in a vacuum, but in a dense, laser-generated plume of gas. In a dense gas, the M^+ ions are stabilized by gas-phase solvation, $M^+(S)_n$. The neutral molecule/ion stabilization energy depends on the extent of localization of the positive charge in the M^+ molecule. The more localized the charge within a molecule, the more stabilized is the molecular ion. In the carbazole molecular ion the charge is localized on the nitrogen by the strong tendency for electron pair donation by the nitrogen. In contrast, the charge is delocalized in the pyrene molecular ion around all four fused aromatic rings. This argument may well explain the greater LD peak intensity of carbazole over pyrene.

Laser Desorption (LD) MS on Lab Aged Asphalt Samples

LD mass spectra were obtained for the eight SHRP asphalts including the unaged samples and the Western Research Institute (WRI) POV and TFO/POV aged samples (as described in the NMR sections in Results and Discussion). All spectra were acquired under the same experimental conditions which included laser energy, number of laser pulses, grid voltage, acceleration voltage, etc. Figure 54 compares the LD mass spectra of SHRP AAA-1, AAA-1

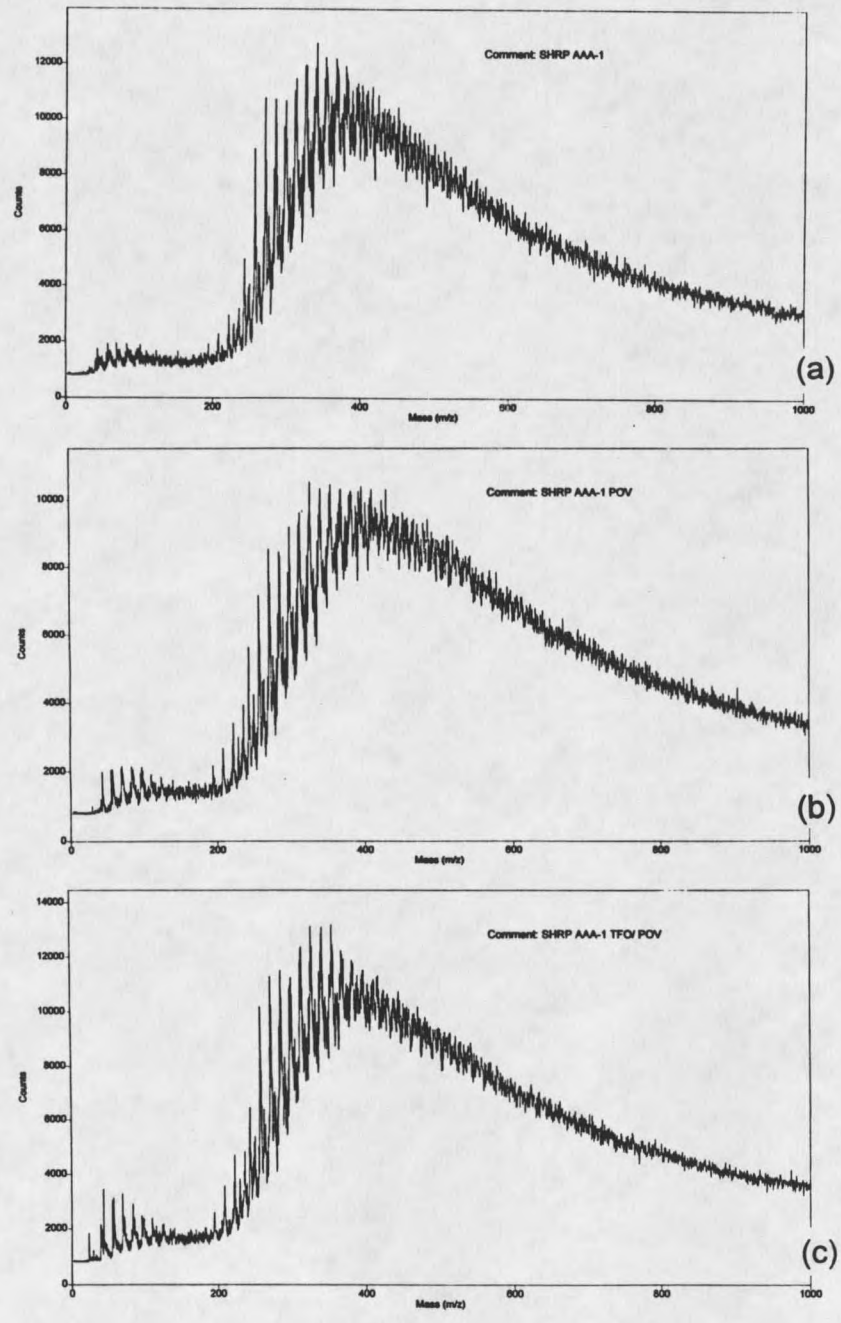

Figure 54. LD spectrum of a.) AAA-1, b.) AAA-1 POV, and c.) AAA-1 TFO/POV asphalt.

POV, and AAA-1 TFO/POV. It is seen that the overall appearance of these spectra is very similar; there are essentially no spectral differences among the unaged and aged samples in Figure 54. Indeed, this was the case for all asphalt samples in the SHRP series. The LD spectra of the SHRP POV or TFO/POV asphalt samples showed the same "envelope" pattern as had the LD spectra of their unaged counterparts. However, the LD spectra varied significantly from one asphalt to another.

One of the SHRP asphalts, namely AAD-1, gave a very different spectrum. The LD spectra of this unique asphalt can be seen in Figure 55. The spectrum of unaged AAD-1 (Figure 55a) is compared to the spectra of the (TFO and TFO/POV) aged samples (Figures 55b and c). As with the other SHRP asphalts, no changes in the mass spectra were observed as a result of WRI aging. The truly unusual aspect of the LD spectra of AAD-1 was the fact that they showed complete base line resolution of integral mass peaks up to about 600 Da. The other asphalts have similar patterns, but they were harder or impossible to analyze. Because of the higher mass resolution in the LD spectra of AAD-1, patterns of resolved peak sequences could be observed. This peak sequence pattern will be discussed in greater detail in the Resolved Peak Sequence subsection.

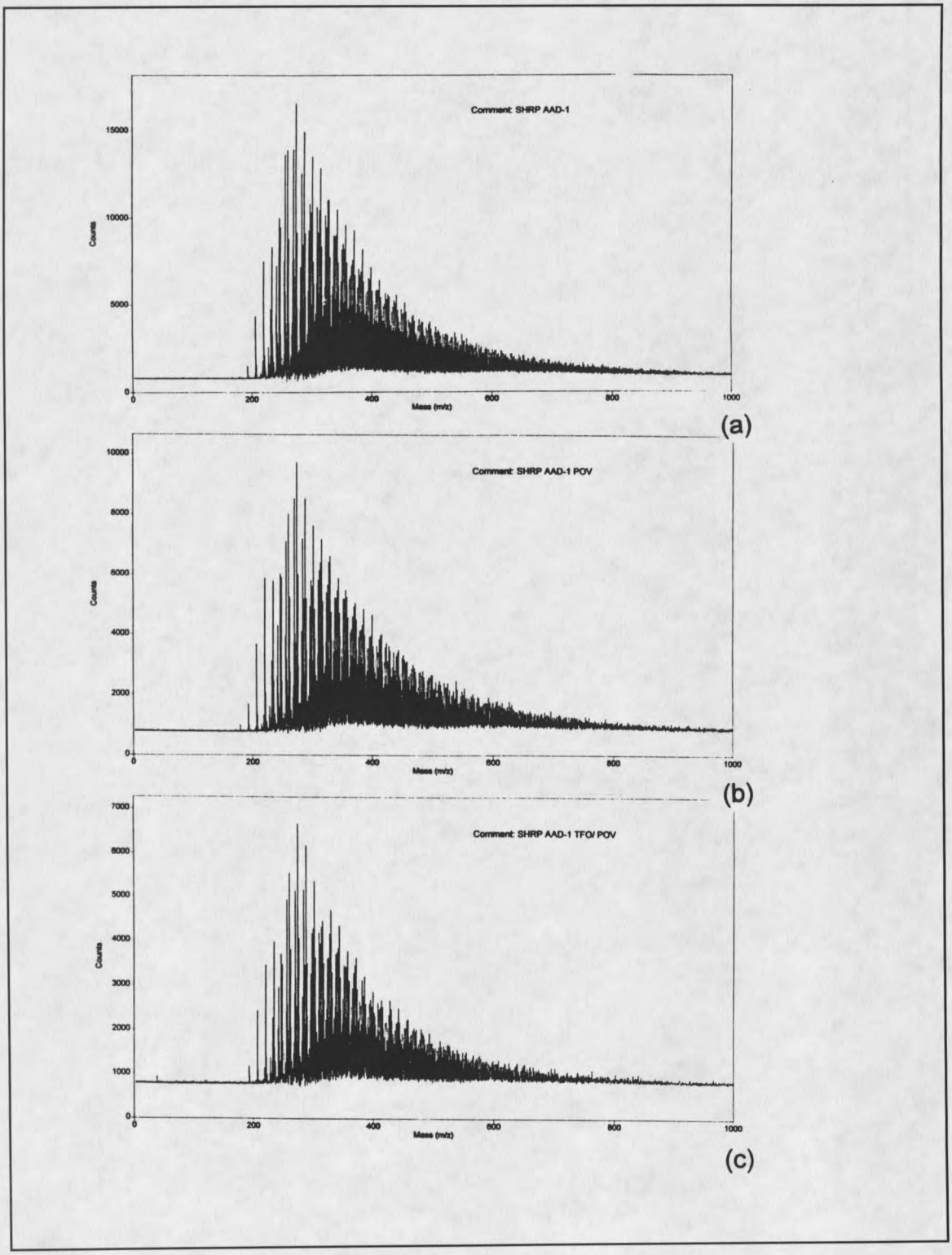

Figure 55. LD spectrum of a.) AAD-1, b.) AAD-1 POV, and c.) AAD-1 TFO/POV asphalt.

Laser Desorption MS on Big Timber Asphalts

Although no significant changes were observed in the LD spectra of the SHRP asphalts upon TFO/POV aging, it was not clear that actual road weathered asphalt samples would behave in the same manner. Figures 56a and b show the LD mass spectra of T18, and TG18, respectively. As discussed previously, T18 was an asphalt included in a road aging study near Big Timber, Montana, that spanned a four year period of yearly core sampling.(61) Figure 56b shows that the broad mass envelope has shifted to higher mass for the road aged TG18 asphalt. Also, the intensity of the peak progression that protrudes from the left shoulder of the broad mass envelope has decreased. This was an indication that actual road weathering of an asphalt could cause the mass distribution to shift towards higher masses. This suggests a possible free-radical polymerization.

Free radicals in asphalt could arise from several sources. For example, they might be produced through aggregate/asphalt contact (10), by UV initiation, or by the introduction of an additive to the asphalt. Once formed, a free radical could react with the aromatic rings in asphalt by substitution.(67) Scheme 1 suggests a possible polymerization reaction.

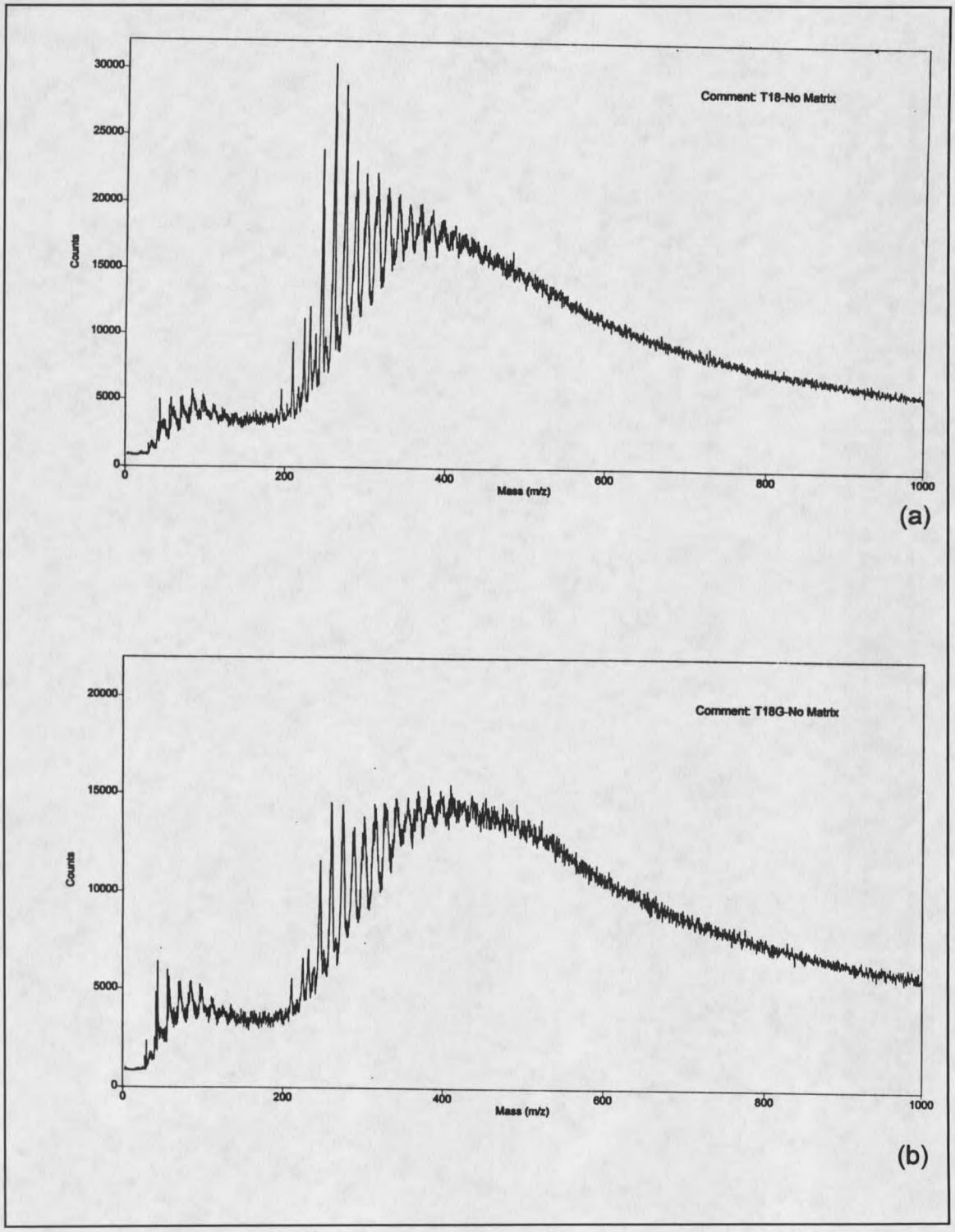

Figure 56. LD spectrum of a.) T18 and b.) TG18. There is a definite shift to higher masses in TG18 and a decrease in intensities of the semiresolved peaks on the left shoulder of the "broad" curve.

Scheme 1:

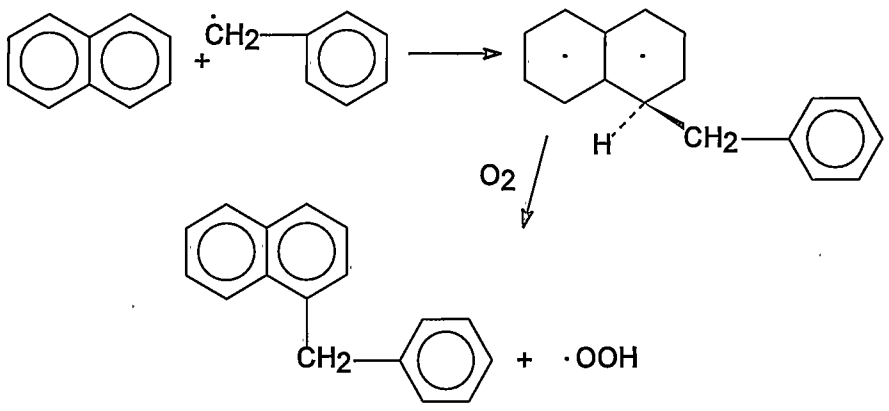

The initial reaction in Scheme 1 forms a resonance stabilized conjugated radical. The only way that the hydrogen can be removed from this system is by interaction with some other radical or oxidizing agent. In asphalt, for example, atmospheric oxygen, O_2, could be the agent needed to drive the reaction forward.

In order to determine whether the increase of molecular waight was a standard observation for road aged asphalts, LD spectra of additional road aged asphalt samples had to be obtained. Four additional asphalt samples used in the Big Timber test section experiment were selected. These had exhibited a broad range of road performance over the four year project.(61) The asphalts included: T12 (unaged), TG12 (aged), T14 (unaged), TG14 (aged), T15 (unaged), TG15 (aged), T16 (unaged), and TG16 (aged). Figures 57-60 compare the mass spectra of the aged versus the unaged asphalts. T12, an asphalt which cracked very little over the four year road study, exhibited little

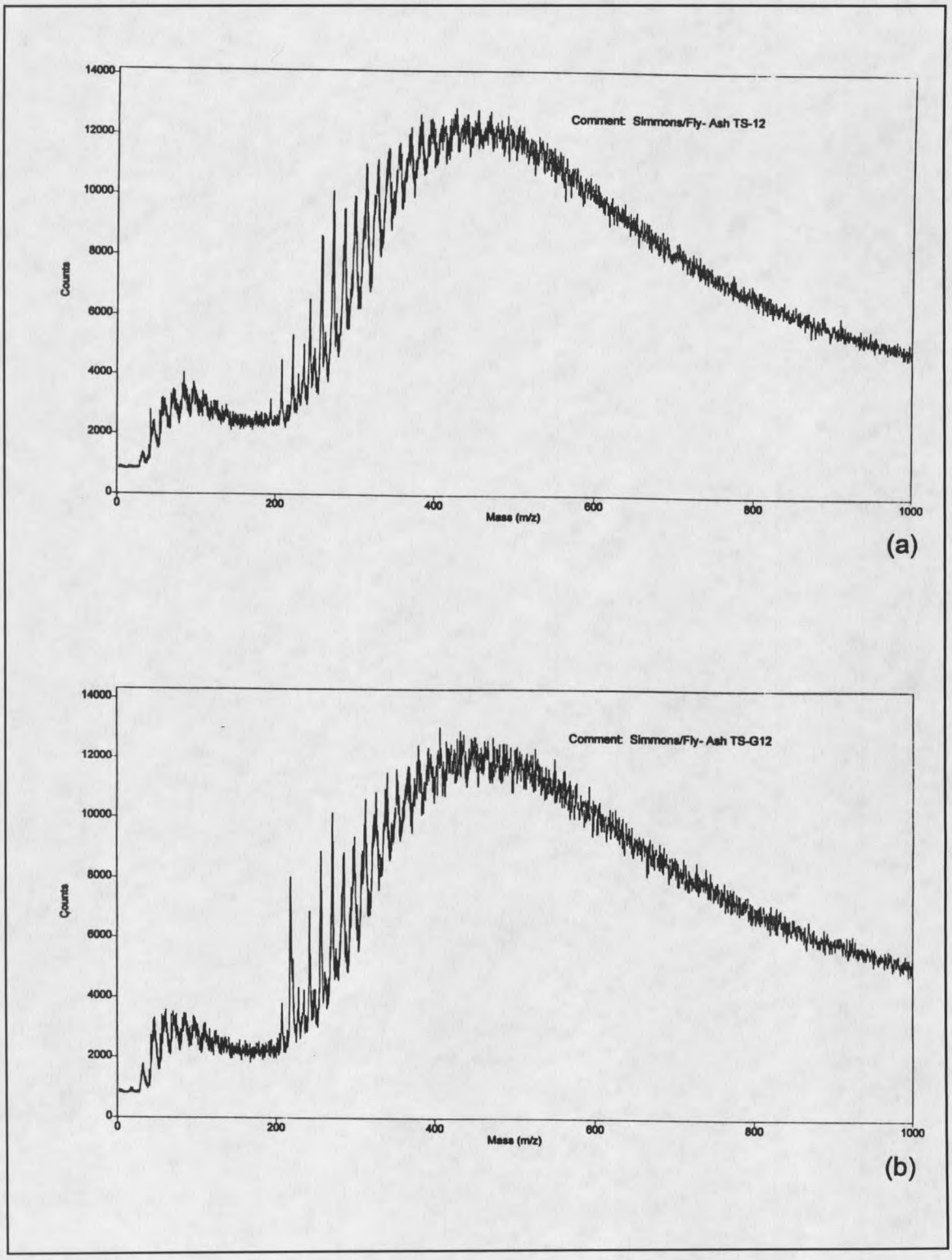

Figure 57. LD spectrum of a.) T12 and b.) TG12. No obvious differences between spectra.

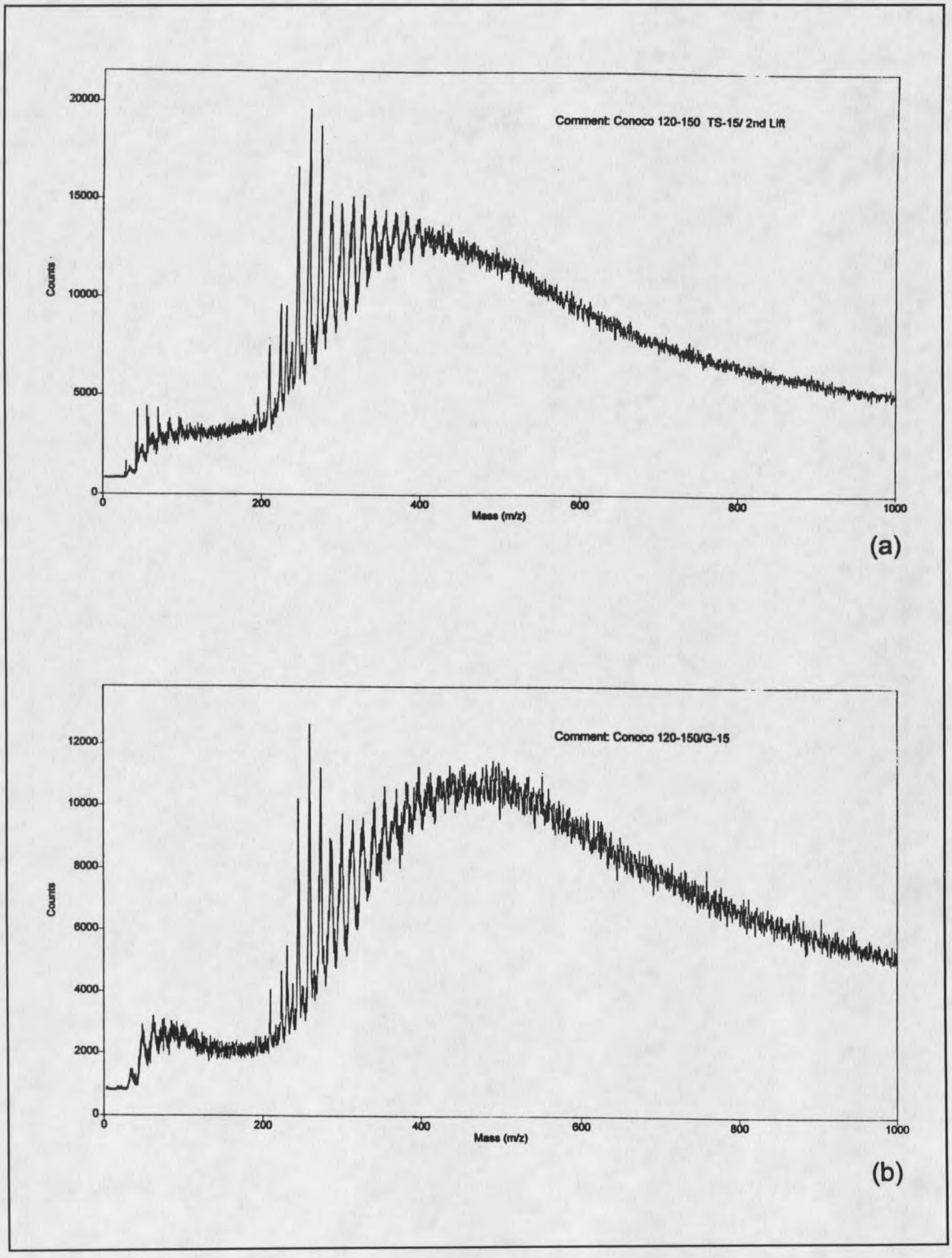

Figure 58. LD spectrum of a.) T15 and b.) TG15. Shift to higher masses in TG15.

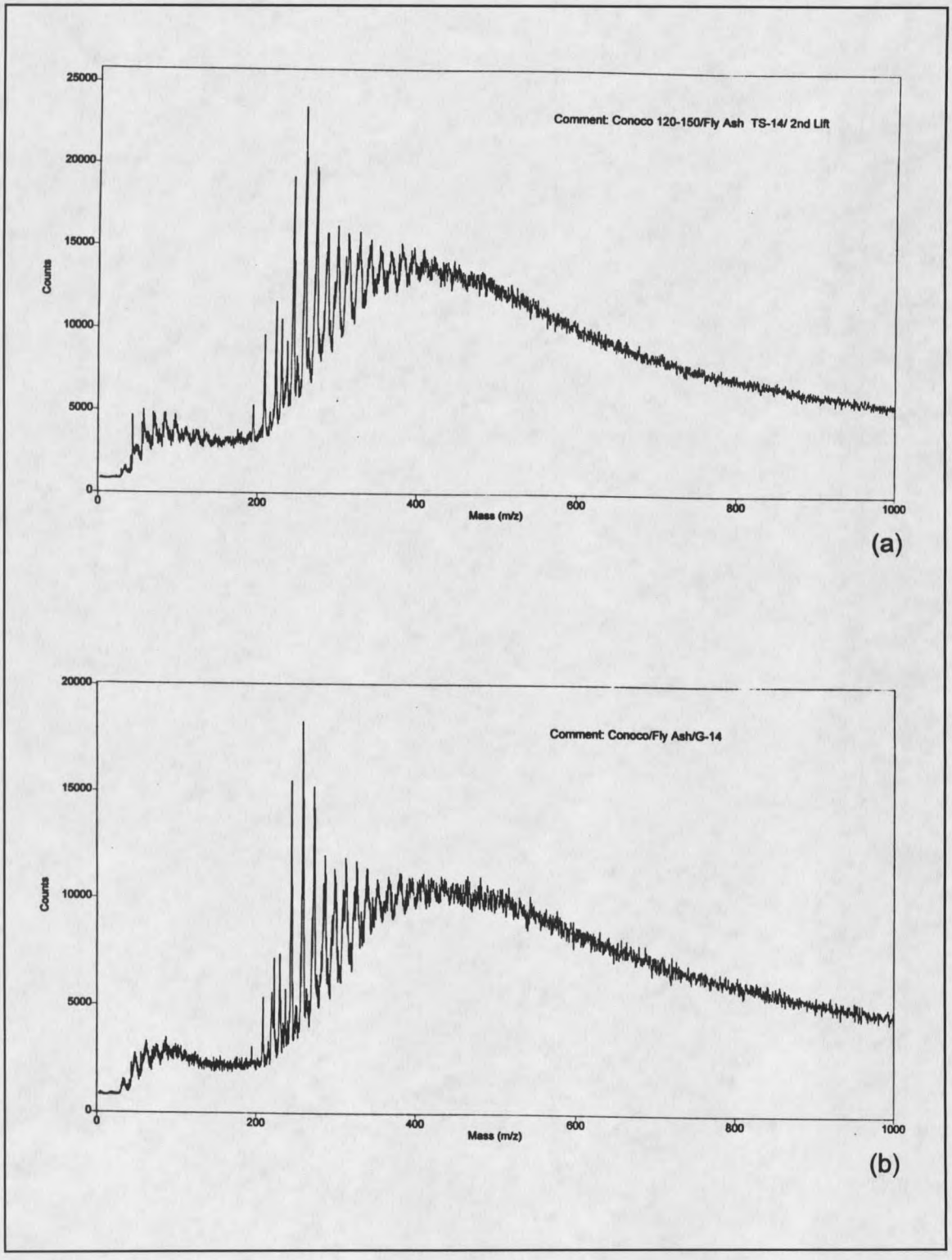

Figure 59. LD spectrum of a.) T14 and b.) TG14. Slight increase in intensity of the right shoulder of the broad curve in TG14.

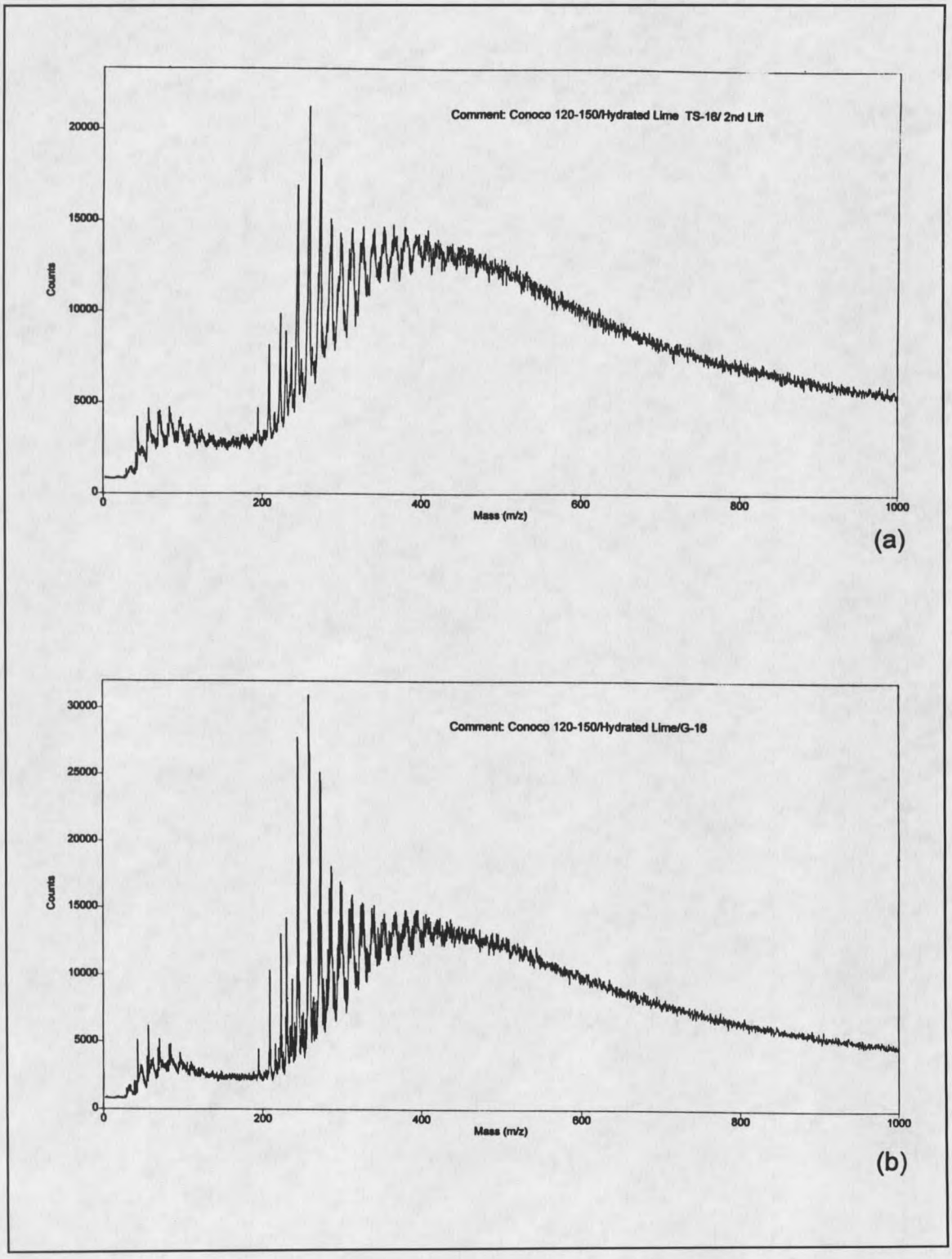

Figure 60. LD spectrum of a.) T16 and b.) TG16. Increase of peak intensities on left shoulder of the broad curve in TG16.

change in its LD mass spectrum, (Figure 57b) as compared to the spectrum of the unaged T12, (Figure 57a). Sample T15, which cracked moderately over the four years, exhibited changes in its aged mass spectrum, shown in Figure 58b. There is a significant shift to higher masses in the broad envelope along with some decrease in the intensity of the peak progression on the left shoulder of the broad envelope. Figure 59b shows the LD mass spectrum of aged T14, which was the most severely cracked asphalt after four years. There is a distinct broadening of the LD mass envelope and a significant mass increase in the intensity above 500 Da. But, in this case, no decrease of the peak progression on the left shoulder of the mass envelope is observed. Finally, in the mass spectrum of aged T16 shown in Figure 60b (another asphalt that only cracked moderately after four years), an increase in the intensity of the peak progression on the left shoulder of the mass envelope is observed without the accompanied broad curve shift to higher masses. Table 13 gives the number of transverse cracks counted within each test section after four years of road service for these Big Timber test section asphalts, as well as comments on the changes in the LD spectra upon aging.

Redistribution of masses has been demonstrated in all of the observed Big Timber asphalts that showed moderate to severe cracking, but there was no apparent change in mass distribution in the asphalt (T12) that cracked only slightly.

The results of the LD mass analysis indicate that poor asphalt road

performance can correlate with a redistribution of asphalt molecular size.

Table 13. Number of cracks in selected Big Timber Asphalts after four years of road aging and comments on their Laser Desorption spectra.

Original Asphalt	# of Cracks After Four Years	Comments Upon Mass Spectral Differences Observed After Four Years of Road Service
T12	2	Very little change in mass spectrum
T14	38	Shift to larger masses in main mass distribution
T15	16	Obvious shift to larger masses
T18	33	Obvious shift to larger masses
T16	19	Increase in intensity of small mass peak progression

However, poor road performance does not necessarily result in a shift to larger masses as would occur if polymerization was a factor. The LD spectrum of TG16 (Figure 60b) provides evidence that other variables must affect poor asphalt road performance as well.

One of the variables affecting asphalt aging could be the types of additives used. For example, Jennings discussed the possibility that the various additives in asphalt affect the way they perform.(61) More samples of this type must be studied.

Resolved Peak Sequence

As mentioned previously, the LD spectra of SHRP asphalt AAD-1 were

unique because integral mass peaks were completely resolved. Figure 61 shows the LD spectrum of whole AAD-1 asphalt between 200 and 400 Da. Within this mass range one can see several overlapping peak series. Each peak series consists of baseline resolved peaks 14 mass units apart indicating that the ions within each series are alkyl substituted to varying degrees on the same core molecule. There are fourteen of these series; however, for simplicity, only four were traced in Figure 61.

The resolved peak series traced out on the LD spectrum in Figure 61, will now be given an identifying nomenclature. Consider first, the series that begins at mass 209 Da continuing with 223, 234, etc. The core molecule of this peak should have a mass of 209 Da or an integral of 14 Da lower in mass. Because this molecule has an odd mass, it should contain an odd number of nitrogens.(66) A reasonable guess as to the identity of this core molecule is carbazole (167 Da). The mass peak at m/z=209 would then be due to carbazole substituted with three methylene groups. Carbazole and methyl and ethyl substituted carbazole should appear in Figure 61 at 167 Da, 181 Da, and 195 Da respectively. However, these compounds do not appear in the mass spectrum. It can be concluded that the corresponding compounds are essentially not present in the asphalt, since carbazole does appear in the mass spectrum when spiked into the sample. Presumably, carbazole and its methyl and ethyl substituted analogs are not present in the asphalt because they were lost in the high temperature petroleum distillation. This peak series will now be

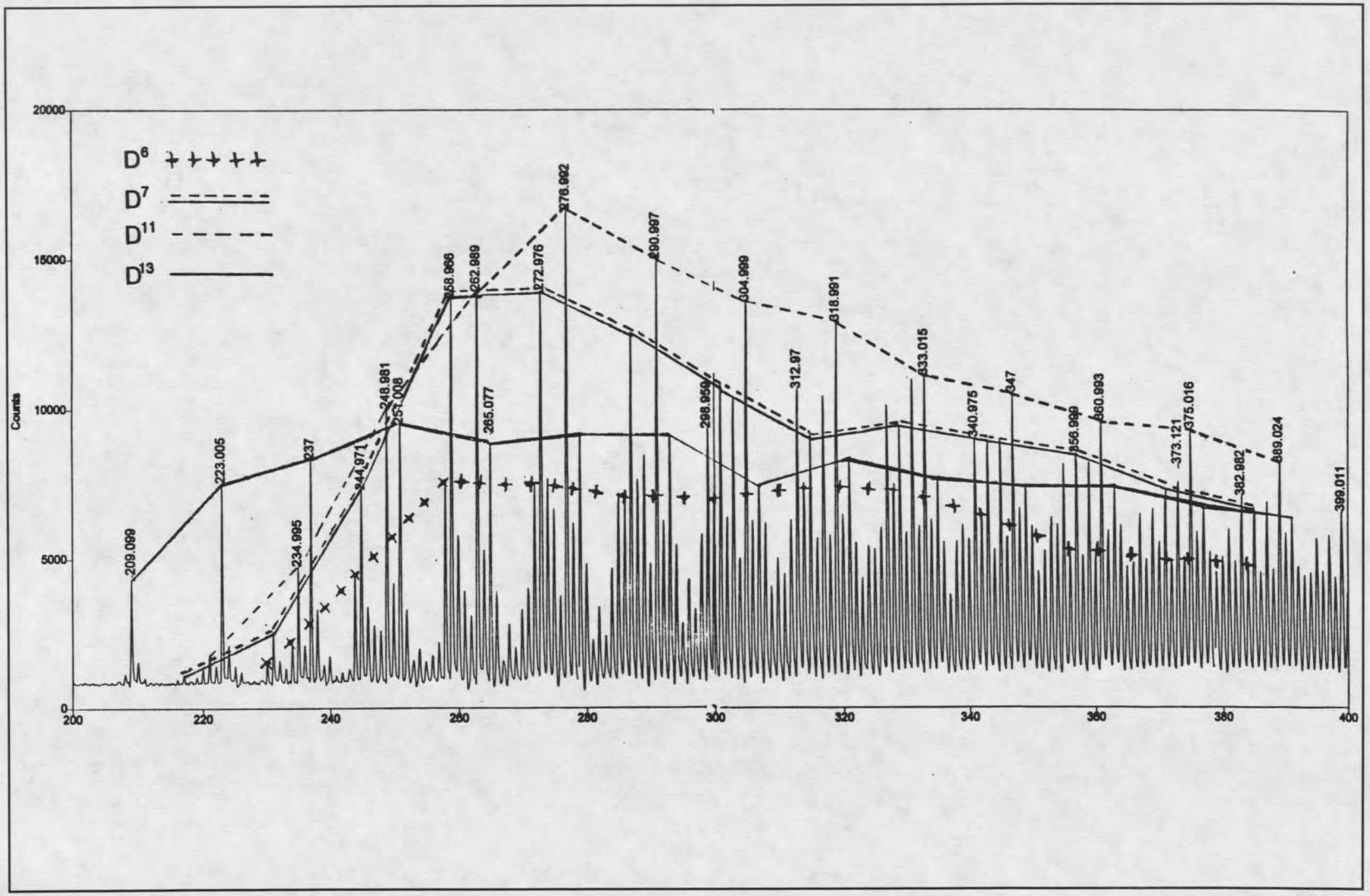

Figure 61. Resolved peak sequences in whole asphalt AAD-1. Four such sequences are traced out.

referred to as the "carbazole" series. All other peak series in the spectrum in Figure 61 will be defined relative to the carbazole series. However, to define all of these series systematically, the following general formula was used:

$$m = 14n + \Delta$$

The m value represents the mass of any peak within a peak series. In this example, m=181 Da will be used. The n value is the integer which, when multiplied by 14, should be 0 to 13 Da less than m. Delta, Δ, is the integer needed for the equation to equal m, i.e.181 Da, for example Δ=13. Hence, the "carbazole" series is defined as the 14n + 13 series. To simplify, it will be referred to as the D^{13} series. In Figure 61, notice the peak series denoted D^{11}. This peak series is staggered 2 Da below the carbazole D^{13} series. Similarly, the D^{7} peak series is staggered 6 Da below the D^{13} series. And, the D^{6} series is staggered 7 Da below the D^{13} series. This simple subtraction method simplifies the identification of each peak sequence enabling one to forego using the equation above to determine the D^{Δ} number.

An interesting feature of the AAD-1 mass spectrum (Figure 61) is that "odd" masses dominate its LD spectrum. Series D^{7}, D^{11}, and D^{13}, for example, are all "odd" mass series whose LD mass peaks are more intense than the D^{6} "even" mass series. As we have seen, the asphalt LD spectra consist primarily of odd electron M^{+} molecular ions. This indicates the presence of compounds containing an odd number of nitrogen atoms. The "even" mass series are much less intense in the asphalt. This observation is reasonable because, as

discussed previously, the LD sensitivity for nitrogen containing compounds appears to be greater than that for PAHs that contain only carbon and hydrogen.

Gel Permeation Chromatography (GPC) LD TOF MS of Selected Asphalts

It was shown above that mass resolution was low in the LD mass spectra of all of the asphalts, except AAD-1, and the reasons are unknown. However, by separating the complex asphalt mixtures into somewhat less complex fractions it might be possible to improve mass resolution such that more chemical information could be obtained from the LD spectra. One method, extensively used for separating asphalt into molecular size groups, is Gel Permeation Chromatography (GPC).(21,25) Here, results of analyzing GPC fractions by LD will be described.

Five asphalt samples were selected for GPC fractionation. SHRP AAF-1, AAD-1, and AAG-1 were chosen because they had previously shown, in a GPC study by Jennings *et al.* (21), distinct differences among their chromatograms as can be seen in Figure 62a, b and c. The Big Timber T18 and TG18 asphalts were chosen because they had shown obvious differences in their LD mass spectra. Figures 62d and e show their GPC chromatograms. In the chromatograms in Figure 62 the x-axis represents elution time and the y-axis represents milli-absorbance at 230 nm. The principal in GPC is that the largest

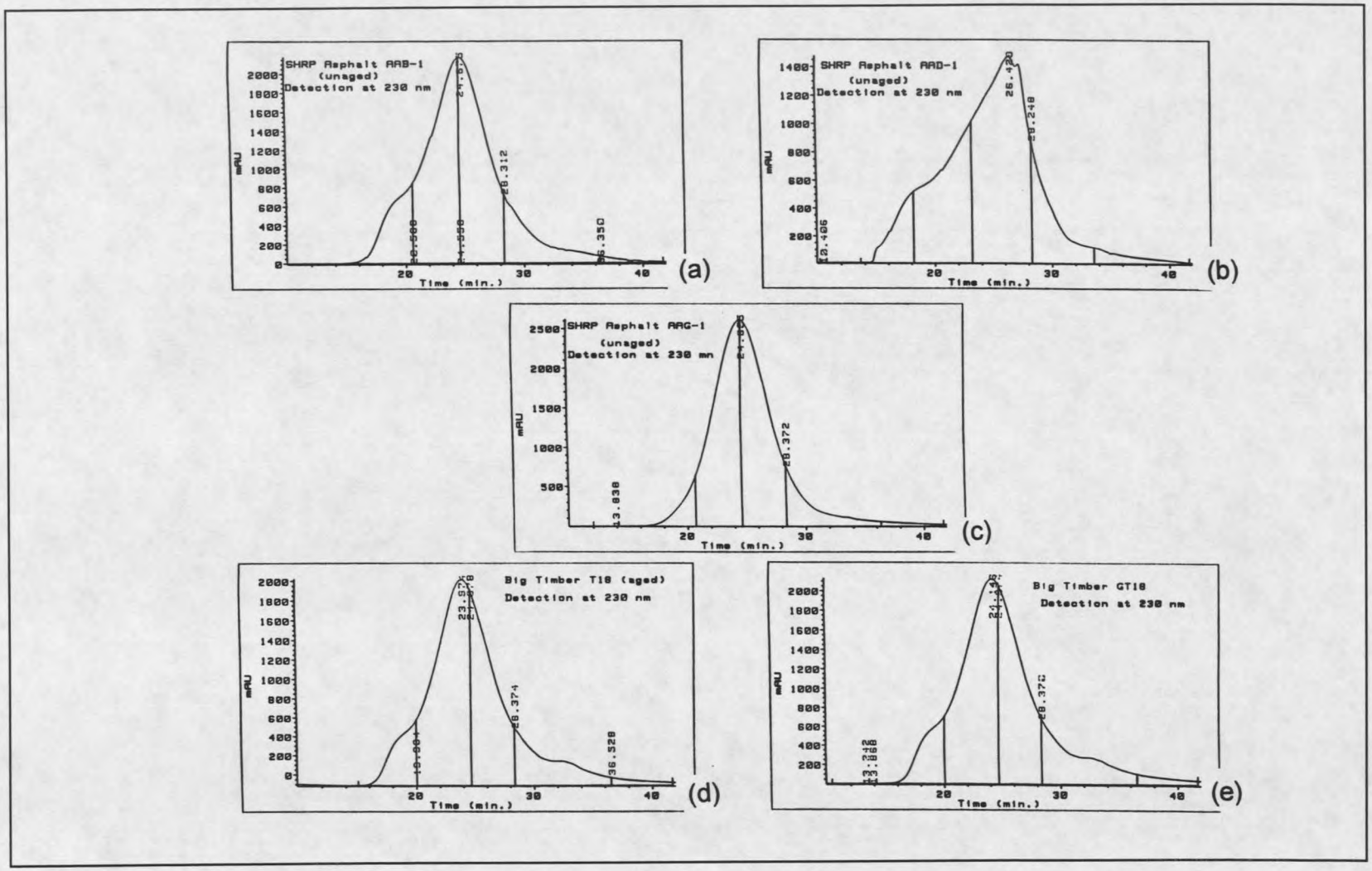

Figure 62. GPC chromatograms indicating when fractions were collected from a.) AAB-1, b.) AAD-1, c.) AAG-1, d.) T18, and e.) TG18.

molecules elute first from the column followed by the elution of increasingly smaller molecules. Upon viewing Figure 62, one can see distinct gel permeation chromatogram regions. The elution times depend on several variables including flowrate and column used. Although the GPC instrument was the same and the experimental parameters were identical to those used by Jennings, *et al.*(61) in their study of the SHRP and the Big Timber asphalts, the column had since been replaced. For this reason, the GPC elution times for these asphalts were different. The asphalt GPC elution times were longer than in the Jennings study, but the chromatogram line shapes were the same. Therefore, direct comparisons can be made between the previous GPC chromatograms and the chromatograms obtained in this work. Hence, the region referred to by Jennings as the Large Molecular Size (LMS) region between elutes between 15 and 20 minutes when using the new column. The Medium Molecular Size (MMS) region falls between approximately 20 and 30 minutes (Figure 62). The Small Molecular Size (SMS) region falls between approximately 30 and 42 minutes. The vertical lines within each GPC chromatogram in Figure 62 delineate the time interval during which each of five fractions per sample was collected.

GPC Mass Calibration

The molecular mass distribution within asphalt samples is an important issue. A GPC mass calibration was performed to construct a mass calibration curve from the elution times for a series of known compounds. From the calibration curve, the approximate molecular size range in each GPC fraction can be determined.

The GPC calibration standards used are listed in Table 14. These standards were chosen because they are similar to molecules present in asphalt. The standards included polyaromatics, alkyl substituted polyaromatics, and polyaromatics containing heteroatoms (O and N). For molecular sizes above 1,000 Da, it is difficult to find substances which would be typical of molecules in asphalt because of the complex nature of these molecules. Therefore, polystyrene standards with molecular masses ranging from 2,350 to 35,000 Da had to be used. Table 14 lists the elution times of these standards. Figure 63 is the calibration curve derived from the data in Table 14. Upon looking at Table 14 and viewing the graph in Figure 63, it appears that masses below 350 Da no longer follow a linear elution trend between elution time and ln(mass). This inconsistency is most likely due to chromatographic effects and effects due to the molecular shape of the standard compounds used. From these observations, it is apparent that the calibration curve can only be used at a lower mass limit of 350 Da.

Table 14. Gel Permeation Chromatography elution times of various standards.

Standard	Structure	Mass (Da)	Elution Time (min)
1,2,4,5-tetramethyl-benzene	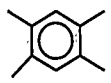	134	29.9
carbazole	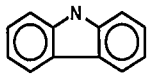	167	29.5
1-(2-naphthyl)ethanol	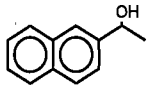	172	30.6
benzo[a]pyrene	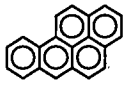	252	33.8
coronene		300	33.6
1-methyl-3,4-di-phenanthrene	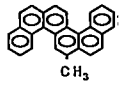	342	29.6
rubrene	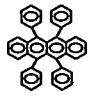	533	26.4
polystyrene	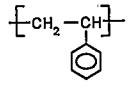	2350	20.9
polystyrene	"	3600	19.7
polystyrene	"	15000	18.1
polystyrene	"	35000	14.9

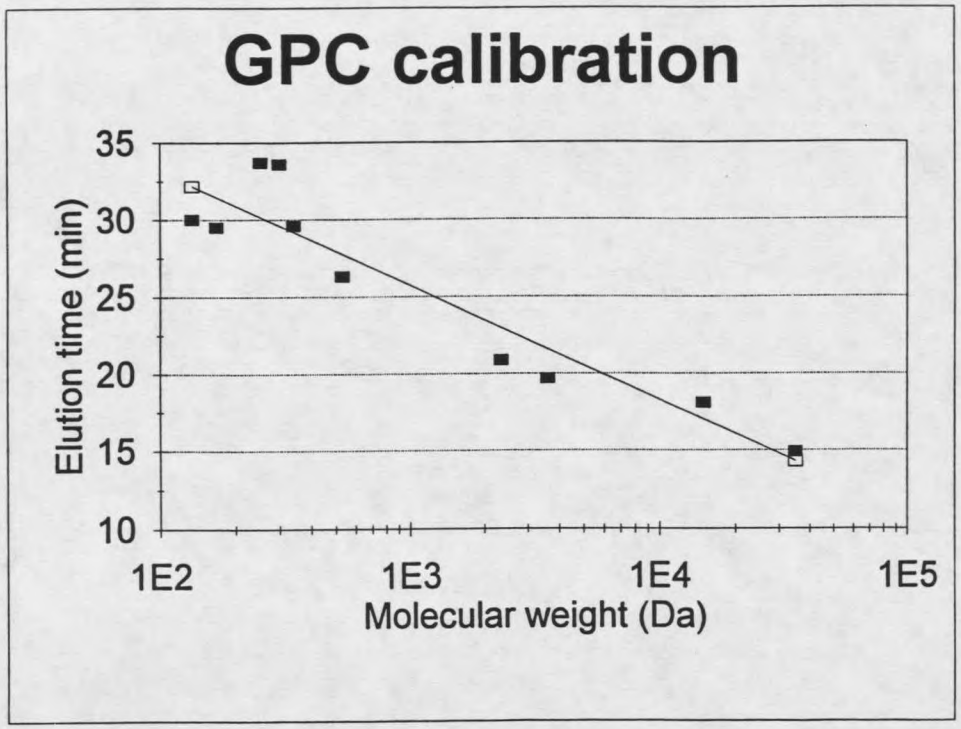

Figure 63. GPC calibration curve for asphalt.

Laser Desorption TOF MS of Asphalt GPC Fractions

LD mass spectra of the five GPC fractions of AAB-1 are shown in Figures 64-66 for comparison. Figure 64a shows the LD spectrum of whole AAB-1 asphalt. Figure 64b shows the LD spectrum of AAB-1 GPC fraction 1. The spectrum shows a distribution of masses ranging from about 900 Da to 10,000 Da. The m/z axis does not span out to 10,000 Da in Figure 64b, however, there is a gradual decrease of intensity until the curve evens out at 10,000 Da. The highest intensity is shown to be at m_{max} =1,400 Da. From the GPC chromatogram in Figure 62a, one sees that fraction 1 was collected between 15 and 20 minutes. The mass range of the molecules that are expected to elute from the GPC column within that time range can be determined from the calibration curve in Figure 63. The expected masses in fraction 1 should range from about 6,000 to 30,000 Da. However, m_{max} = 1,400 Da in fraction 1 is much lower than expected from the calibration curve. Fraction 2 in Figure 65a shows an m_{max} of approximately 900 Da. From the calibration curve in Figure 63 it is seen that the GPC mass range, expected for the elution time range, is between 1,600 and 6,000 Da. The agreement between m_{max} and the expected GPC mass range is closer for fraction 2 than for fraction 1. The LD spectrum of fraction 3 in Figure 65b shows an m_{max} at about 600 Da. The expected GPC mass range is from 400 to 1,600 Da. The 600 Da m_{max} value is well within the expected GPC elution mass range. Figure

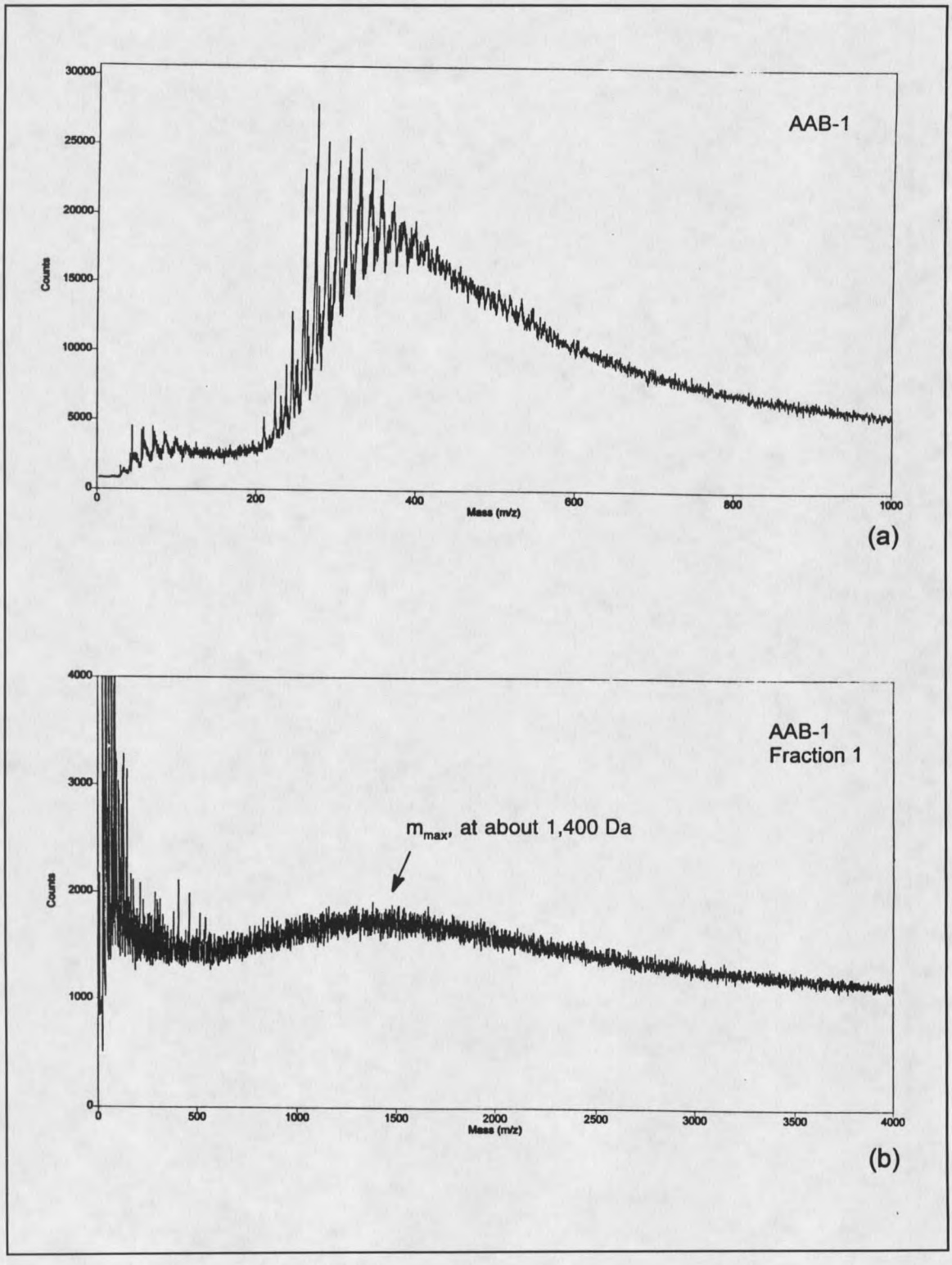

Figure 64. LD spectrum of a.) whole asphalt AAB-1, and b.) GPC fraction 1 of AAB-1.

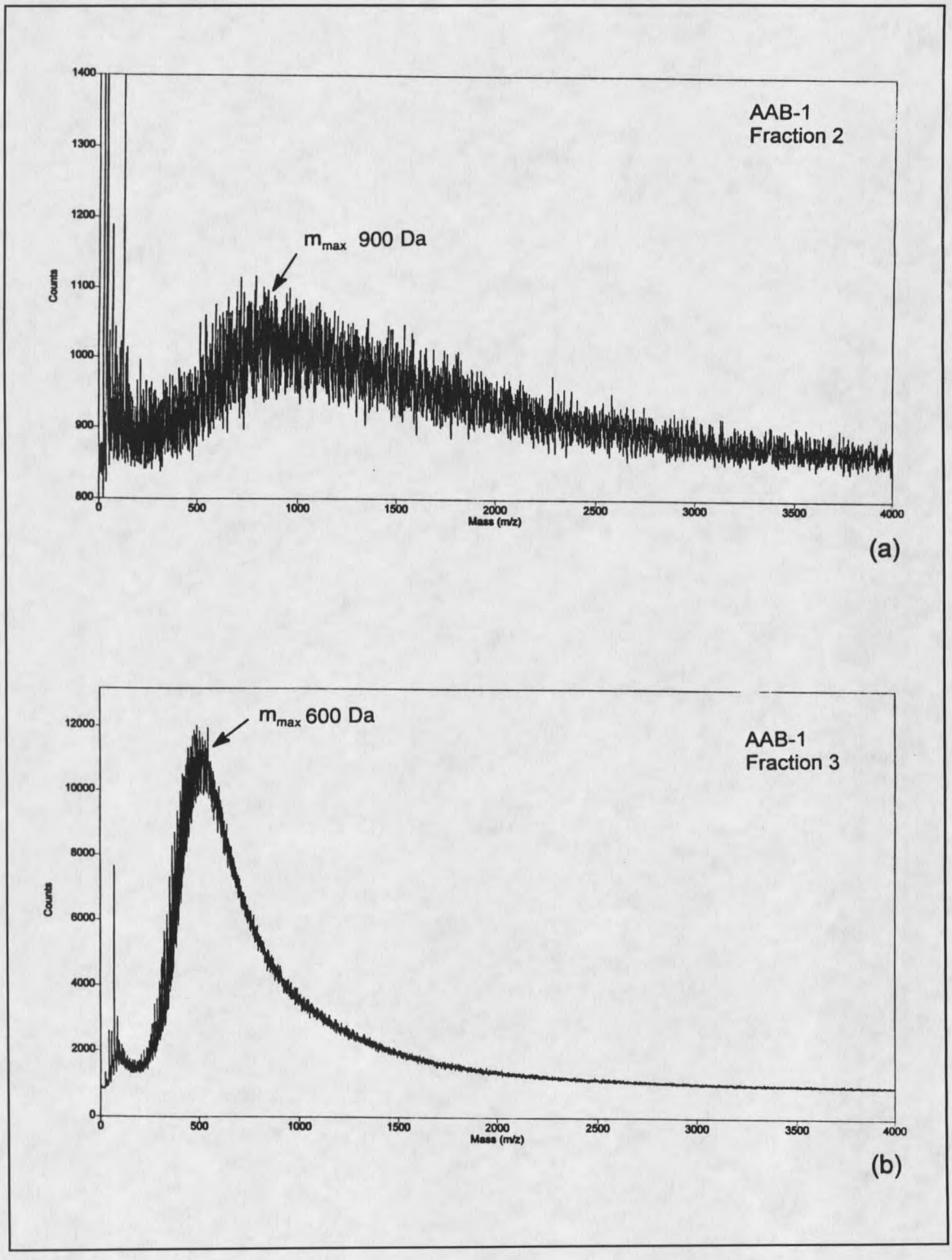

Figure 65. LD spectrum of a.) GPC fraction 2 of AAB-1, and b.) GPC fraction 3 of AAB-1.

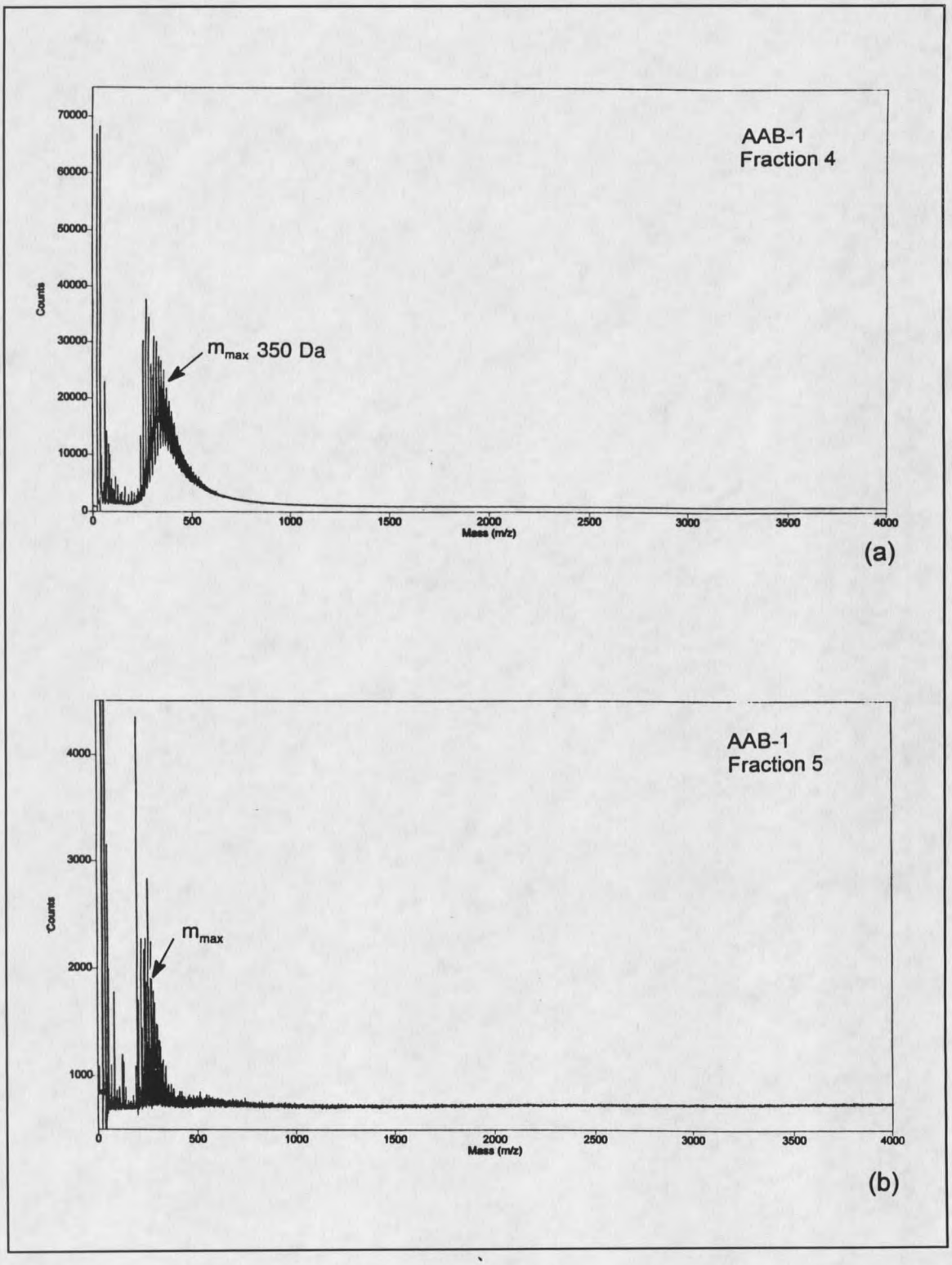

Figure 66. LD spectrum of a.) GPC fraction 4 of AAB-1, and b.) GPC fraction 5 of AAB-1.

66a shows the LD spectrum of fraction 4. This fraction, interestingly enough, exhibits partial peak resolution up to 350 Da. The m_{max} is about 350 Da and according to Figures 62a and 63, the expected GPC mass range is from a high mass of 400 Da to a lower mass limit which cannot be determined from the calibration curve. This situation also applied to fraction 5 (Figure 66b) whose LD mass spectrum showed resolution of integral masses. However, as stated in the GPC calibration subsection, masses below approximately 350 Da seem to have similar elution times. In agreement with this, the LD mass range for fraction 5 does not show as large of a mass shift to lower mass relative to fraction 4 than do the other fractions relative to the fractions that proceeded them.

The LD results from all asphalt GPC fractions in Figure 62 can be summarized as follows. The general trend seen in the LD mass spectra of the GPC fractions showed separation of steadily decreasing masses from fractions 1 through 5 in each of the asphalt samples. However, between fractions, there was substantial LD mass overlap; there were no sharp mass separation boundaries. The typical LD mass spectra of GPC fractions 1, 2, and 3 of the asphalt samples showed broad unresolved mass envelopes. The LD spectral intensities of fractions 1 and 2 were low. The LD peak intensity was invariably the highest in fraction 3. Fraction 4 either gave a partially resolved or a resolved LD spectrum. The LD spectrum of fraction 5 always showed unit resolution of peaks. The peak intensity pattern that repeated itself every 14 Da

as previously seen in AAD-1 was now obtained in fractions 4 and 5. It was now possible to identify peak sequences which corresponded to core compounds that appeared alkylated to varying degrees for the asphalt GPC fractions 4 and 5. One such series, for example, was previously defined as the "carbazole series", or, to be more concise, the "D^{13}" series.

It is important to consider one possible explanation for the discrepancy between the mass distributions of the largest asphalt molecules in fractions 1 and 2 observed by LD and by GPC. It could be that fragmentation of large molecules in asphalt occurs upon laser desorption ionization. However, it was observed and discussed earlier that only a low intensity of fragment ions is observed in the low mass region below 100 Da in the asphalt LD spectra. It has been concluded that the DLD ionization method is softer than MALDI and that asphalt serves itself as a type of "liquid" matrix. Therefore, fragmentation seems unlikely.

Another explanation for the discrepancy between LD and GPC would take into consideration the theory of asphalt "self-assembly" in solutions, as discussed in the Introduction. It is possible that the GPC chromatograms at the high molecular weight end, represent not large individual molecules, but rather assemblies of smaller molecules. Then the asphalt molecules that are eluting from the column in the LMS region are much smaller than predicted from the GPC chromatograms. The discrepancy between the GPC calibration curve and the LD mass spectra could then be explained. The mass ranges seen in the

LD spectra would be the actual masses present in these GPC fractions.

The LD spectra of the GPC fractions of AAD-1 will now be discussed. Figure 62b shows a fairly large LMS area in the GPC chromatogram of AAD-1. In accordance to the past GPC experiments on asphalt self-assembly,(21) one could say that AAD-1 has a greater tendency, compared to the other asphalt samples used in this work, towards self-assembly. But, one cannot determine directly from the GPC chromatograms how large the individual molecules are of which these assemblies are comprised. However, the LD spectrum (not shown) of AAD-1 fraction 1 shows only small molecules ranging from 200 to 400 Da. Fraction 1 is the fraction containing the largest supposed assemblies in the GPC LMS range. It would seem from this data that, for AAD-1, the self-assembly in the GPC LMS region is dominated by small molecules.

Resolved Peak Sequence in Asphalt GPC Fractions As mentioned above, all of the asphalt samples that were GPC fractionated showed unit resolution in the LD mass spectra of fraction 5 and all but one of the LD spectra of fraction 4. Peak identification was now possible in the LD spectra of these GPC fractions because they showed similar peak series patterns as described earlier for the AAD-1 whole asphalt. Each series was shown to consist of consecutive peaks with an incremental mass difference of 14 Da. The typical series profile exhibited a steady increase in peak intensity with each addition of a methylene group until an apex of peak intensity was reached. From the

apex, as the series continued toward higher masses, the peak intensity declined (some more sharply than others) until eventually disappearing into the baseline noise.

Table 15 lists the most intense, D^{Δ}, peak series observed in the GPC asphalt fractions together with the mass at the intensity apex for each peak series. It also lists probable core molecules for each series. All of the molecules in the asphalt fractions that were studied, appeared to be alkyl substituted to varying degrees. This is illustrated by the following example. Figure 67 shows a LD spectrum of GPC fraction 4 of the T18 asphalt. The appearance of the resolved peak sequence is very similar to that seen for the AAD-1 asphalt in Figure 61. Notice the D^{13} series also called the "carbazole" series. Although the mass of carbazole is 167 Da (Table 15), the D^{13} series in this asphalt fraction begins at 181 Da which indicates a methyl (CH_3) substituted carbazole. From now on, the degree of alkylation will be given by the number of methylene groups, n_s, substituted on the proposed core molecule. Table 16 lists the n_s value at the peak apexes for each asphalt GPC fraction. The D^{13} series climbs to maximum intensity at m_{max}=209 Da, where n_s=3 (Tables 15 and 16). The D^{7} and the D^{11} series behave similarly to the D^{13} "carbazole" series in that they both climb to a peak apex at m_{max}=259 Da (n_s=3) and 277 Da (n_s=6.5) respectively (Tables 15 and 16).

The D^{6} series, also referred to as the "pyrene" series, also climbs from a minimum at 216 Da and reaches a maximum peak intensity at m_{max}=258 Da

Table 15. Prominent LD peak series in asphalt GPC fractions.

Suggested Core Molecule (CM)	Mass of CM	D^{Δ}	Peak Mass at Series Apex (m_{max})				
			AAB-1 Frac.4	AAD-1 Frac.4	AAG-1 Frac.5	T18 Frac.4	TG18 Frac.4
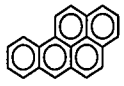	252	D^{0}	392	a	280	308 & 364[b]	a
 & ?	202 & ?	D^{6}	258	N.O.	272	258	258
	?	$D^{6\prime}$	356	314	314	314	314
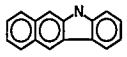	217	D^{7}	287	259	287	259	a
?	?	D^{8}	287	274	274	274	274
?	?	$D^{8\prime}$	372	N.O.	316	330	N.O.
?	?	D^{10}	N.O.	304	318	290	290
?	?	$D^{10\prime}$	346			346	346
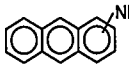 & 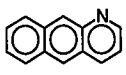	193 & 179	D^{11}	375	277	277	277[a]	N.O.
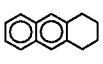 & 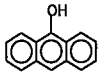	180 & 194	D^{12}	390 & 404[c]	292[a]	306	390 & 404[c]	a
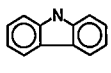	167	D^{13}	237 & 349[b]	223	307[a]	209	N.O

a) Very low intensity.
b) Peak with the highest intensity.
c) Both peaks are of equal intensity.
N.O. = Not Observed

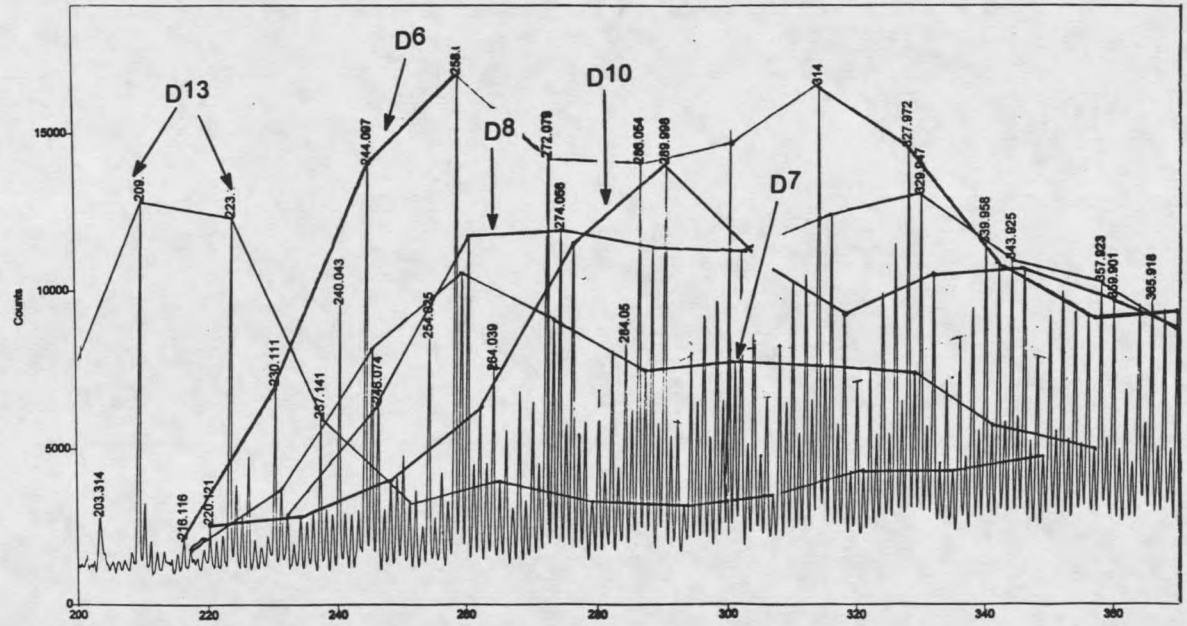

Figure 67. Resolved peak sequence in the LD spectrum of T18 GPC fraction 4. As shown, the traced peak series include: D^6, D^7, D^8, D^{10}, and D^{13} .

Table 16. Average number of carbons at LD peak apexes for asphalt GPC fractions.

Series Term	Number of Carbons (n_s) at Peak Apex				
	AAB-1 Frac.4	AAD-1 Frac.4	AAG-1 Frac.5	T18 Frac.4	TG18 Frac.4
D^0	10	N.O.	2	4 (8)[a]	N.O
D^6	4	N.O.	5	4	4
$D^{6'}$	11	8	9	8	8
D^7	5	3	5	3	N.O.
D^8	?	?	?	?	?
$D^{8'}$	?	?	?	?	?
D^{10}	?	?	?	?	?
$D^{10'}$	?	?	?	?	?
D^{11}	13 & 14	6 & 7	6 & 7	6 & 7	N.O.
D^{12}	16 & 15	8 & 7	9 & 8	16 & 15	N.O.
D^{13}	5 (13)[a]	4	10	3	N.O

a) Second peak apex of which the peak intensity was highest of the two apexes.
N.O. = None Observed
? = Core molecule cannot be guessed therefore, extent of alkylation cannot be determined.

where n_s=4 (Tables 15 and 16). The series peak intensity then declines, reaching a minimum at mass 286 Da (n_s=6) where it then begins another increase to reach a second maximum at m_{max}=314 Da (Tables 15 and 16) at n_s=8. From 314 Da the D^6 series begins a steady decline in peak intensitiy until it disappears into the background noise at about 600 Da (not shown in Figure 67). From Figure 67 it was observed that two other series had two peak apexes; they were the D^8 and D^{10} series.

The degree of alkylation in T18 fraction 4 varies somewhat. However, the fact that alkylation of each series reached peak intensity apexes in the LD spectrum in Figure 67, indicated that there could be points of maximum abundance for these alkyl substituted core molecules, the most stable alkylated number being the point of greatest peak intensity. However, for those series showing two peak maxima (D^6, D^8, and D^{10}), it is highly unlikely that there would be two points of alkylation stability for the core molecules. A reasonable interpretation seems to be that there are two or more core molecules for these series. Tables 15 and 16 list the m_{max} and n_s values for the D^6, D^8, and D^{10} series, however, the core molecules that cannot be identified are designated with question marks.

A speculative conclusion is that the degree of alkylation is fairly low and for T18 fraction 4 in Figure 67 the mass spectrum indicates that the average alkylation number for each series is n_{ave}=4.

The LD mass spectra of fraction 4 of AAB-1 and AAD-1 and fraction 5 of AAG-1 show differences from T18. Road aged TG18 showed differences from unaged T18 as well which will be discussed in the following subsection. The LD spectrum of AAB-1 fraction 4 in Figure 68 will now be used as an example for comparison against the LD spectrum of T18 fraction 4 in Figure 67. It is seen that the D^{13} series has two peak apexes, at 237 and 349 Da, and the peak at 349 Da is more intense than the peak at 237 Da. However, in the LD spectrum of T18 fraction 4 in Figure 67, there is only one peak apex at 209 Da

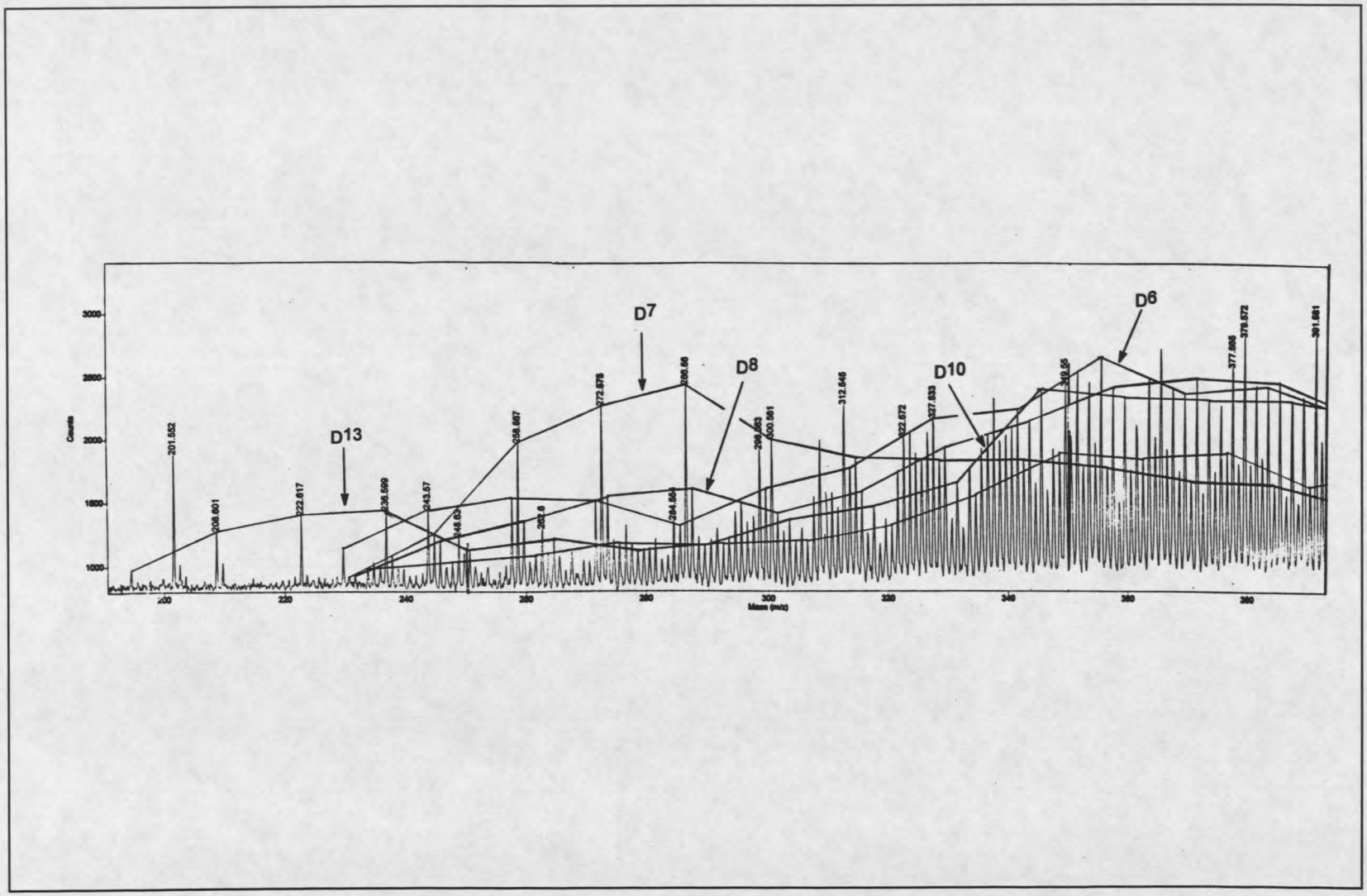

Figure 68. Resolved peak sequence in the LD spectrum of AAB-1 GPC fraction 4.

in the D^{13} series. Relative to the other series, the D^{13} peak apex is much more intense in T18 than in AAB-1. However, relative to the other series, D^7 is much more dominant in AAB-1 than in T18. The two peak apexes for the D^6 series are quite prominent in T18 (358 & 314 Da) and in AAB-1 the second peak apex (356 Da) is dominant whereas the first (258 Da) has very low intensity. D^{10} has only one peak apex at 346 Da in AAB-1. There are two D^{10} apexes at 290 and 346 Da in T18 with the 290 Da peak dominanting.

The AAD-1, fraction 4, LD spectrum (not shown) shows that the D^7, D^{11}, and the D^{13} series dominate over the other series. Whereas the AAG-1, fraction 5, LD spectrum (not shown) shows that the D^0, D^6, D^8, D^{10}, and D^{12} series dominate. It is clear that the importance of core molecules varies widely in these asphalts.

LD Spectral Differences Between T18 and TG18 GPC Fractions As mentioned earlier, at the beginning of the LD subsection of the Big Timber asphalts, T18 exhibited a definite shift to higher mass in the broad mass curve of its LD spectrum after four years of road service (Figure 56b). This particular asphalt pavement was not resilient to weathering and was cracked heavily. As a result of the GPC fractionation method it is now possible to observe additional differences between T18 and TG18.

Figure 69 shows the LD spectra of fraction 4 of T18 and TG18. Figure 70 shows the LD spectra of fraction 5 of T18 and TG18. One can see in Figure 69

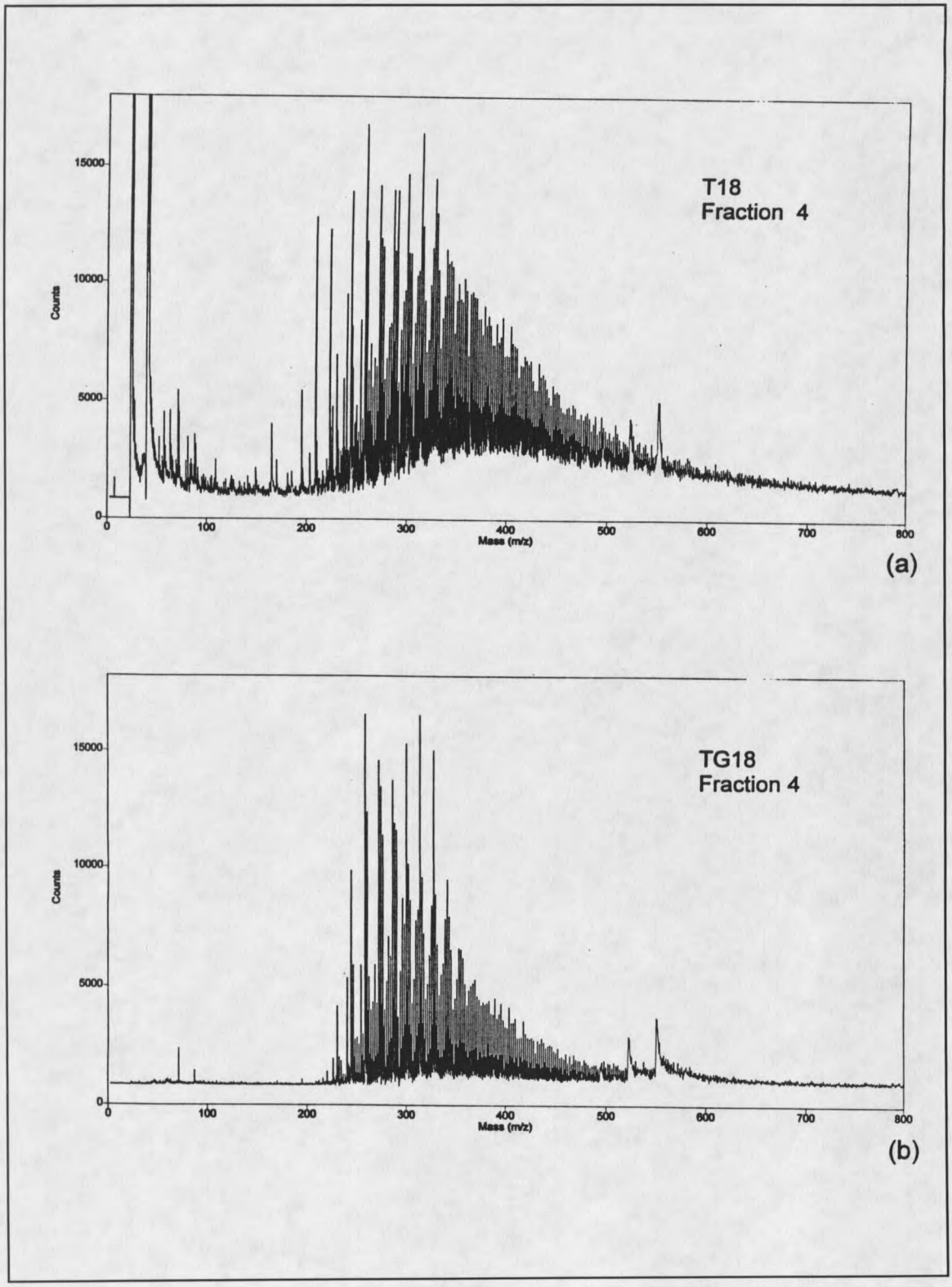

Figure 69. LD spectrum of GPC fraction 4 for a.) T18 and b.) TG18.

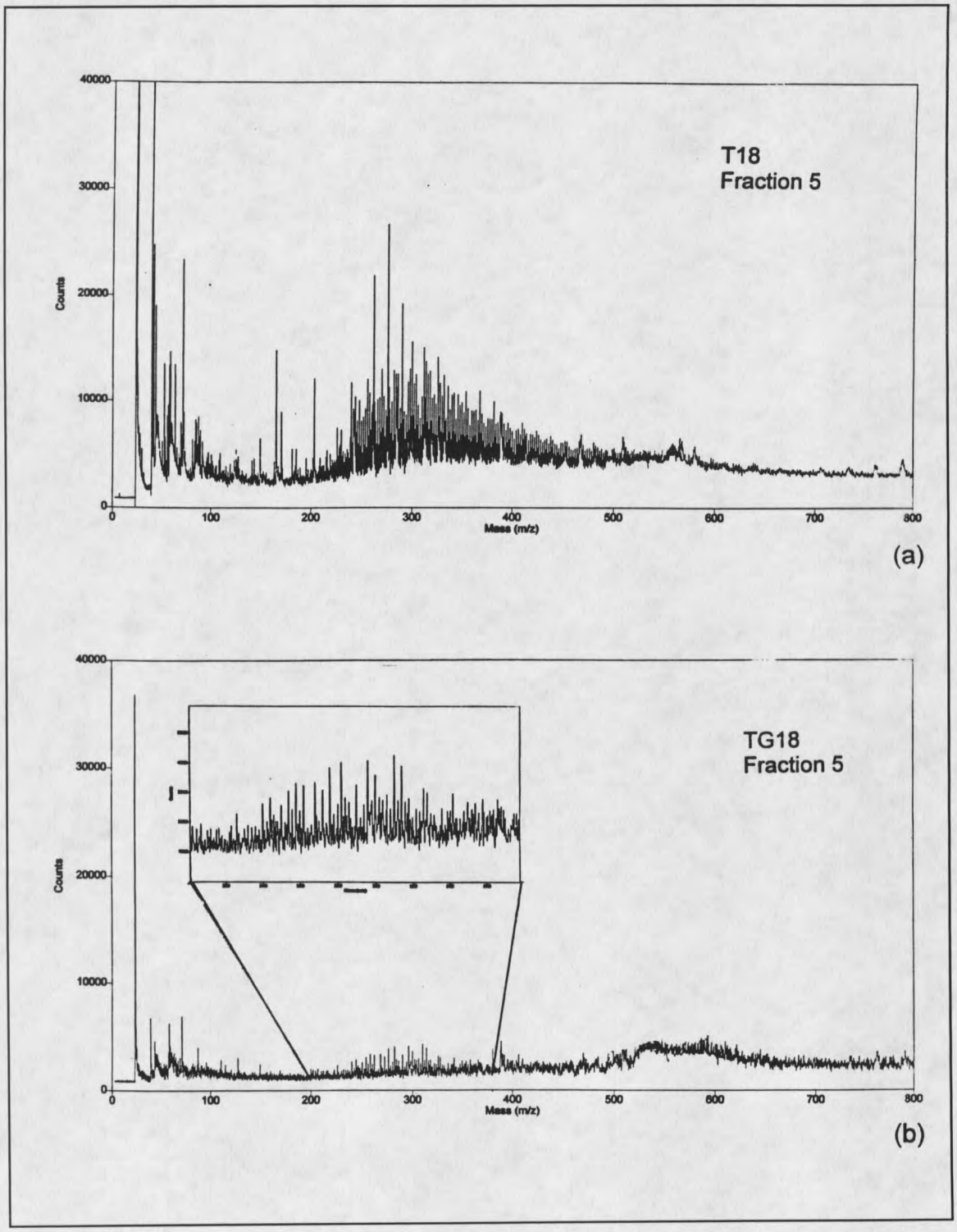

Figure 70. LD spectrum of GPC fraction 5 for a.) T18 and b.) TG18. The inset in b.) Is the magnified portion which shows that there are some small molecules left in TG18.

that the ion current is lower in the LD spectrum for TG18 than for T18. In addition, in the low mass region of the T18 LD spectrum (< 150 Da), one can see fragment type peaks as well as two very high intensity sodium (23 Da) and potassium (40 Da) peaks whereas these peaks are absent in the TG18 LD spectrum. The origin of these peaks is unknown.

In Figure 70, there is little evidence of any ion current for the small molecules in TG18. However, the inset in Figure 69b is a magnified view from 200 to 380 Da which shows that small molecules are still present in this fraction but the peak intensity is very low. In Figure 69a, there appears to be fragment ions and high intensity sodium and potassium peaks in the spectrum of T18. Figure 70b shows some low mass fragment type peaks and a sodium peak. The origin of these peaks, as stated above, is unknown.

Figures 67 and 71 show magnified views of the LD between 200 and 370 Da in the LD spectra of T18 and TG18 fraction 4. One can see that series D^6, D7, D^8, D^{10}, and D^{13} are traced out in both spectra. By comparing both spectra, one can see that the D^6, D^8, and D^{10} "even" mass series are still present in asphalt TG18 in Figure 71. However, there are no remaining peaks associated with the D^{13} "odd" mass series as well as very little D^7 "odd" mass series remaining in TG18.

Upon speculation of the disappearance of the smaller "odd" masses in TG18, one might first assume that evaporation has occured. However, this is highly unlikely due to the fact that neither the odd nor the low mass species in asphalt are very volatile. Even the "Hot Mix" cycle (at ~132° C) used just prior to

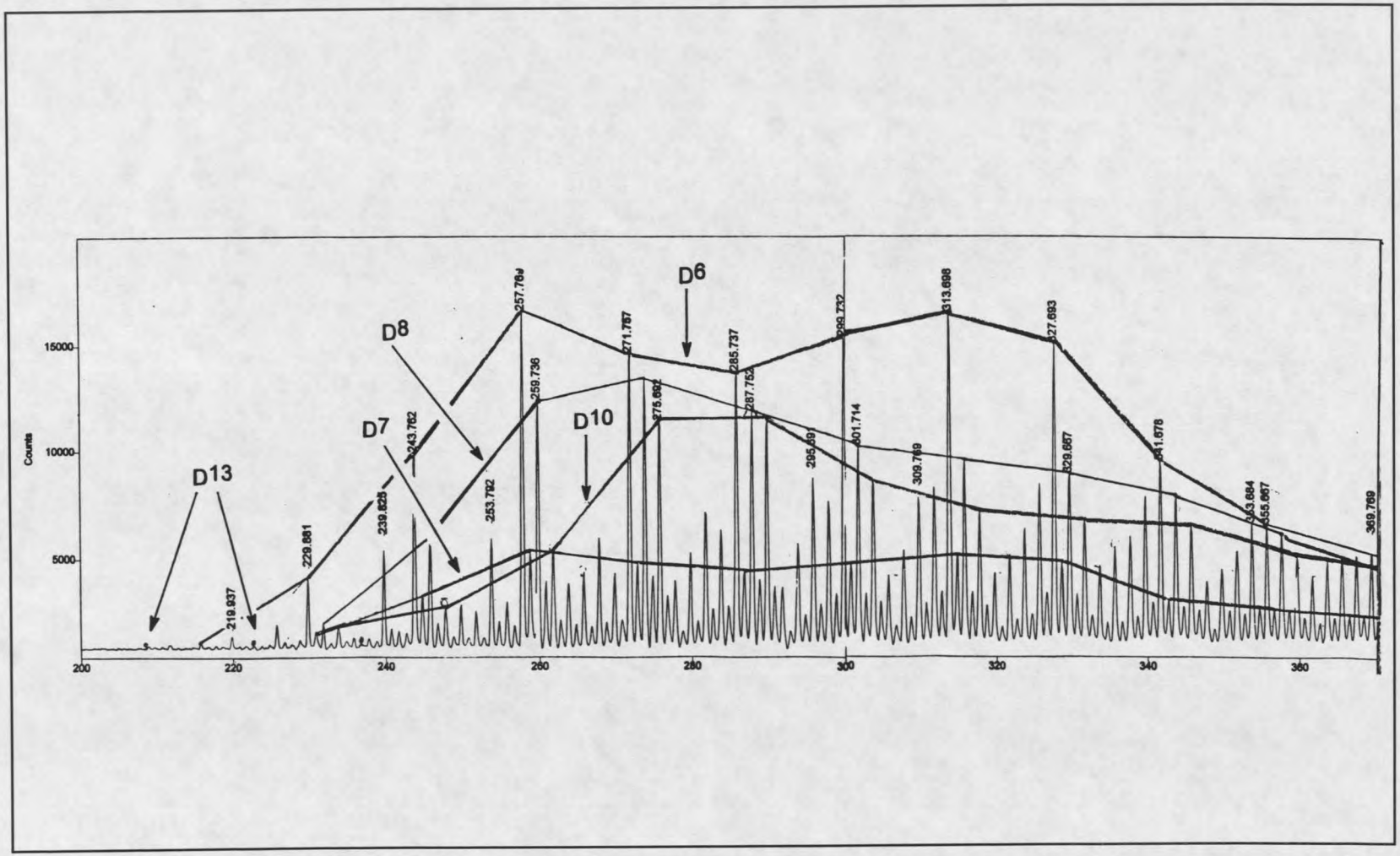

Figure 71. Resolved peak sequence in the LD spectrum of TG18 GPC fraction 4. Peak series D^{13} is gone here however, it was present in T18 fraction 4 (Figure 67). The D^{7} series is greatly diminished. D^{6}, D^{8}, and D^{10} are still present.

paving, when the asphalt binder is mixed with the aggregate material, does not reach temperatures sufficient to evaporate off even the smaller PAHs and nitrogen containing molecules in asphalt. For instance, carbazole has a boiling point of 355° C which is well above 132° C.

The actual cause of the disappearance is not known. However, Meng, *et al.* (67) discovered that photochemical free-radical polymerization of nitrogen containing heterocycles, including carbazole, occurs with fused polycyclic aromatic hydrocarbons. See Figure 72 for the photochemical polymerization reaction between carbazole and anthracene which is one of the reactions accomplished by Meng, *et al.* Although conjectural, the same process could have occured in T18 through UV free-radical initiation.

Pattern Recognition of Individual Asphalts

It has been shown that lower mass GPC fractions 4 and 5 gave LD spectra with baseline resolution of peaks. A large number of peaks are obtained, and it has been seen that large differences are observed in the peak pattern between different asphalts. If the LD spectra can be made reproducible by using similar experimental parameters, then peak patterns could be used to identify individual asphalts by fingerprinting.

Laser desorption reproducibility of the resolved peak sequence was investigated by repeating laser desorption on two separate samples of AAD-1

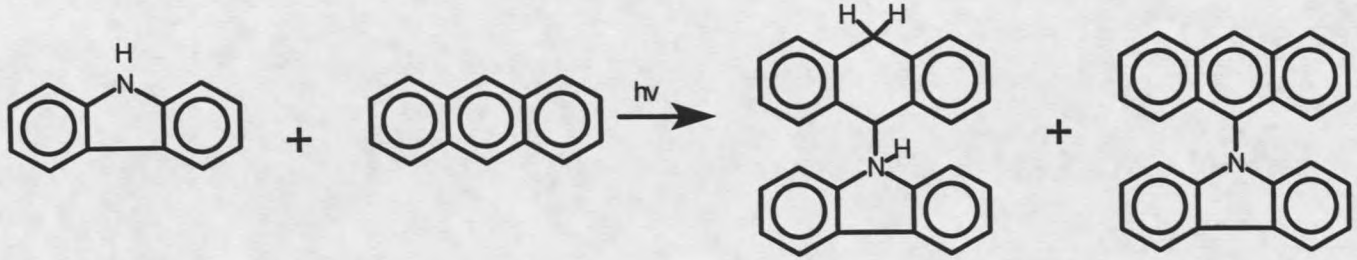

Figure 72. Photochemical reaction between carbazole and anthracene.(67)

keeping the experimental parameters constant. These parameters included the laser energy, number of scans, accelerating voltage, and the time that the acquisition started after the ionization chamber reached constant pressure. Figure 73 compares two spectra in the mass from 250 to 350 Da. It is seen that, by treating these samples in a similar manner, reproducible spectra can be obtained. Some minor differences can be noticed, but overall, the peak pattern remained the same.

Five GPC fractionated asphalts were chosen for experiments on the possibility of identifying asphalts by their LD spectral patterns. The fractions chosen were: AAB-1 fraction 4, AAD-1 fraction 4, AAG-1 fraction 5, T18 fraction 4, and TG18 fraction 4. Figures 74 and 75 show the characteristic peak profiles of these asphalt fractions in the range from 287 to 300 Da. Notice, in Figure 75, that very similar profiles are obtained for T18 and TG18. This is not surprising because they are both from the same refinery "batch", however TG18 has been road aged for four years.

It has been demonstrated here that asphalts show reproducible laser desorption mass spectra as well as individual, characteristic LD peak patterns. Therefore, the combined use of GPC fractionation and LD MS offers a novel approach for distinguishing one asphalt from another.

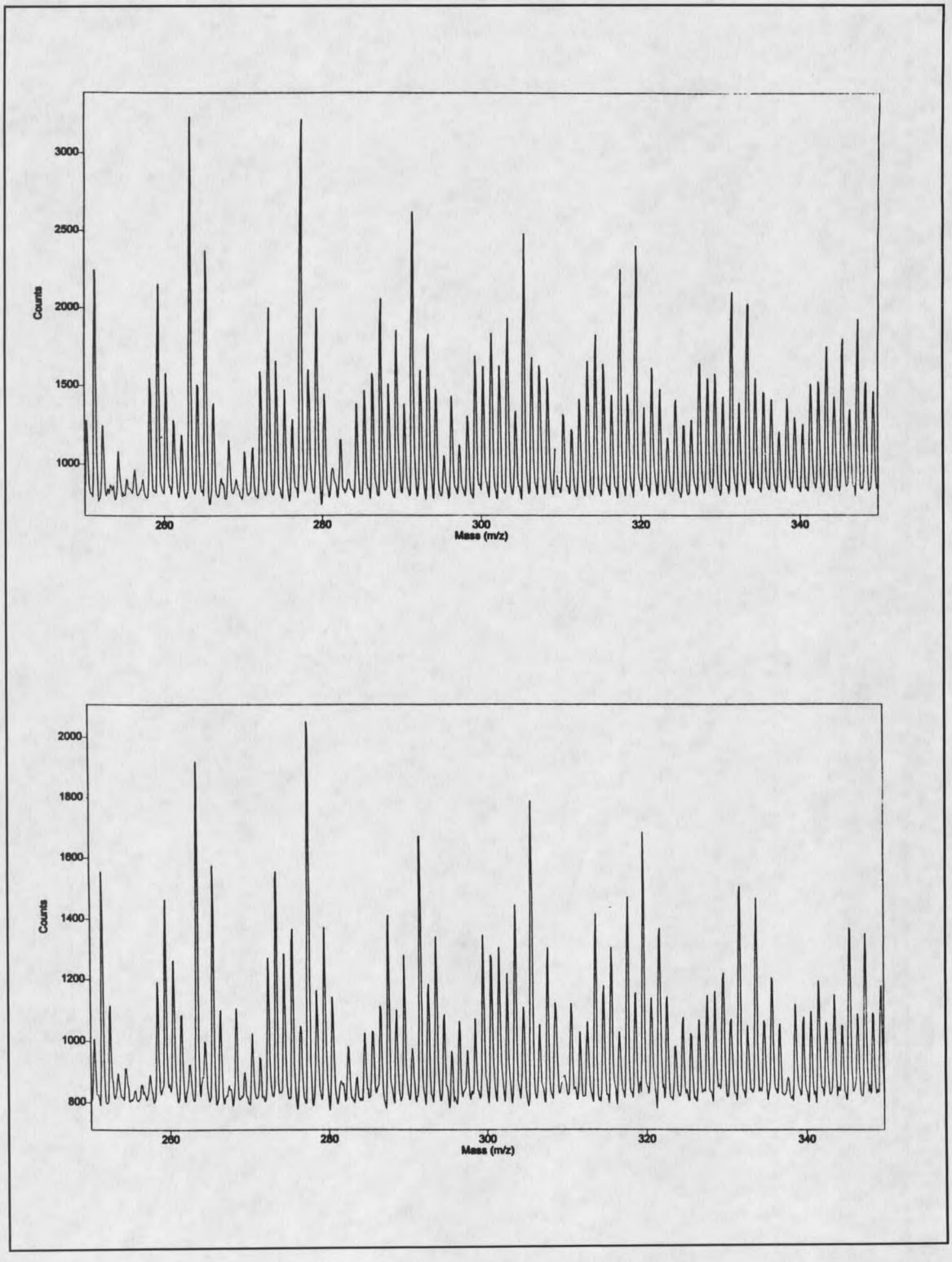

Figure 73. Reproducible LD spectra of AAD-1 showing mass range between 250 and 350 Da.

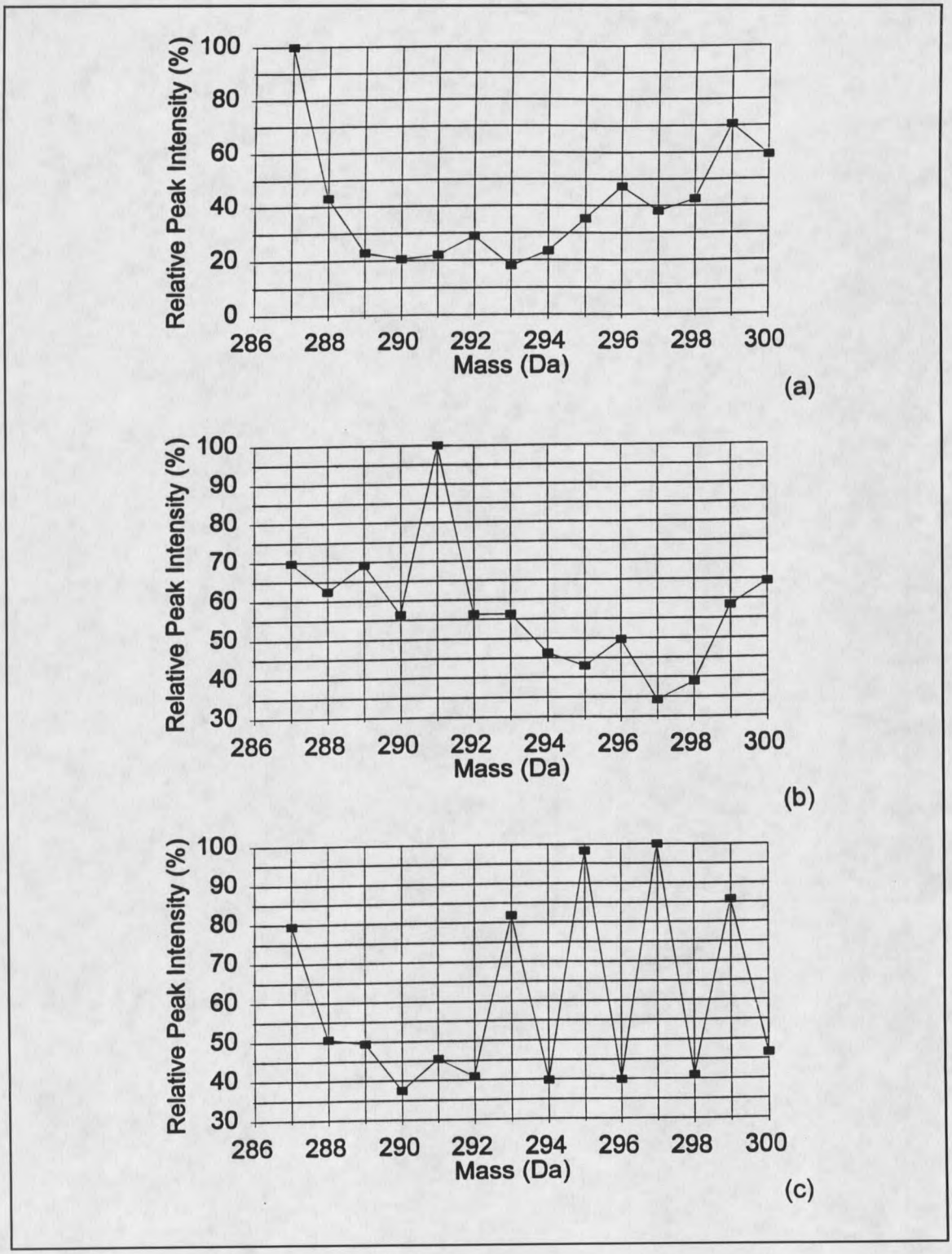

Figure 74. Graphed LD peak profiles for pattern recognition of a.) AAB-1 GPC fraction 4, b.) AAD-1 GPC fraction 4, and c.) AAG-1 GPC fraction 5.

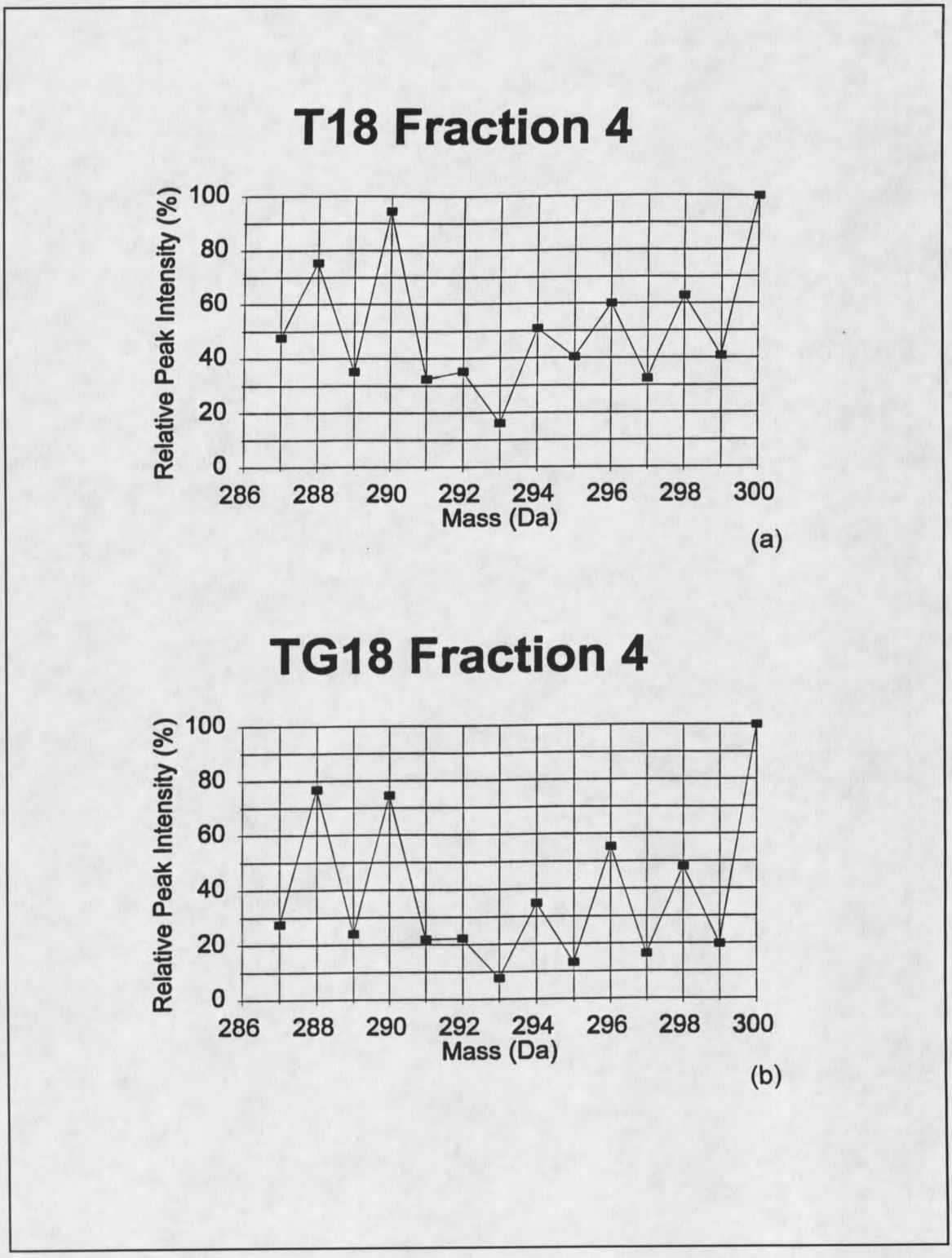

Figure 75. Graphed LD peak profiles for pattern recognition of a.) T18 GPC fraction 4 and b.) TG18 GPC fraction 4.

SUMMARY

Three major accomplishments have been discussed within this dissertation, and they include the following:

First, the characterization of phenols in asphalt has been successfully accomplished by employing a unique methylation process which can be carried out using minimal chemistry. It has been found, by first using model phenol compounds, that the sodium hydride/methyl iodide ($NaH/^{13}CH_3I$) method can quantitatively and specifically methylate small concentrations of phenols fairly rapidly inside of an NMR tube. The reaction is complete after only approximately two hours. The reaction "vessel" containing the unseparated reaction products is used to acquire the INVERSE GATED ^{13}C NMR experiment. The resulting ^{13}C NMR spectra are always clean and integratable. This expedient method for characterizing phenols in asphalt offers an on-line method for analyzing many samples. In addition, when using this method on asphalt, there appears to be an additional sharp peak within the NMR spectral region of the hindered methoxy carbon. This sharp peak indicates the presence of a small molecule which is supported by results obtained from the GPC LD MS experiments. It has been shown that asphalt does indeed contain not only large molecules but smaller molecules as well. It has been found that 9-hydroxyanthracene is a molecule present in the asphalts that were studied. This molecule is considered a hindered phenol.

Second, NMR spectroscopy has also been used to characterize benzylic carbons in asphalt and to relatively quantify changes that occur to the benzylic protons upon age weathering of asphalt pavement. A decrease in benzylic protons would support the theory of the free-radical air oxidation of benzylic carbons to benzylic ketones. The NMR experiment used to accomplish this is the 2D INVERSE COLOC experiment which optimizes long-range couplings between two nuclei. The benzylic carbon in asphalt cannot be directly observed, however by employing the COLOC experiment, the ^{2}J coupling between the benzylic proton and the quaternary aromatic carbon two bonds away can be seen as a cross peak in the 2D spectrum. 9,10-dimethylanthracene, whose benzylic protons chemical shift is sufficiently downfield from those of asphalt, was used as the "off-resonance" standard to ratio the relative changes in benzylic proton peak area upon age weathering. It was found that the WRI TFO/POV aging method was not harsh enough to cause a substantial decrease in benzylic protons. In some cases there was an increase. However, when a real road weathered asphalt pavement was used for comparison, a substantial decrease in benzylic protons was observed. A sample of this unaged asphalt containing a MnO_2 additive was also shown to contain fewer benzylic protons. MnO_2 is a fairly strong oxidant. An asphalt treated with hydrogen peroxide (H_2O_2) showed a definite decrease in benzylic protons which proves that these positions are labile and reactive under certain conditions. Carbonyl concentration has been determined by FT-IR

spectroscopy. Although the IR absorbance spectra showed the presence of carbonyl in the TFO/POV samples, there was a higher concentration in the actual weathered sample and in its MnO_2 containing counterpart. This was especially true with the H_2O_2 treated asphalt. Benzylic carbon oxidation is not neccessarily the only contributor to the formation of carbonyl group as evinced by the IR data. But, the IR data has helped as supportive evidence showing that when benzylic protons have actually decreased after aging or upon addition of an oxidizing agent there is a substantial increase in the IR absorbance in the carbonyl region.

Third, peak profiling for fingerprinting asphalts and mass identification has been determined using GPC LD MS. Fractionating asphalt by GPC has shown that asphalts can be individually identified. The GPC fractions of the low mass molecules in individual asphalts seem to show unique, resolvable LD mass patterns of peak sequences. These small molecule patterns can now be defined as series of overlaping peak sequences of mass 14 Da differences. These peak series have also revealed that there are masses common to all of the asphalts. However, they are present in varying concentrations. The extent of alkylation also varies from asphalt to asphalt.

Both "even" and "odd" mass series are in asphalt. The even masses appear to be alkylated PAHs and the odd masses are alkylated nitrogen containing molecules. It was observed that upon actual road aging, there was a shift in LD masses. A free-radical polymerization scheme was proposed that

could explain an LD spectral shift to higher masses. One of the most startling observations was made between an unaged (T18) versus a road aged (TG18) asphalt. There had been a distinct LD higher mass shift in TG18 along with the decrease of peak intensity in the small mass region. Upon GPC separation of the smaller mass fractions it was shown that the "odd" mass series (the nitrogen containing molecules) had completely disappeared or decreased substantially in TG18. A photochemical polymerization reaction between the small mass nitrogen compounds and PAHs was proposed as a possibility for the above mentioned observations in the LD spectra of TG18.

REFERENCES

1. The Asphalt Institute. "The Asphalt Handbook", College Park, Maryland. Manual series No. 4. (1961).

2. Petersen, J.C., "Chemical Composition of Asphalt as related to Asphalt Durability-State of the Art", *Transportaion Research Record 999*, TRB, National Research Council, Washington, D.C., 13, (1985).

3. Jennings, P.W., Pribanic, J.A.S., Desando, M.A., Raub, M.F., Stewart, F.F., Hoberg, J., Moats, R., Smith, J.A., Mendes, T.M., and McGrane, M., "Binder Characterization and Evaluation by NMR Spectroscopy", Dept. Of Chemistry, Montana State University, Final Report, (February 1991).

4. Yen, T.F. "A Macrostructure of Petroleum Asphalt", PREPRINTS, *Div of Petrol. Chem.*, ACS, 35(3), 314 (1990).

5. Yen, T.F., "The Coloidal Aspect of a Macrostructure of Petroleum Asphalt", *Fuel Science and Technology Int'l.*, 10(4-6), 723 (1992).

6. World Book Encyclopedia. Field Enterprises Educational Corpaoration. Chicago, IL., Vol II., (1963).

7. Grolier Encyclopedia. The Grolier Society. New York, N.Y., Vol VII., (1954).

8. Jennings, P.W., Desando, M.A., Raub, M.F., Moats, R., Mendez, T.M., Stewart, F.F., Hoberg, J.D., Pribanic, J.A.S., and Smith, J.A., "NMR Spectroscopy in the Characterization of Eight Selected Asphalts", *Fuel Science and Technology Int'l.*,10 (4-6), 887, (1992).

9. Petersen, J.C., "An Infrared Study of Hydrogen Bonding in Asphalt", *Fuel*, 46, 295 (1967).

10. Petersen, J.C., Barbour, F.A., and Dorrence, S.M., "Catalysis of Asphalt Oxidation by Mineral Aggregate Surfaces and Asphalt Components", Proceedings, Association of Asphalt Paving Technologists, 43, 1622 (1974).

11. Glover, C.J., Davison, R.R., Ghoreishi, S.M., Jemison, H.B., and Bullin, J.A., "Evaluation of Oven Simulation of Hot-Mix Aging by and FT-IR Pellet Procedure and Other Methods", *TRR 1228*. TRB, National Research Council, Wishington D.C.

12. Petersen, J.C., Barbour, F.A., and Dorrence, S.M., "Identification of Dicarboxylic Anhydrides in Oxidized Asphalts", *Anal. Chem.*, 47(1), 107 (1975).

13. McKay, J.F. and Wolf, J.M., "Infrared Study of the Aging of Asphalts in Contact with Aggregates", *Fuel Science and Technology Int'l.*,10(4-6), 935 (1992).

14. Davis, T.C. and Petersen, J.C., "An Inverse GLC Study of Asphalts Used in the Zaca-Wigmore Experimental Test Roads", *Proc., Association of Asphalt Paving Technologists*, 36, 1 (1967).

15. Petersen, J.C., "Quantitative Method Using Differential Infrared Spectrometry for the Determination of Compound Types Absorbing in the Carbonyl Region in Asphalts", *Anal. Chem.*, 47(1) (1975).

16. Petersen J.C., "Quantitative Functional Group Analysis of Asphalts Using Differential Infrared Spectrometry and Selective Chemical Reactions-Theory and Application", *TRR 1096*, TRB, National Research Council, Washington, D.C.

17. Zakar, P., Asphalt, Chemical Publishing Company, INC. New York. pg. 6, (1971).

18. Rostler, F.S. and Sternberg, H.W., "Analytical Procedure for Chemical Fractionation of Asphalts Rostler-Sternberg Analysis", *Assoc. Paving Tech.*, 31, 72 (1962).

19. Brule', B., "Characterization of Bituminous Compounds by Gel Permeation Chromatography (GPC)", *J. Liquid Chromatography*, 2(2),165 (1979).

20. Brule', B., Such, C., and Baluja-Santos, C., "Characterization of a Road Asphalt by Chromatographic Techniques (GPC & HPLC)", *J. Liquid Chromatography*, 2(3), 437(1979).

21. Pribanic, J.A.S., Jennings, P.W., Smith, J.A., and Mendes, T.M., "HP-GPC Analysis of Asphalt Fractions in the Study of Molecular Self-Assembly in Asphalt", PREPRINTS, *Div. Of Fuel Chemistry*, ACS, 37, 1312 (1992).

22. Fessenden R.J., and Fessenden J.S., Organic Chemistry, Willard Grant Press. Boston Massachusettes. Third Printing. pg. 23, (1980).

23. Planche, J.P., "Relationships between Characterization of Asphalt Cements by Differential Scanning Calorimetry and their Physical Properties", PREPRINTS, *Div. Of Petroleum Chemistry*, ACS, 35(3), 330 (1990).

24. Brule' B., *TRR 1096*, 22 (1986).

25. Jennings, P.W., Pribanic, J.A.S., Raub, M.F., Smith, J.A., and Mendes, T.M., "Advanced High Performance Gel Permeation Chromatography Methodology", Quarterly Report, Montana State Univ., non-published results. (July-Sept. 1990).

26. Guin, J.A., Chang, H.-S., Yen, S.-C., and Kuo, C.-T., "Absorption of Asphalt into Porous Aggregates: Test of a Simple Physiochemical Model", *Fuel Science and Technology Int'l*, 10 (4-6) (1992).

27. Corbett, L.W., "Reaction Variables in the Air Blowing of Asphalt", *Ind. Eng. Chem. Process Des. Dev.*, 14(2) 181 (1975).

28. Dunning, R.L. and Meeks. "Comparison Between Air Blowing and Accelerated Aging", Proceedings of the *Association of Asphalt Paving Technologists (AAPT)*, 37, 529 (1968).

29. Dickinson, E.J., "The Constitution and Quality of Paving Grade Asphalts Produced by Air Blowing Distillation Residues of Kuwait and Light Arabian Crude Oil", Proceedings of the *Association of Asphalt Paving Technologists (AAPT)*, 43, 132 (1974).

30. Clark, M.F. and Culley, R.W., "Evaluation of Air-Blown Asphalts to Reduce Thermal Cracking of Asphalt Pavements", Proceedings of the *Association of Asphalt Paving Technologists (AAPT)*, 539 (1976).

31. Mill, T. And Tse, D., "Oxidation and Photooxidation of Asphalts", Proceedings of the Symposium on Chemistry and Characterization of Asphalts, Washington, Division of Petroleum Chemistry, 483-489 (1990).

32. Lau, C.K., Lunsford, K.M., Glover, C.J., Davison, R.R., and Bullin, J.A., "Reaction Rates and Hardening Susceptibilities as Determined from Pressure Oxygen Vessel Aging of Asphalts", *TRR 1342*, TRB, National Research Council, Washington D.C.

33. Jennings,P.W., Stewart, F.F., Smith, J.A., Desando, M.A., Mendes, T.M., and Pribanic, J.A.S., "Nuclear Magnetic Resonance Spectroscopy for the Characterization of Asphalt", PREPRINTS, *ACS Division Fuel Chemistry*. 37, 1320 (1992).

34. Hagen, A.P., Johnson, M.P., and Randolph, B.B., "^{13}C NMR Studies on Roadway Asphalts", *Fuel Science and Technology Int'l.*, 7, 1289 (1989).

35. Jennings, P.W., Desando, M.A., Raub, M.F., Hoberg, J.O., Moats, R., and Stewart, F.F., "NMR Spectroscopy in the Characterization of Asphalt", Symposium on Chemistry and Characterization of Asphalts, Div. of Petroleum Chemistry, Inc., and Fuel Chemistry, ACS, Washington, D.C., Aug. 26-31, 440 (1990).

36. Rose, K.D. and Francisco, M.A., "A Two-Step Chemistry for Highlighting Heteroatom Species in Petroleum Materials Using ^{13}C NMR Spectroscopy", *J. Am. Chem. Soc.* 110, 637 (1988).

37. Stoochnoff, B.A. and Benoiton, L.N., "The Methylation of some Phenols and Alcohols with Sodium Hydride/Methyl Iodide in Tetrahydrofuran", *Tetrahedron Letters*, 1, 21 (1973).

38. Brown, C.A., Barton, D., and Sivaram, S. "Rapid Stereospecific Methylation of Alcohols and Glycols with Sodium Hydride/Methyl Iodide", *Communications*, pg. 434. June (1994).

39. Jemison, H.B., Burr, B.L., Davison, R.R., Bullin, J.A., and Glover, C.J., "Application and Use of the ATR FT-IR Method to Asphalt Aging Studies", *Fuel Science and Technology Int'l.*,10(4-6), 795 (1992).

40. Haley, B.A., "Molecular and Unit Sheet Weights of Asphalt Fractions Separated by Gel Permeation Chromatography", *Anal. Chem.*, 43(3), 371 (1971).

41. Farcasiu, M., Forbus, T.R., and LaPierre, R.B., "Transalkylation Reactions in Fossil Fuels and Related Model Compounds", PREPRINTS, *ACS Div. Petrol. Chem.*, 28, 279 (1983).

42. Dorronsoro, D., Garcia, M.R., and Grimalt, J.O., "Triterpane Distributions in Diapir-Related Asphalts", *Fuel*, 73(1), 83 (1994).

43. Gale, P.J. and Bentz, B.L., "Chemical Characterization of Asphalt Using Thermal Chromatography with Mass Spectrometry", *Fuel Science and Technology Int'l.*, 10(4-6), 1059 (1992).

44. Sebor, G., Kubelka, V., and Weisser, O., "Mass Spectrometric Characterization of Petroleum", *Chem.-Technol.* 213 (1980).

45. Barber, M., Bordoli, R.S., Elliot, G.J., Sedgwick, R.D., and Tyler, A.N., *J Chem. Soc. Chem. Commun.*, 325 (1981).

46. Roepstorff, P. And Sundquist, B., in Biochemical Applications of Mass Spectrometry, ed. By S. Gaskell, pg. 269. Wiley, Chichester (1986).

47. Fenn, J.B., Mann, M., Meng, C., Wong, S., "Electrospray Ionization-Principles and Practice", *Mass Spec. Rev.*, 9(1), 37 (1990).

48. Smith, R.D., Loo, J.A., Loo, R.R.O., Busman, M., and Udseth, H.R., "Principles and Practice of Electrospray Ionization-Mass Spectrometry for Large Polypeptides and Proteins", *Mass Spec. Rev.*, 10(5), 359 (1991).

49. Beavis, R.C. and Chait, B.T., Hillenkamp, F., and Karas, M., "Matrix-Assisted Laser Desorption Ionization Mass Spectrometry of Biopolymers", *Anal. Chem.*, 63(24), 1193 (1991).

50. Hunt, J.E., Drinkwater, D.E., and Winans, R.E., "Comparison of Several Contemporary Ionization/Mass Analyzer Techniques for Large Components of Comples Fossil-Derived Materials", Poster Presented at the 41st ASMS Conference on Mass Spectrometry (524a).

51. Burroughs, J.A., Cadre, B.M., and Hanley, L., "Laser Desorption Ion Trap Mass Spectrometry of the Polymeric Component of Coal", Poster Presented at the 41st ASMS Conference on Mass Spectrometry (441a).

52. Greenwood, P.F., Strachan, M.G., Willett, G.D., and Wilson, M.A., "Laser-Induced Molecular Ion Formation and Gas-Phase Ion Formation from Polycyclic Aromatic Hydrocarbons, Coals, and Coal Products Detected by Fourier Transform Mass Spectrometry", *Organic Mass Spectrometry.*, 25, 353 (1990).

53. Karas, M., Bachman, D., Bahr, U., and Hillenkamp, F., "Matrix-Assisted Ultraviolet Laser Desorption of Non-Volatile Compounds", *Int. J. Mass Spectrom.* Ion Proc., 78, 53 (1987).

54. John, P., Johnson, C.A.F., Parker, J.E., Smith, G.P., Herod, A.A., Li, C., Humphrey, P., Chapman, J.R., and Kandiyoti, R., "Molecular Masses up to 270,000μ in Coal and Coal Derived Products by Matrix Assisted Laser Desorption Ionization Mass Spectrometry (MALDI-MS)", *Fuel*, 93(10), 1606 (1994).

55. Altgelt, K.H. and Hirsh,E., "GPC Separation and Integrated Structural Analysis of Petroleum Heavy Ends", *Separation Science*, 5(6), 855 (1970).

56. Altgelt, K.H., "Fractionation of Asphaltenes by Gel Permeation Chromatography", *Journal of Appled Polymer Science*, 9, 3389 (1965).

57. Reerink, H. And Lijzenga, J., "Gel Permeation Chromatography Calibration Curve for Asphaltenes and Bituminous Resins", *Analytical Chemistry*, 47(13) (1975).

58. Rose, K.D. and Francisco, M.A., "Characterization of Acidic Heteroatoms in Heavy Petroleum Fractions by Phase-Transfer Methylation and NMR Spectroscopy", *Energy and Fuels*, 1, 233 (1987).

59. Atta-ur-Rahman. Nuclear Magnetic Resonance, Basic Principles, Springer-Verlag. New York N.Y. (1986).

60. Abraham, R.J., Fisher, J., and Loftus, P., Introduction to NMR Spectroscopy, John Wiley & Sons. Chichester, England (1988).

61. Jennings, P.W., Pribanic, J.A.S., and Mullaney, M., "Asphalt as a Variable. The Big Timber Test Sections", Presented at the annual meeting of the Association of Asphalt Paving Technologists, Reno, Nevada. Feb 22-25 (1987).

62. Vastola, F.J., Mumma, R.O., and Pirone, A.J., *Org. Mass Spectrom.* 3, 101-104 (1970).

63. Harrison, A.G., Chemical Ionization Mass Spectrometry, 2nd Ed., CRC Press, Boca Raton (1992).

64. Lias, S.G., Liebman, J.F., Levin, R.D., Kafafi, S.A., and Stein, S.E., Positive Ion Energetics, Ver. 2.0, NIST Standard Reference Database 19A (1993).

65. Lowry, T.H. and Richardson, K.S., Mechanisms and Theory in Organic Chemistry, Third Edition. Harper & Row, Publishers, New York. Pg 742 (1987).

66. McLafferty, F.W. Interpretation of Mass Spectra, University Science Books. Mill Valley, CA. Third edition. (1980).

67. Meng, J., Wang, W., Wang, Y., and Wang, H., "Solid State Photoreaction of N-Heterocyclic Compounds", *Chin Chem Lett*, 4(2), 115-118 (1993).

APPENDIX

SHRP ASPHALT BACKGROUND INFORMATION

Appendix

ASPHALT CODE		AAA-1	AAB-1	AAC-1	AAD-1	AAF-1	AAG-1	AAK-1	AAM-1
CRUDE OIL SOURCE		Lloydminster	WY Sour	Redwater	Ca	W Tx Sour	Ca Valley	Boscan	W Tx Inter.
VISC./PEN GRADE		150/200	AC-10	AC-8	AR-4000	AC-20	AR-4000	AC-30	AC-20
SHRP PG GRADE		PG58-28	PG58-22	PG58-16	PG58-28	PG64-10	PG58-10	PG64-22	PG64-16
Viscosity:	140° F, poise	864	1029	419	1055	1872	1862	3256	1992
	275° F, cSt	283	289	179	309	327	243	562	569
Penetration:	77° F,100g,5s	160	98	133	135	55	53	70	64
	39.2° F,100g,5s	15	6	7	9	0	2	2	4
Ductility, cm:	39.2° F,1cm/min	150+	40.1	137	150+	7.6	0.0	27.8	4.6
	Softening Point,°F	112	118	109	118	122	120	121	125
Asphaltenes:	(n-heptane)	16.2	17.3	10.1	20.5	13.3	5.0	20.1	4.0
	(Iso-octane)	3.4	2.0	3.1	3.4	3.1	3.3	2.8	5.4
Polar Aromatics		37.3	38.3	37.4	41.3	38.3	51.2	41.8	50.3
Naphthene Aromatics		31.8	33.4	37.1	25.1	37.7	32.5	30.0	41.9
Saturates		10.6	8.6	12.9	8.6	9.6	8.5	5.1	1.9
Elemental Analysis:	C%	83.9	82.3	86.5	81.6	84.5	85.6	83.7	86.8
	H%	10.0	10.6	11.3	10.8	10.4	10.5	10.2	11.2

Appendix cont. . .

Asphalt Code		AAA-1	AAB-1	AAC-1	AAD-1	AAF-1	AAG-1	AAK-1	AAM-1
Elemental Analysis:	O%	0.6	0.8	0.9	0.9	1.1	1.1	0.8	0.5
	Nitrogen,%	0.50	0.54	0.66	0.77	0.55	1.10	0.70	0.55
	Sulfur,%	5.50	4.7	1.90	6.90	3.40	1.30	6.40	1.20
	Vanadium, ppm	174	220	146	310	87	37	1480	58
	Nickel, ppm	86	56	63	145	35	95	142	36
	Iron, ppm	4	16	------	13	100	48	24	255
	Aromatic C, %	28.1	31.9	24.7	23.7	32.8	28.8	31.9	24.7
	Aromatic H, %	7.68	7.12	6.41	6.81	8.66	7.27	6.88	6.51

For more information on the above listed SHRP asphalts as well as additional SHRP asphalts contact:

Nichols Consulting Engineering
1885 S. Arlington, #111
Reno, NV 89509

Phone #: (702) 329-4955

This address is current up to May 1, 1997.